

**Investigating the Roles of *Drosophila ppk20* in
Cellular Iron Import**

by
Qian Wang

A thesis submitted in partial fulfillment of the requirements for the degree of

Master of Science

Department of Biological Sciences
University of Alberta

©Qian Wang, 2022

Abstract

The *ppk20* (*pickpocket 20*) gene was identified from a two-step screen that was aimed at identifying genes relevant to *Drosophila* iron and heme homeostasis. Initially, our lab collaborated with two other labs and carried out a prothoracic gland (PG)-specific genome-wide screen of 12,500 RNA interference (RNAi) lines seeking genes that might be relevant to ecdysone synthesis. Ecdysone is an insect steroid hormone that regulates *Drosophila* development. This initial screen identified 1,906 RNAi lines with developmental defects, including different larval stage arrest/delay and pupal lethality. The secondary screen was conducted in our lab, using ~800 lines that showed development defects, but survived to the third instar stage. This strategy identified 13 RNAi lines that showed enlargement of the PG (no red autofluorescence) and 21 RNAi lines that exhibited enlarged PGs together with a red autofluorescence signal. Due to the high iron demand in PG associated with heme and ecdysone synthesis, our lab has used the PG phenotype to study poorly characterized aspects of *Drosophila* iron and heme homeostasis.

The heme production pathway is a multi-step biosynthesis process, and it requires the incorporation of iron at the last step. Several heme precursors contain the porphyrin ring structure, making them autofluoresce a red colour when exposed to ultraviolet (UV) light. The final product, heme, is a necessary cofactor for cytochrome P450 enzymes (CYPs) that are essential for *Drosophila* ecdysone biosynthesis. Ecdysone regulates all developmental transitions from embryonic to adult stages. Hence, an inappropriate drop in ecdysone concentration can lead to developmental defects. The PG maintains high iron levels to sustain heme production, thus supporting ecdysone biosynthesis. The red-fluorescing, protoporphyrin IX (PPIX), is the immediate precursor to heme, and without iron incorporation, it might halt and reduce heme production, causing PPIX to accumulate. In addition, interruption at other steps may result in the accumulation of other red-fluorescing precursors. Under UV light, the PG will fluoresce bright red with enough red-fluorescent precursor accumulation. Knocking down *ppk20* in the PG causes developmental defects and red PG phenotype, possibly due to the lack of ecdysone and the accumulation of red-fluorescing precursors.

PPK20 is a member of the epithelial sodium channel (ENaC) family, and some of its vertebrate homologs have been shown to exhibit sodium channel activity. No previous studies

have shown the relevance of *ppk20* or any other *ppk* genes in iron and heme homeostasis. In this thesis, I explored how *ppk20* this possible relevance.

Iron might be imported into the cells through the iron-containing proteins, transferrin (Tsf) and ferritin, or through a non-protein-binding form. In humans, primary iron intake involves importing Tsf via Tsf receptor-mediated endocytosis. However, there is no identified fly Tsf receptor. Heme feeding and *human transferrin receptor (hTfR)* cDNA expression, but not iron feeding, rescued the loss-of-*ppk20* animals. When *ppk20* function was impaired in the larval intestine, free iron uptake from the midgut was interrupted. Moreover, ferritin injection could partially rescue the *ppk20*-deficient animals. Interestingly, the larval tracheal necrotic phenotype was present in the loss-of-*ppk20* animals, which indicates its role in tracheal function.

Taken together, this thesis presents evidence that *ppk20* may play a role in cellular iron import via regulating the free iron and Tsf import pathways due to its possible function as the Tsf receptor-like protein or sodium channel. Additionally, *ppk20* might play a role in larval tracheal development and water clearance, contributing to the porphyria-like PG phenotype and developmental defects observed in the loss-of-*ppk20* animals.

Acknowledgments

Throughout the writing of this thesis and this degree, I have received a great deal of help and support. Although it has been difficult for us all during the unprecedented COVID-19 pandemic, especially in academic research, a generous amount of assistance from my support system was given to me.

First of all, I would like to thank my supervisor Dr. Kirst King-Jones for giving me the opportunity to carry out the research project in your lab. Moreover, you had provided me with valuable feedback when I needed guidance.

I would also like to thank committee members Dr. Martin Srayko and Dr. Anna Phan for giving me feedback and guidance throughout my degree. Without their help, I would not have come up with some novel ideas for the project.

For the past and current members of King-Jones's lab, I would really like to say a big thank you to all of them. They provided me with the guidance and training, despite doing it on their own private time. Thank you for being so patient when I have a million questions regarding the project or the techniques for you. In addition, I would also like to thank some colleagues from other labs for lending us the reagents equipment and kindly giving us the fly lines we needed for research.

During the time of getting the master's degree, there were many dark days, my lovely friends helped me through it all when my mental health was not at best because of the stress. Thank you for talking to me in person before the pandemic and zooming with me during the pandemic regardless of whichever time zone you are in. After the pandemic, I could not travel, which really took a toll on my mental health, and suffering the loss of some family member made it extra difficult. My support system, including my family and friends, pulled me through the most challenging time of my academic life. Furthermore, I am grateful for those of you who have supported my artistic creation, without that outlet, I could not have made it. Thank you for modelling for me and listening to me talking about apocalypse nonstop.

Special thanks to Dr. Sarah Hughes, Dr. Andrew Waskiewicz, Dr. Greg Goss and Dr. Ted Allison for the encouragement and for pointing out the directions for me. They have educated and provided me with guidance on various levels and during different stages of the degree. Last but not least, I would like to thank the University of Alberta for providing me with the teaching opportunity as the financial support. I gained experience in teaching and problem-solving.

TABLE OF CONTENTS

Chapter 1. Introduction.....	1
1.1 The significance of iron.....	1
1.2 Iron storage and import via iron-bound proteins.....	2
1.3 Comparison of human and <i>Drosophila</i> iron metabolism.....	3
1.4 Intracellular iron regulation.....	6
1.5 Ecdysteroid biosynthesis in the prothoracic gland.....	8
1.6 Heme biosynthesis.....	10
1.7 <i>ppk20</i> was found in a two-step screen.....	13
1.8 <i>ppk20</i> is a member of the DEG/ENaC family.....	13
1.9 HIF functions in hypoxia.....	17
1.10 Summary of iron import in human and <i>Drosophila</i>	18
1.11 Current gaps in our understanding and overall hypothesis.....	20
Chapter 2. Materials and Methods.....	21
2.1 Fly stock maintenance and fly development study.....	21
2.1.1 Basic fly husbandry.....	21
2.1.2 Setting up fly crosses and embryo collection.....	21
2.1.3 Survival rate studies.....	21
2.2 Survival rate quantification of animals with delay and arrest phenotypes.....	22
2.3 Supplemental rescue experiments.....	23
2.4 Grape juice plate.....	23
2.5 Larval tissue immunofluorescence (IF).....	24

2.6 Immunoprecipitation (IP)	25
2.7 Coomassie Brilliant Blue staining.....	28
2.8 Western blot analysis.....	29
2.9 Mass spectrometry (MS).....	31
2.10 Confocal microscopy.....	31
2.11 RNA-sequencing (RNAseq)	31
2.12 Ferric iron staining.....	32
2.13 Larval ferritin injection.....	32
2.14 <i>Drosophila</i> whole-body DNA extraction using “DNAzol”	33
2.15 High-efficiency transformation.....	34
2.16 Plasmid DNA extraction.....	35
2.17 Statistics.....	36
2.18 Tables.....	37
Chapter 3. The study of how <i>ppk20</i> is involved in cellular iron import.....	47
3.1 Introduction and rationale.....	47
3.1.1 The primary scenarios by which PPK20 may be involved in cellular iron import.....	47
3.1.2 Other possibilities of how PPK20 is involved in fly iron and heme homeostasis.....	50
3.2 Results and discussion.....	50
3.2.1 The phenotypes study of other <i>ppk</i> loss-of-function animals.....	50
3.2.2 Characterization of PG phenotype and survival rate of the loss-of- <i>ppk20</i> animals.....	51

3.2.2 Supplement food rescue experiment of <i>PG>ppk20</i> -RNAi and <i>ppk20^{KO}</i> animals.....	58
3.2.3 Loss of <i>ppk20</i> may disturb the function of enzymes involved in the heme synthesis pathway.....	67
3.2.4 The possibilities of how <i>ppk20</i> mediates cellular iron import: (1) PPK20 directly affects non-transferrin-binding iron (NTBI) cellular import.....	69
3.2.5 The possibilities of how <i>ppk20</i> mediates cellular iron import: (2) <i>ppk20</i> is the potential receptor for Tsf/ferritin or affects their receptor (unknown) function in cellular iron import.....	73
3.3 Discussion.....	80
3.4 Tables.....	81
Chapter 4. Characterization of PPK20 protein and its interaction with other proteins	84
4.1 Introduction and rationale.....	84
4.1.1 PPK20 expression pattern study.....	84
4.1.2 Proteins that may interact with PPK20.....	87
4.2 Results and discussion.....	87
4.2.1 Localization of PPK20 in the larval PG using various Gal4 drivers.....	87
4.2.2 Localization of PPK20 in various larval tissues using <i>actin-Gal4</i> driver.....	90
4.2.3 Immunoprecipitation and Western blot analysis of PPK20 expression.....	95
4.2.4 Mass spectrometry analysis.....	97
4.2.5 Predicted PPK20 functional network.....	97
4.2.6 RNAseq result.....	99
4.3 Discussion.....	100

4.4 Tables.....	101
Chapter 5. PPK20 may be involved in larval tracheal liquid clearance.....	103
5.1 Introduction and rationale.....	103
5.2 Results and discussion.....	104
5.2.1 Tracheal necrosis in <i>PG>ppk20-RNAi</i> and <i>ppk20^{KO}</i> animals.....	104
5.2.2 Expression of <i>ppk20</i> in larval trachea.....	107
5.2.3 Loss-of- <i>ppk20</i> animals had less extensive tracheal branching.....	107
5.3 Discussion.....	108
Chapter 6. Future directions and Conclusion.....	109
6.1 Future directions.....	109
6.1.1 PPK20 mediates cellular iron import.....	109
6.1.2 PPK20 functional network.....	112
6.1.3 PPK20 function in the tracheal system.....	114
6.1.4 The putative sodium channel function of PPK20.....	116
6.2 The summary of the study.....	117
Literature cited.....	119

List of Figures

Figure 1-1. Iron absorption and metabolism in humans.....	5
Figure 1-2. Mammalian intracellular iron regulation via Iron Regulatory Protein 1 (IRP1)/ Iron-Responsive Element (IRE)	7
Figure 1-3. Ecdysteroid biosynthesis pathway in the prothoracic gland (PG)	9
Figure 1-4. The heme synthesis pathway.....	12
Figure 1-5. The transmembrane protein structure of a generic mammalian epithelial sodium channel (ENaC) protein.....	16
Figure 1-6. Summary of iron import in mammals and <i>Drosophila</i>	19
Figure 2-1. Western blot gel transfer stack.....	30
Figure 3-1. The constructs of the two <i>ppk20</i> mutant lines.....	53
Figure 3-2. The PG phenotypes in different loss-of- <i>ppk20</i> and wild-type animals.....	54
Figure 3-3. The survival rate study of the loss-of- <i>ppk20</i> animals.....	57
Figure 3-4. Food supplement rescue experiment of <i>ppk20</i> -RNAi animals (heme synthesis pathway).....	64
Figure 3-5. The survival rate and the PG phenotype of <i>ppk20</i> ^{KO} animals in different supplemented foods.....	65
Figure 3-6. Food supplement rescue experiment of <i>ppk20</i> -RNAi animals (ecdysone synthesis pathway).....	66
Figure 3-7. The transcript level of ALAS was significantly upregulated by knocking down or knocking out <i>ppk20</i>	68
Figure 3-8. Larval gut ferric iron staining.....	72

Figure 3-9. <i>hTfR</i> cDNA could partially rescue <i>ppk20</i> RNAi animals.....	77
Figure 3-10. Larval ferritin dietary feeding, injection and overexpression in <i>ppk20^{KO}</i> and <i>Fer1HCH⁰⁰⁴⁵¹</i> animals.....	78
Figure 4-1. ModENCODE predicted temporal expression data of <i>ppk20</i>	86
Figure 4-2. Localization of PPK20 in larval PG.....	89
Figure 4-3. Localization of PPK20 in various larval tissues using the <i>actin-Gal4</i> driver....	93
Figure 4-4. Validation of <i>ppk20</i> expression induced by the <i>tubulin-Gal4</i> driver using Western blot analysis.....	96
Figure 4-5. PPK20 protein interaction network based on the prediction of String.....	98
Figure 5-1. Loss of PPK20 causes larval trachea necrosis phenotype.....	106
Figure 6-1. The overall summary of PPK20 might mediate Tsf, NTBI and ferritin import.....	118

List of Tables

Table 2-1. The concentration of various supplements in Nutrifly food.....	37
Table 2-2. The antibodies used in this study.....	38
Table 2-3. The recipe for 2x buffer used in immunoprecipitation (IP).....	39
Table 2-4. The recipe for 1x lysis buffer used in immunoprecipitation (IP)	40
Table 2-5. The composition of wash buffer 1 used in immunoprecipitation (IP).....	41
Table 2-6. The composition of wash buffer 2 used in immunoprecipitation (IP).....	42
Table 2-7. The composition of SDS-PAGE separating gel using 40% acrylamide.....	43
Table 2-8. The composition of SDS-PAGE stacking gel using 40% acrylamide.....	44
Table 2-9. The SDS-PAGE gel acrylamide percentage in response to the protein size.....	45
Table 2-10. List of <i>Drosophila</i> stocks used in this study.....	46
Table 3-1. Validation of PG-specific RNAi phenotypes of all 31 <i>ppk</i> genes.....	81
Table 4-1. The overexpression constructs of <i>ppk20</i> and their properties.....	101
Table 4-2. Genes identified in RNAseq.....	102

LIST OF ABBREVIATIONS

μL: microliter

μM: micromolar

20E: 20-hydroxyecdysone

7dC: 7-dehydro-cholesterol

AGBE: 1,4-Alpha-Glucan Branching Enzyme

ALA: aminolevulinic acid

ALAD: aminolevulinate dehydratase

ALAS: aminolevulinic acid synthase

AP: ammonium persulfate

ASIC: acid sensing ion channel

BDSC: Bloomington *Drosophila* stock center

BPS: bathophenanthrolinedisulfonic acid disodium salt trihydrate

BRGC: brain ring gland complex

BSA: bovine serum albumin

CA: corpora allata

CC: corpora cardiaca

cDNA: complementary DNA

cm: centimeter

CNS: central nervous system

CO-IP: co-immunoprecipitation

COPRO'GEN III: coproporphyrinogen III

CPO/CPOX: coproporphyrinogen oxidase

CRISPR: clustered regularly interspaced short palindromic repeats

CYP: cytochrome P450

DAPI: 4', 6-diamidino-2-phenylindole

ddH₂O: double-distilled water

DEG/ENaC: degenerin/epithelial sodium channel

DMT1: divalent metal transporter 1

E. coli: Escherichia coli

ECL: enhanced chemiluminescence

ER: endoplasmic reticulum

FAC: ferric ammonium (III) citrate

Fe²⁺: ferrous iron

Fe³⁺: ferric iron

FECH: ferrochelatase

Fer1HCH: ferritin 1 heavy chain homolog

Fer2LCH: ferritin 2 light chain homolog

Fe-S: iron-sulfur

FRT: flippase recombinase target

g: gram

GFP: green fluorescent protein

HA: hemagglutinin

HMB: hydroxymethylbilane

hr: hour

ID: iron deficiency

IDA: iron deficiency anemia

IF: immunofluorescence

IRE: iron-responsive element

IRP: iron-regulatory protein

KD: knock down

KO: knock out

L: liter

L1: first instar

L2: second instar

L3: third instar

LB: lysogeny broth

Lsp1: larval serum protein one

M: molar

mA: milliamp

MCO: multicopper oxidase

mg: milligram

min: minute

mL: milliliter

mm: millimeter

mRNA: messenger ribonucleic acid

MS: mass spectrometry

nemy: no extended memory

ng: nanogram

NTBI: non-transferrin-bound iron

Osi: Osiris

PBG: porphobilinogen

PBGD: porphobilinogen deaminase

PBS: phosphate buffered saline

PBST/PBT: phosphate buffered saline + triton-X

PBTB: phosphate buffered saline + triton-X + blocking reagents

pg: picogram

phm: phantom

PL: proximity labeling

pM: picomolar

PNS: peripheral nervous systems

PPI: protein-protein interaction

PPIX: protoporphyrin IX

PPK: pickpocket

PPO/PPOX: protoporphyrinogen oxidase

psa: puromycin-sensitive aminopeptidase

PVDF: polyvinylidene difluoride

PY: Pro-Pro-x-Ty

qPCR: quantitative polymerase chain reaction

RG: ring gland

RNA: ribonucleic acid

RNAi: RNA interference

RNAseq: RNA sequencing

rpm: revolutions per minute

RT: room temperature

SDS-PAGE: sodium dodecyl sulfate–polyacrylamide gel electrophoresis

sec: second

SG: salivary gland

TBS: tris-buffered saline

TfR: transferrin receptor

Tsf: transferrin

Tub: tubulin

TurboID: turboID-mediated biotinylation

UAS: upstream activation sequence

URO3: uroporphyrinogen III

URO3S: uroporphyrinogen III synthase

UROD: uroporphyrinogen decarboxylase

UTR: untranslated region

V: volt

VDRC: Vienna *Drosophila* research center

WB: Western blot

WT: wild-type

Chapter 1. Introduction

1.1 The significance of iron

Iron is essential for the survival of nearly all living organisms on the planet because it is involved in many critical biological processes such as DNA metabolism [1-3], oxidation/reduction reactions and oxygen transport [4-7]. An average human body stores 2-3 grams of iron as a trace element [8, 9]. Iron primarily exists in complex forms, namely, heme-binding proteins (hemoprotein), which harbor heme moieties (*e.g.*, hemoglobin and myoglobin) and heme enzymes (peroxidases and cytochrome P450 enzymes), and non-heme molecules (ferritin and transferrin) [10]. Globin proteins combine with heme to form hemoglobin and myoglobin. Hemoglobin is localized in erythrocytes and is critical for oxygen transport, and myoglobin can be found in cardiac and skeletal muscle tissues functioning in oxygen supply [11-13]. In comparison, heme enzymes can catalyze both reductive and oxidative reactions [14, 15]. Non-heme iron-containing compounds, such as ferritin and transferrin, mainly function in intracellular iron storage and extracellular iron trafficking, respectively [16-19]. Moreover, iron can also be found in the form of iron-sulfur (Fe-S) clusters that commonly exist in proteins participating in oxidation-reduction reactions and catalysis [20, 21].

Although iron is essential for organismal survival, it can also be a double-edged sword, where too much or too little can lead to different problems [22]. For example, iron can cause oxidative damage because of its involvement in redox reactions. Consequently, an inappropriately high amount of iron is cytotoxic, which might cause organ injury [23-25]. Therefore, it is vital to maintain a proper iron balance [26, 27].

Iron deficiency (ID) and iron deficiency anemia (IDA) cause one of the most prevalent nutrient deficiencies, leading to serious global health concerns [28-30]. Approximately two billion people are affected by ID and IDA worldwide [31, 32]. ID may develop into IDA, the most prevalent form of anemia characterized by the loss of iron storage. Lack of iron can lead to reduced

activity of iron-containing enzymes and lowered erythrocyte hemoglobin levels. The symptoms of IDA include fatigue, weakness and pale skin, and some cases are asymptomatic [33-35].

1.2 Iron storage and import via iron-bound proteins

Two vital non-heme iron-containing proteins, ferritin and transferrin (Tsf), play separate roles in iron storage and systemic iron trafficking [10].

In both humans and *Drosophila*, intracellular iron can be stored in ferritin nanocages to avoid cytotoxicity and be released when needed [16, 36-38]. Ferritin consists of 24 subunits made of ferritin 1 heavy chain homolog (Fer1HCH) and ferritin 2 light chain homolog (Fer2LCH) in a 1:1 ratio. Up to 4,500 iron ions (Fe^{3+}) can be stored in each ferritin protein cage [39, 40]. Most mammalian ferritin resides in the cytoplasm, while some are found extracellularly (123 ng/mL in human males, 56 ng/mL in females) [41]. The extracellular ferritin is known as human serum ferritin, the function of which is not well-studied. Some research showed that the serum ferritin may be secreted through a nonclassical secretory pathway and thus may play a role in systemic iron delivery [42, 43]. In *Drosophila*, most ferritin is exocytosed from cells and, thus, enriched in the hemolymph (insect blood). It remains unclear whether circulating ferritin can be imported into fly cells and thus function as a systemic iron carrier [44]. Therefore, *Drosophila* ferritin might function in cellular iron detoxification and systemic iron transport [45, 46].

Another essential iron-containing protein, Tsf, is a glycoprotein and is considered the primary form of the human systemic iron carrier supplying cells with iron [19, 47]. Most mammalian Tsf protein originates from the liver [48]. Almost all circulating iron is bound to Tsf in the plasma. Iron is loaded onto Tsf from the iron absorption sites in the intestine and transported to the target sites to be utilized. These target sites include the intestine, liver, spleen, and bone marrow, where hemoproteins can be produced [36, 49]. In the human cells, Tsf is endocytosed through cell-surface transferrin receptor (TfR), during which clathrin is recruited as a co-protein to form the endocytotic vesicles [50-52]. There are two types of human TfRs, transferrin receptor 1 (TfR1) and transferrin receptor 2 (TfR2), and they are 45% identical in their extracellular domain [53, 54]. The distribution of TfR1 is less limited than TfR2, as TfR2 is mainly located in tissues that are involved in iron metabolism, *i.e.*, the liver tissue [55-57]. This study mainly focuses on

TfR1; therefore, TfR1 will be referred to as TfR hereafter, unless stated otherwise. Currently, no *Drosophila TfR* ortholog or functional equivalent has been identified. However, there are three *Drosophila Tsf* genes, of which transferrin 1 (Tsf1) is likely the main transport vessel for serum iron [45]. Thus, it is still unclear whether or not the Tsf-TfR pathway is the primary *Drosophila* cellular iron transport mechanism and if the TfR-mediated Tsf endocytosis is conserved in flies.

1.3 Comparison of human and *Drosophila* iron metabolism

Compared to the relatively well-established human iron homeostasis model, many aspects of *Drosophila* iron homeostasis remain undetermined [58] (Figure 1-1). In humans, the primary iron uptake site is the intestine, where non-heme dietary iron is imported into the enterocytes via divalent metal transporter 1 (DMT1) [59, 60]. In *Drosophila*, the *DMT1* ortholog is called *Malvolio* [61, 62], which is thought to play a similar role in *Drosophila* iron uptake. The membrane ferric reductase of enterocytes, duodenal cytochrome b (*Dcytb*), converts Fe^{3+} into Fe^{2+} before DMT1 can import the iron into the enterocytes [63, 64]. In *Drosophila*, *CG1275* and *no extended memory (nemy)* (CG8776) genes are the orthologs of human *Dcytb* [65]. The function of *CG1275* remains unknown, while *nemy* has a role in learning and memory [66-68].

The iron uptake site for *Drosophila* is between the middle and posterior region of the intestine, and iron accumulates at the anterior midgut when enough iron is present in the food [69, 70]. In human enterocytes, absorbed iron is stored in ferritin or becomes part of the labile iron pool. When iron is needed at target sites, such as the liver and bone marrow, the stored iron can be transported across the basolateral membrane of the enterocyte by an iron export protein, ferroportin 1 (FPN1), into the blood [71-73]. There is no identified fly ortholog of *FPN1*. Hephaestin is the human transmembrane multi-copper oxidase (MCO) that converts Fe^{2+} into Fe^{3+} . Once converted, Fe^{3+} is picked up by serum Tsf [74, 75]. In *Drosophila*, there are four paralogous *MCO* genes, *MCO1-4* [76], in which *MCO3* is the most likely fly candidate to be a functional equivalent of human hephaestin due to its documented function in iron export [77, 78]. In addition, *MCO3* showed *in vitro* ferroxidase activity in some studies [62, 79]. When there is enough iron in the human blood, the expression of FPN1 is downregulated by the iron-homeostasis master regulator

hormone hepcidin, which is mainly secreted by the liver [80, 81]. Consequently, the downregulation of FPN1 will reduce iron export from the enterocytes to the blood [6, 82].

Although almost all circulating plasma iron is bound to Tsf in the blood [36, 83], there is a group of iron that is not bound to Tsf or other iron-containing molecules like heme, hemosiderin and ferritin. This non-protein-bound iron (*i.e.*, free iron in plasma) is known as the non-transferrin-bound iron (NTBI) [84]. NTBI is considered labile and potentially toxic due to its ability to form reactive oxygen species (ROS), which damages cellular organelles and interrupts normal cellular processes [85, 86]. Circulating NTBI in human plasma can be taken up by cells in the form of Fe-citrate. However, the NTBI cellular uptake mechanism remains elusive [87, 88].

In short, compared to the known human iron import pathway (Tsf-TfR endocytosis), the mechanisms by which iron enters cells in *Drosophila* remain unclear. However, the fly genome encodes orthologs for Tsf and ferritin, which are both candidates for acting as systemic iron carriers. Corresponding receptors for Tsf and ferritin, if they exist, are unknown. Additionally, in *Drosophila*, NTBI could be a minor source of cellular iron, independent from potential major iron sources like Tsf and ferritin.

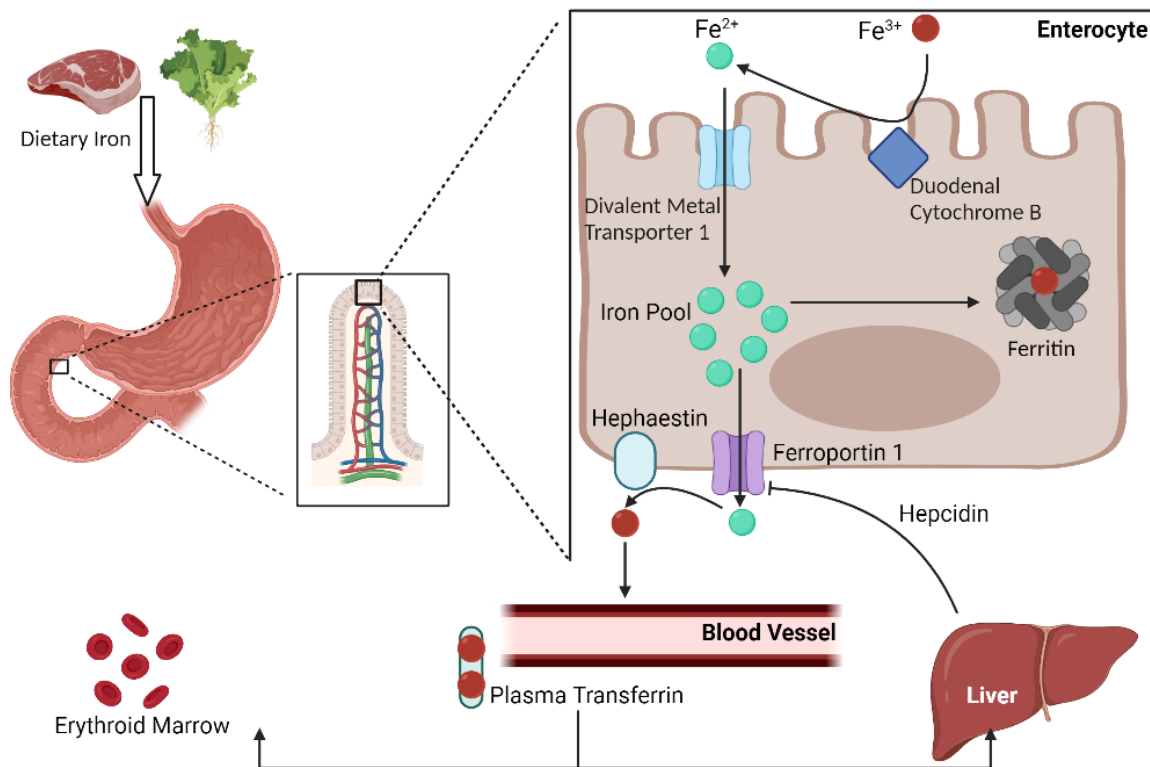


Figure 1-1. Iron absorption and metabolism in humans.

The intestinal enterocytes are the primary iron uptake site in humans, where non-heme dietary iron can be imported via DMT1. Before the iron is imported into the enterocytes by DMT1, the membrane ferric reductase of enterocytes, Dcytb, needs to convert Fe³⁺ into Fe²⁺. Intracellular iron can be stored in ferritin, and it can be transported across the basolateral membrane of the enterocyte and into the blood by an iron export protein, FPN1. The human transmembrane copper-dependent ferroxidase, hephaestin, converts Fe²⁺ into Fe³⁺ before the iron is loaded onto Tsf. Iron-bound Tsf travels in the blood vessels to deliver iron to the target sites, such as the liver and bone marrow. When iron levels in the body are sufficient, the expression of FPN1 is downregulated by liver-derived hepcidin, a master regulatory hormone controlling systemic iron-homeostasis. Thus, FPN1 downregulation results in a reduction in iron export from the intestine. This figure is adapted and modified from [22, 89].

1.4 Intracellular iron regulation

In mammals, cellular iron metabolism is mainly regulated through the binding of the iron regulatory proteins (IRP1 and IRP2) to the iron-responsive elements (IREs). The IRP/IRE system regulates iron homeostasis by controlling the expression of different genes post-transcriptionally in response to different cellular iron conditions [90, 91].

IRP1 is a bifunctional protein that can reversibly bind to Fe-S clusters [92]. Under normal and abundant iron conditions, holo IRP1 harbors a Fe-S cluster (4Fe-4S) and functions only as a cytosolic aconitase, which interconverts citrate and isocitrate. At the same time, IRP2 undergoes degradation mediated by the proteasome [93, 94]. Hence, when cellular iron levels are sufficient, IRPs are not bound to IREs. Consequently, mRNAs that contain IREs in the 3'-UTR (untranslated region) are degraded, and mRNAs that contain IREs in the 5'-UTR will be translated due to the lack of IRP1 binding. As a result, the 3'-UTR TfR1 mRNA degrades since there is no need for iron import, and 5'-UTR ferritin mRNA will be translated to facilitate the need for increased iron storage [95].

When iron levels are low, IRP1 loses the Fe-S clusters and turns into the apo form, and IRP2 does not undergo degradation. As such, IRP1 and IRP2 bind to the 5'-IRE and repress mRNA translation only when cellular iron levels are below a critical threshold. For example, ferritin cannot be made when the mRNAs of Fer1HCH and Fer2LCH are not translated, resulting in less cellular iron storage. In opposition, IRP1/IRP2 binding to the 3'-IRE will stabilize the translation of TfR1 and DMT1 mRNAs, which favours iron import [95-97] (Figure 1-2).

In *Drosophila*, there are two *IRP1* orthologs, *IRP-1A* and *IRP-1B*, while *IRP2* is absent in this species [98]. Evidence suggested that IRP-1A and IRP-1B both have aconitase activity, while only IRP-1A can bind to IRE [99]. The mechanism of how IRP-1A might regulate intracellular iron needs to be elucidated as it might be the functional equivalent to human IRP1.

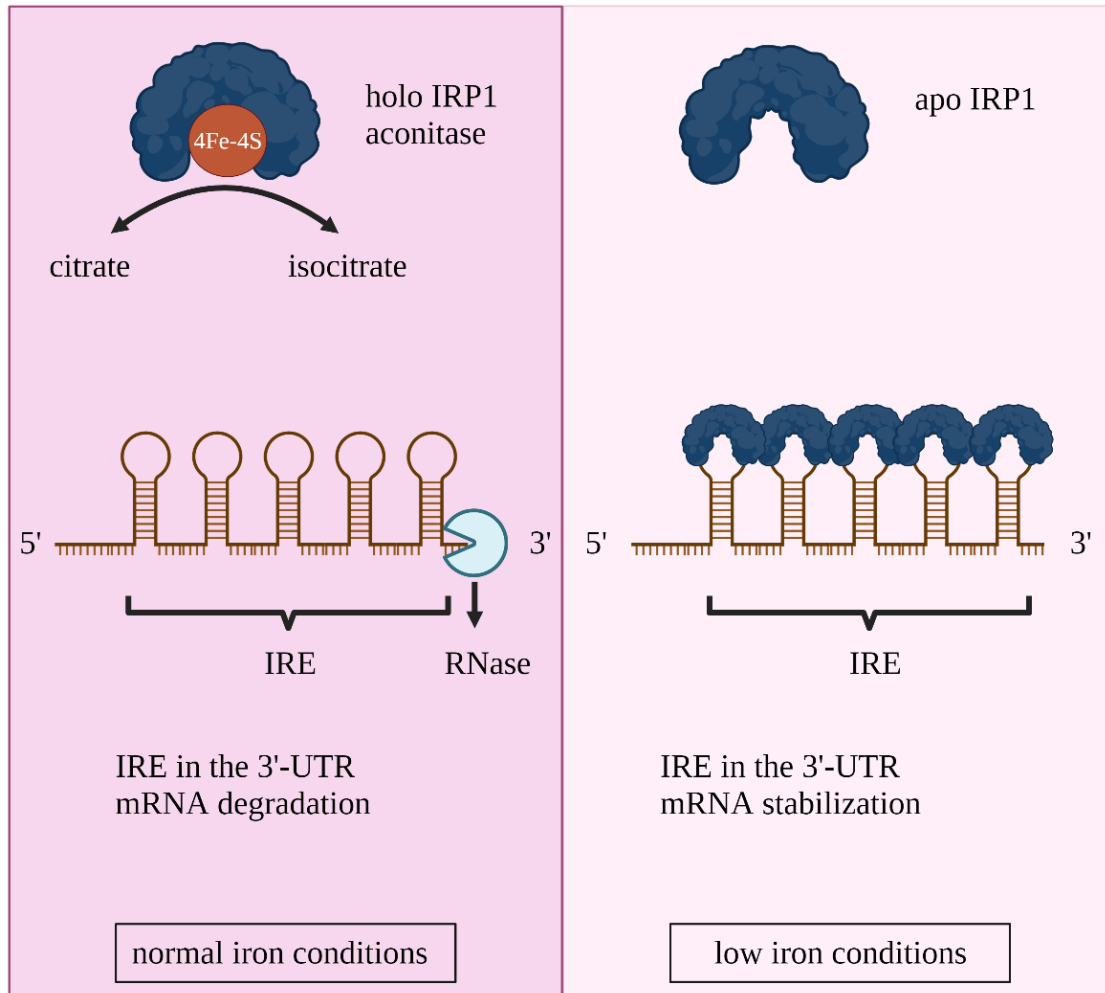


Figure 1-2. Mammalian intracellular iron regulation via Iron Regulatory Protein 1 (IRP1)/Iron-Responsive Element (IRE).

Intracellular iron metabolism is mainly regulated via the binding of IRP1 and IRP2 to IREs. Under normal/abundant iron conditions, the holo-IRP1 harbors a 4Fe-4S cluster and functions as a cytosolic aconitase, which can interconvert citrate and isocitrate. Whereas IRP2 undergoes degradation mediated by the proteasome. In this case, no IRPs bind to IRE. Consequently, mRNAs that contain IREs in the 3'-UTR will be degraded, and mRNAs that harbor IREs in the 5'-UTR will be translated due to the lack of IRP1 binding. Under low iron conditions, IRP1 loses the Fe-S clusters and assumes the apo form. IRP1/IRP2 can now bind to 5'-IRE and repress mRNA translation, in which ferritin production is reduced to lower the cellular iron storage. In contrast, the binding of IRP1/IRP2 to 3'-IRE will stabilize the translation of TfR1 and DMT1 mRNAs, which favours iron importing.

1.5 Ecdysteroid biosynthesis in the prothoracic gland

The model organism used in this study was *Drosophila melanogaster*. Thus, it is crucial to understand this organism's genetics, morphology, and physiology with respect to iron-dependent processes, heme and ecdysteroid synthesis, in which ecdysteroid production requires heme as a cofactor for some of its enzymes function. The survival rate of the flies was observed as an essential phenotype in this thesis, of which steroid hormones tightly regulate the fly life cycle [100, 101].

Derived from cholesterol, steroid hormones are lipophilic hormones that play critical roles in physiological and biological processes in mammals, plants, and insects, *e.g.*, carbohydrate regulation, mineral balance, reproductive functions, and inflammatory responses [102, 103].

The ring gland (RG) is a critical endocrine organ of *Drosophila* [104, 105]. The larval RG consists of three different endocrine glands: the corpora cardiaca (CC), the corpora allata (CA), and the prothoracic gland (PG). The CA and CC play roles in juvenile and adipokinetic hormone production, respectively [106, 107]. In comparison, the PG is where the fly ecdysteroid, ecdysone, is produced. *Drosophila* ecdysone regulates all major developmental transitions [108] (Figure 1-3A). These developmental stages include embryo, larva, pupa and adult [101]. In the larval *Drosophila* PG, ecdysone secretion is mediated by calcium signalling via a regulated vesicular trafficking mechanism and simple diffusion [109, 110].

Ecdysteroid production is a multi-step pathway that requires at least eight enzymes. Six out of eight known ecdysteroidogenic enzymes belong to the cytochrome P450 enzyme family (CYPs), and the two other enzymes, Neverland and Shroud, are not members of the CYP family. *Neverland* encodes an oxygenase-like protein (cholesterol 7,8-dehydrogenase) with a Rieske electron carrier domain and harbors a Fe-S cluster [111-113], while *Shroud* encodes a short-chain dehydrogenase/reductase [114, 115] (Figure 1-3B). The six CYPs include Spookier, Cyp6t3, Phantom, Disembodied, Shadow and Shade, and they all require heme as a cofactor. Moreover, after ecdysone is secreted to peripheral tissues, the CYP Shade converts ecdysone to 20 hydroxyecdysone (20E), which is the best-characterized active form of ecdysone. A lack of ecdysone production leads to larval developmental defects, *i.e.*, delay or arrest at certain stages [116, 117].

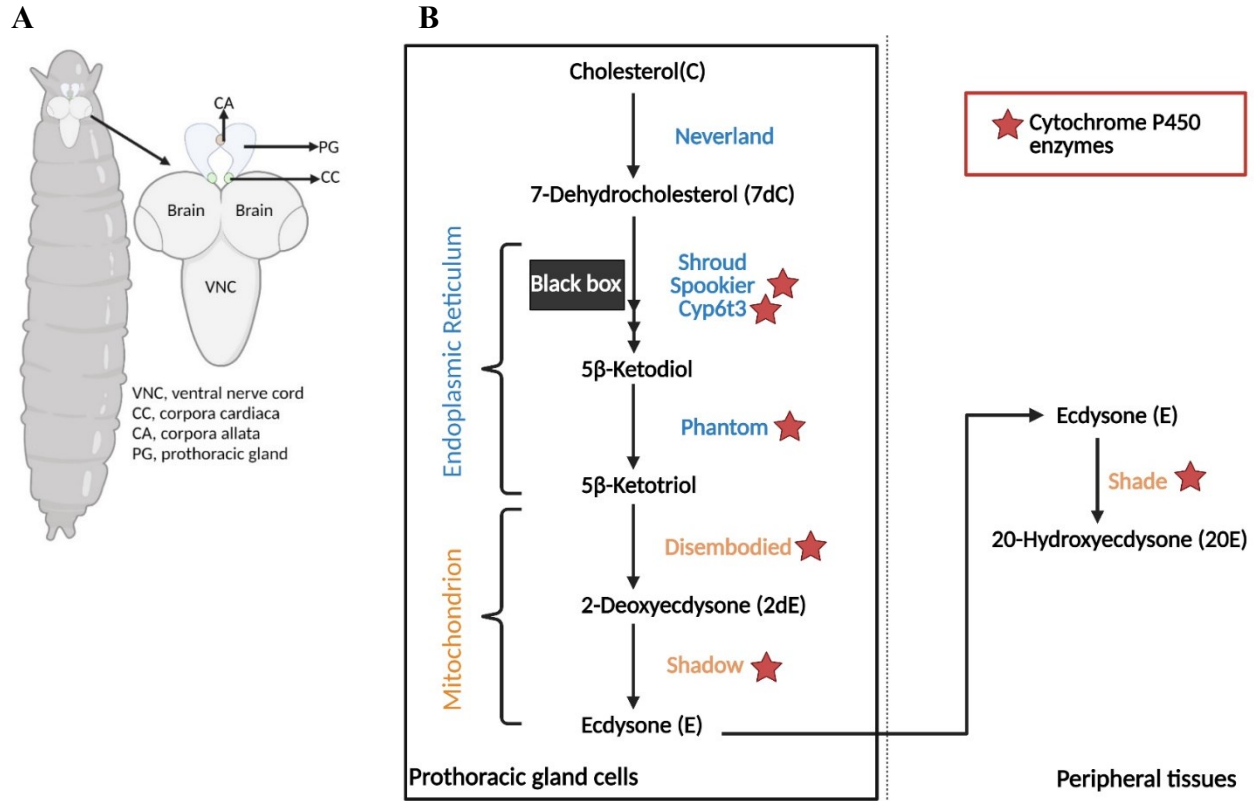


Figure 1-3. Ecdysteroid biosynthesis pathway in the prothoracic gland (PG).

A. The RG is an endocrine organ and consists of three different organs: CC, CA and PG, in the fly larva. The CA and CC function in juvenile and adipokinetic hormone production, respectively, while the PG is the primary site for producing the ecdysteroids. B. The synthesis of ecdysteroids is a pathway involving at least eight enzymes belonging to the cytochrome P450 enzyme family (CYPs), except Neverland and Shroud. These CYPs include Spookier, Cyp6t3, Phantom, Disembodied, Shadow and Shade. All the CYPs require heme as a cofactor. Neverland harbors a Fe-S cluster. 20-hydroxyecdysone is the best-studied active form of ecdysone.

1.6 Heme biosynthesis

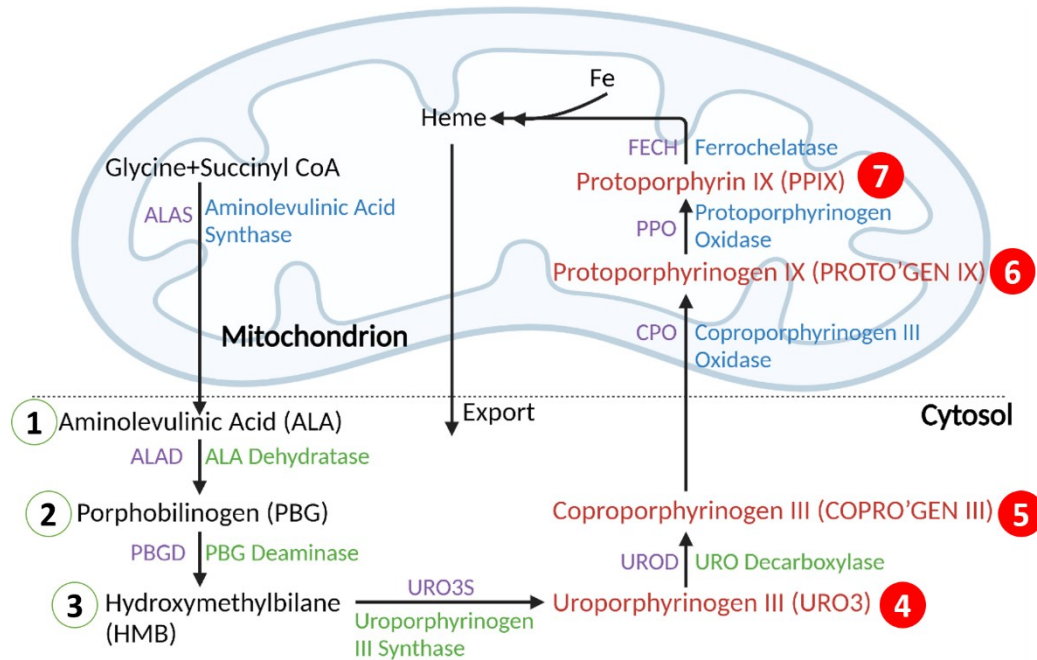
In mammals, most iron (65%) is found in the hemoglobin inside the red blood cells [118]. Hemoglobin is a tetramer made of four heme-containing polypeptide globin chains and plays a vital role in mammalian oxygen transport [119, 120]. As mentioned, heme is the cofactor for CYPs required in the ecdysone production pathway in flies, indicating its necessity in ecdysteroid synthesis; hence, heme is essential for *Drosophila* larval development and survival [121-124]. The heme synthesis pathway (Figure 1-4A) is a multi-enzyme process [125], in which the first and last three steps occur in the mitochondrion, and the remaining steps occur inside the cytoplasm. From steps four to seven, the precursors have a porphyrin ring structure, which autofluoresces red when exposed to UV light [126, 127]. In the last step, protoporphyrin IX (PPIX exhibits red autofluorescence) incorporates Fe^{2+} to form heme (a colourless compound) [128, 129] (Figure 1-4B). Thus, when heme is synthesized under normal iron conditions, red fluorescence is not observed. Likewise, no red autofluorescence is observed in wild-type fly larvae. If mitochondrial iron levels are insufficient, PPIX may accumulate and result in red autofluorescence in the PG, which requires a high level of heme production to support ecdysone synthesis [130].

On the other hand, when the heme synthesis is disrupted specifically by affecting the function of certain biosynthetic enzymes involved in the process, the accumulation of other autofluorescent precursors will occur. These enzymes include uroporphyrinogen decarboxylase (UROD), coproporphyrinogen oxidase (CPO or CPOX), protoporphyrinogen oxidase (PPO or PPOX), and ferrochelatase (FECH) [131]. As a result, the PG tissue will autofluoresce red when exposed to UV light [132].

In humans, mutations of heme biosynthetic genes (nine enzymes and eight steps) can cause a group of disorders collectively known as porphyria [133], which is characterized by excessive buildup of porphyrins and their precursors depending on the type of porphyria. Various porphyria subtypes correspond to the disruption of different steps in the heme biosynthesis pathway [134]. For example, disruption of aminolevulinatase (ALAD) and FECH will lead to ALAD porphyria and erythropoietic protoporphyria [135, 136]. Nine different disorders have been described, and they vary in severity. The symptoms of porphyria include red deposits on the skin, teeth, and other tissues due to the release of heme precursors from bursting cells, and anemic phenotypes caused by low hemoglobin production [136, 137]. According to the National Institutes

of Health (NIH), the estimated porphyria prevalence is between 1/500 to 1/50,000 people worldwide ([https://ghr.nlm.nih.gov/condition/porphyria# definition](https://ghr.nlm.nih.gov/condition/porphyria#definition)). Porphyria cannot be cured, but certain types are more manageable than others [138]. Thus, it is crucial for us to understand the mechanisms and the different causes of iron disorders so that better treatments can be found. Therefore, studying fly heme synthesis and PG phenotype may help further our understanding.

A



B

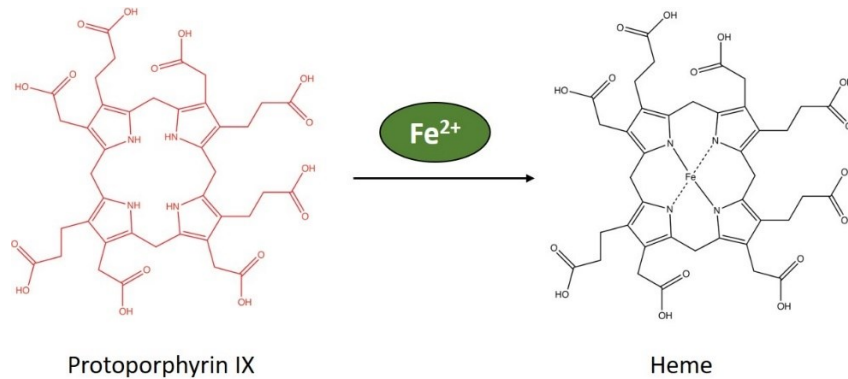


Figure 1-4. The heme synthesis pathway.

A. There are eight steps required for heme synthesis. Part of the process occurs in the cytoplasm, while the first step and the last three steps occur inside the mitochondria. The initial substrates for heme synthesis are succinyl-CoA and glycine. Precursors in red text can autofluoresce under UV light. At the final step, PPIX is converted to heme by FECH when iron is present (modified from [131]). B. In the last step of the heme production pathway, PPIX exhibits red autofluorescence until it incorporates ferrous iron (Fe^{2+}) to form heme, a colourless compound.

1.7 *ppk20* was found in a two-step screen

The remarkable porphyria-like PG phenotype is utilized as a tool in our lab to study the poorly characterized fly iron and heme homeostasis model [96, 132]. In the first round of the screen, our lab collaborated with two other labs and carried out a genome-wide PG-specific RNA interference (RNAi) screen of ~12,500 fly lines [101, 132]. The original intent of the primary screen was to identify genes with critical roles in steroid hormone production. The initial screen identified approximately 1,906 lines with developmental defects, including L1 arrest, L2 arrest pupariation of L2 larvae, L3 arrest, developmental delays (delay), and pupal lethality [101, 132].

The secondary screen was based on ~800 lines that showed lethality in third instar larvae. This 2nd screen was conducted in our lab, where we searched for red autofluorescent RGs as a possible indicator for a disturbance of heme biosynthesis. The second stage screen identified 13 RNAi lines that showed enlargement of the PG (but no red autofluorescence) and 21 RNAi lines that exhibited enlarged PGs together with a red autofluorescence signal. Of these 34 hits, four lines harbored RNAi constructs targeting the heme biosynthesis pathway, indicating that the screen had worked successfully. The *pickpocket 20* (*ppk20*) gene was one of the 21 hits.

1.8 *ppk20* is a member of the DEG/ENaC family

ppk20 gene was one of the 21 genes that showed enlarged autofluorescing PGs and larval developmental arrest when the gene was knocked down in the PG by RNAi. PPK20 is a member of the DEG/ENaC (Degenerin/Epithelial Na⁺ Channel) superfamily, which is mainly known to act as non-voltage-gated amiloride-sensitive sodium channels [139, 140]. In humans, the DEG/ENaC paralogs are encoded by nine genes that can be categorized into two families based on homology: i) four genes encode ENaC homologs that belong to the non-voltage gated sodium channel family; ii) the other five genes encode acid-sensing (proton-gated) ion channel (ASIC) family members [141, 142].

ENaCs function in the bulk transport of Na⁺ into high resistance epithelia to maintain salt and water homeostasis, which means ion transport in these epithelial cells is under the tight control; hence, they can be commonly found in the kidney's collecting duct, where around 180 L of body

fluid is processed daily [143, 144]. Consequently, fluid flow (mostly water) accompanies the Na⁺ transport due to osmolarity changes [145-147]. In humans, disruption of ENaC function may result in Liddle syndrome (gain of sodium channel function) and Pseudohypoaldosteronism Type I (PHA) (loss of sodium channel function). The channel hyperactivity may cause hypertension in patients with Liddle syndrome, while reduced sodium channel activity can lead to salt wasting and hypotension in PHA patients [148-150].

Unlike ENaCs, ASICs are H⁺-gated ion channels that rapidly desensitize after activation and remain closed in the resting state. In mammals, the expression of *ASIC* genes generally occurs in the central and peripheral nervous systems. Here, ASICs may function in mechano-sensation, acid-taste, and learning. Due to these functions, ASICs are excellent pharmaceutical targets for studying PNS (*e.g.*, diabetic neuropathy and peripheral pain) and CNS disorders (*e.g.*, stroke, migraine, neurodegenerative and psychiatric diseases) [151, 152]. In short, although the functions of DEG/ENaC channels are not entirely understood, research showed that they have many physiological functions and can respond to extracellular stimuli as ionotropic receptors, meaning they might be ligand-gated channels [142, 153, 154]. Some *ppk* members of the ENaC family are mostly known to function as non-voltage-gated amiloride-sensitive sodium channels; hence, amiloride can be used as an inhibitor [145-147].

The mammalian ENaC protein has a heterotrimeric structure that comprises three homologous glycoprotein subunits: alpha, beta and gamma (α , β , and γ). Each subunit consists of two membrane-spanning domains (M1 and M2). In addition, the intracellular C terminus of each subunit contains a canonical "PY" (Pro-Pro-x-Tyr) motif (Figure 1-5) [155]. The PY motif allows binding to the WW domain of Nedd4-2, an E3 ubiquitin ligase from the HECT family. The WW domain is a modular protein domain that consists of a double tryptophan (W) residue [156, 157]. Once the PY motif is recognized and bound to the WW domain, Nedd4-2 ligates ubiquitin to the ENaC subunit, resulting in the internalization and subsequent degradation of the membrane-bound ENaC in proteasomes or lysosomes. This process is characterized by reduced ENaC activity and cellular sodium import [158, 159]. In *Drosophila*, no classic PY motif is found in any fly PPK proteins, so it remains unknown whether the cellular sodium trafficking is still associated with the Nedd4 pathway [147].

In *Drosophila*, the function of PPK remains mostly elusive compared to human ENaCs. Several PPK proteins have been studied in detail. The expression of *ppk1* and *ppk26* was found in larval multi-dendritic neurons, and the study showed that they could sense mechanical nociceptive stimuli [147]. *ppk4* and *ppk11* are expressed in the tracheal system, and loss of PPK4 and PPK11 function could lead to a significant defect in liquid clearance, indicating their potential role in larval tracheal liquid clearance [160].

Moreover, one study showed that Na⁺ import is required for intracellular iron accumulation in mammalian cells, in which DEG/ENaC is responsible for sodium import. Their study showed that the iron uptake of human airway epithelial cells could be blocked by using Na⁺-free buffer or the addition of a group of sodium channel inhibitors, including furosemide, bumetanide, and ethylisopropyl amiloride [161]. However, the initial idea for this study was to find out why airway epithelial cells are able to take in extracellular iron to prevent the damaging effects. Therefore, the connection between iron import and ENaC function might only occur in mammalian bronchial epithelial cells.

Therefore, the finding of the concurrent flow of iron and sodium in human cells has motivated a hypothesis in flies for this thesis: the loss of DEG/ENaC channel function could cause reduced cellular sodium import, which may lead to a failure in iron import, thus causing larval developmental defects and the red autofluorescence phenotype in the PG (lack of iron in the last step of heme synthesis pathway). There are several potential human homologs of *ppk20*, including ASIC3 and ASIC4, but the functional similarity is undermined between *ppk20* and ASIC3/4. Thus, there is no identified human ortholog to *Drosophila ppk20*. According to DIOPT Ortholog Finder [162], the similarity of protein alignment PPK20 and human ENaC/ASIC is below 40%; hence the overall score is too low. In summary, no publication has focused on characterizing the expression or function of *ppk20*; therefore, whether PPK20 functions in iron import or the tracheal system is unclear.

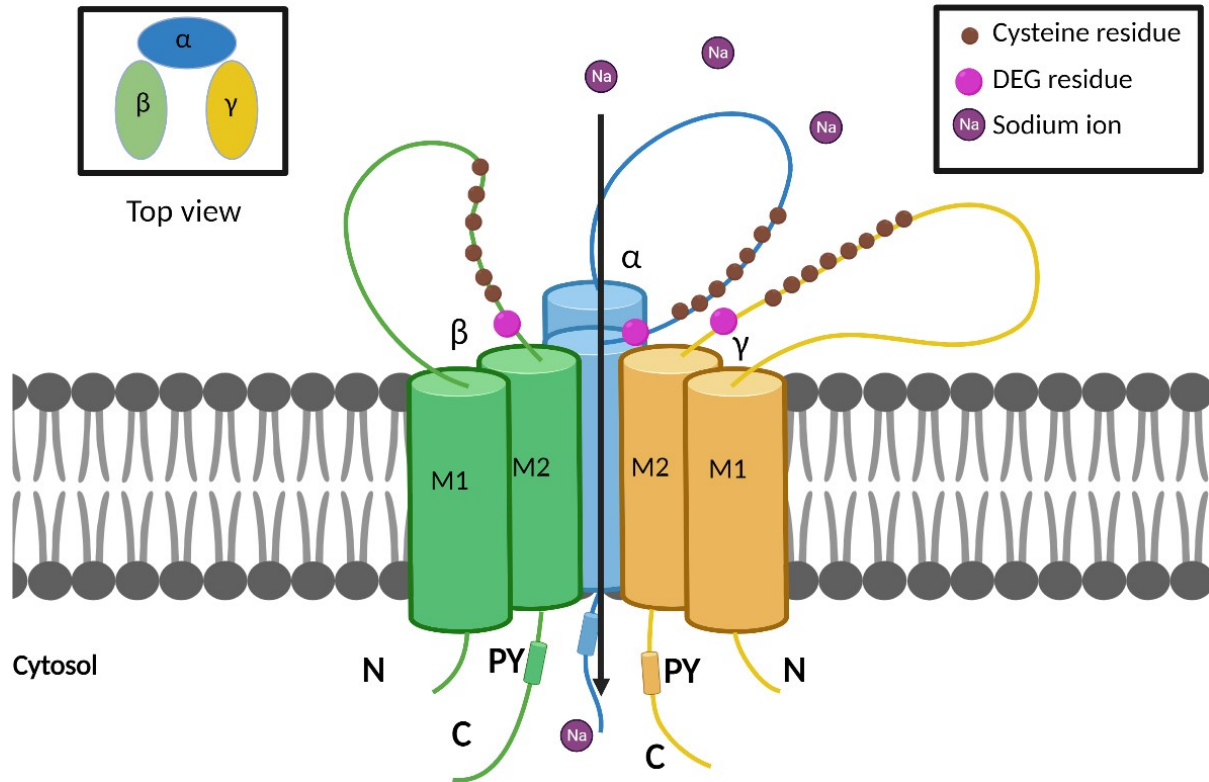


Figure 1-5. The transmembrane protein structure of a generic mammalian epithelial sodium channel (ENaC) protein.

The most common ENaC structure comprises three homologous glycoprotein subunits: alpha, beta, and gamma (α , β , and γ). Each subunit consists of two membrane-spanning domains (M1 and M2) with an intracellular N terminus and a canonical "PY" (Pro-Pro-x-Tyr) motif-containing C terminus [155]. The extracellular cysteine loop is thought to function in sodium trafficking. In *C. elegans*, the DEG channels can respond to mechanical stimulation delivery and removal [163]. Evidence showed it might be playing a similar role in humans [151, 164].

1.9 HIF functions in hypoxia

The tracheal functional impairment was a critical trait in the loss of *ppk4* and *ppk11* animals [160], and the tracheal function is closely related to larval oxygen transport and availability.

In mammals, iron bioavailability affects cellular oxygen transport due to its necessity in hemoglobin formation [118]. And iron bioavailability also affects cellular sensitivity to hypoxia, putatively through the hypoxia-inducible factor (HIF) pathway [165]. The lack of oxygen in the environment causes insufficient oxygen supply in supporting cell survival due to its involvement in respiration and other critical processes. When there is a lack of hemoglobin, not enough oxygen can be transported around the body, mimicking the lack of oxygen [120, 166].

HIF is the central transcriptional regulator in hypoxic response in animals, and it has a heterodimeric structure that comprises one of three α subunits (HIF-1 α , HIF-2 α , and HIF-3 α) and a β subunit (HIF- β , which is known as ARNT) [167-169]. The most well-studied HIF-1 α acts as a transcription factor that helps regain oxygen balance in response to chronically low oxygen conditions by inducing erythropoiesis and glycolysis [170]. In *Drosophila*, the HIF pathway is conserved. There are three homologs, the gene *similar* (*sima*), *trachealess* (*trh*) and *single-minded* [171, 172]. The *Drosophila* ARNT-like protein Tango form heterodimers with Sima, Single-minded and Trachealess [173, 174]. Sima belongs to the basic helix-loop-helix (bHLH)/PAS (Per/ARNT/Sim) transcription factor family, and it has close functional homology to human HIF-1 α [175]. The *trh* plays a critical role in tracheal development [176]. Single-minded functions in midline cell specification in *Drosophila* central nervous system [172, 174, 177].

The insect tracheal system is a tubular network that can transport oxygen from the environment to target cells. The tracheal system shares similarities with the human vascular system, *i.e.*, branching morphology and function in oxygen uptake [177, 178].

Under low oxygen levels, adult flies frequently have reduced body and cell size. Although the mechanisms are not well studied, one hypothesis is that the feeding pattern could be affected. Hence, HIF might play an important role in cell growth reduction, which then causes a reduced body size compared to the control animals [179]; thus, the animals might not reach the critical size to complete growth. Although, another study has shown in *Manduca sexta* that the oxygen supply might be independent of the size-dependent mechanisms of moulting and metamorphosis [180].

Therefore, the fine-tuning of how oxygen conditions mediate fly growth is undetermined, and more evidence is needed.

1.10 Summary of iron import in human and *Drosophila*

There are several ways that iron could be imported intracellular in humans and *Drosophila* (Figure 1-6). In humans, the TfR-mediated Tsf endocytosis is the main way cellular iron import [50-52], but in flies, the TfR is not identified yet, however, based on current understanding, there is one fly TfR. Furthermore, the ferritin import mechanism remains unclear in both models [42, 43]; there are several proposed human ferritin receptors, including TfR, mucin domain 2 (Tim2), and SCARA5 [181-183]. The third way is an ongoing project in our lab, and there is a high-affinity iron transport complex comprised of Multicopper oxidase 4 (MCO4) and an unknown protein that works in iron import under low iron conditions in *Drosophila* (data not published). However, in humans, this pathway is not identified yet. Lastly, in terms of the NTBI import, it is not the main way of iron import, and the mechanism is unknown in both humans and flies [87, 88].

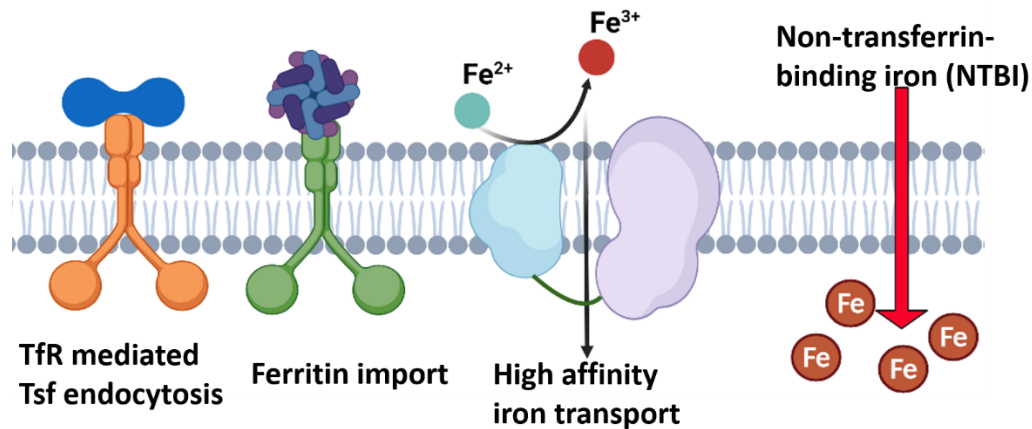


Figure 1-6. Summary of iron import in mammals and *Drosophila*.

The TfR-mediated Tsf endocytosis is the main way in mammalian cellular iron import, but in flies, the TfR is not identified yet. And ferritin import mechanism remains unclear in both models; there are several proposed mammalian ferritin receptors, including TIM2, TfR and SCARA5 (see 3.1.1). The third way is an ongoing project in our lab, and there is a high-affinity iron transport complex comprised of MCO4 and an unknown protein that works in iron import under low iron conditions in *Drosophila*, but this pathway is not identified in mammals yet. The last way is the NTBI import, and it is not the main way of iron import, and the mechanism is unknown to both mammals and flies.

1.11 Current gaps in our understanding and overall hypothesis

This thesis focuses primarily on the role *ppk20* plays in the cellular iron import, which in turn might be closely linked to larval development and tracheal function. The current gap in research is that there is no study focusing on *ppk20* characterization, making this project intriguing and novel.

My overall hypothesis: *ppk20* plays an essential role in cellular iron import on the plasma membrane.

Based on the data, PPK20 might mediate cellular iron import via controlling free iron and Tsf cellular import, possibly through its sodium channel function. PPK20 is also involved in tracheal function, possibly through its sodium channel function, and when PPK20 function is lost, defective iron import might contribute to the loss of tracheal function. On the other hand, tracheal phenotype might be caused by loss of *ppk20* and is independent of lack of cellular import.

Therefore, my plan is to examine the larval PG for developmental phenotypes in loss of *ppk20* animals. Based on the three potential ways by which iron can be imported into *Drosophila* cells, I will examine whether PPK20 mediates iron uptake via NTBI, Tsf or ferritin-based processes.

Chapter 2. Materials and Methods

2.1 Fly stock maintenance and fly development study

2.1.1 Basic fly husbandry

Fly stocks were kept at 18°C for slow growth while the experimental fly lines were reared in a 25°C, 60% relative humidity incubator for faster growth and ready to be used as experimental flies. The tipping cycle for stocks was approximately four weeks to reduce the risk of contamination from fungi and bacteria [184].

2.1.2 Setting up fly crosses and embryo collection

Around 200 3-day-old virgin female flies and 100 5-day-old young male flies were transferred to an embryo collection cage for each cross. The female flies of Gal4 driver lines were often collected to induce gene expression in different tissues depending on different experiments; for example, *phantom-Gal4* (*phm-Gal4*) was used to induce gene expression in the PG [185, 186]. After two days of mating, the embryos were collected on grape juice plates for 1 hr. Consequently, 50 embryos were used for each survival rate quantification experiment (see 2.1.3).

For dissection purposes, the Nutrifly food plates (18 g Nutrifly food powder in 100 mL water and 480 µL propionic acid) were placed directly under the collection cage in order for embryo collection instead of the grape juice plates [184].

2.1.3 Survival rate studies

For quantification studies, three biological crosses were set up for each control or experimental group. Fifty embryos were collected from each of the three biological replicates. The

number of living animals from first, second and third instar larva (L1, L2 and L3), pupa to adult fly were quantified. Then, the survival rate was normalized to the percentage using the formula:

$$\frac{n}{50} \times 100\%$$

n: number of animals in each stage

50 is the number of embryos

For *ppk20^{KO}* animal survival rate quantification, embryos were collected but not quantified until the L2 stage because not all embryos were homozygous *ppk20^{KO}* animals. Therefore, 50 L2 Tubby (Tb) heterozygotes and 50 L2 non-Tb homozygotes were collected for quantification instead of quantifying the numbers from the embryonic stage. The survival rate was normalized to the percentage (formula: $n/50 \times 100\%$).

Depending on the genetic background of the experimental groups, different control groups were used.

For *PG>ppk20* RNAi animals: *w¹¹¹⁸* males crossed with *phm-Gal4* as the control;

For *ppk20^{KO}* animals: Tb heterozygous animals were used as controls.

2.2 Survival rate quantification of animals with delay and arrest phenotypes

The general steps of setting up crosses and collecting embryos follow the same procedure described in 2.1. One extra step was that the L2/L3 moulting stage was used as the standard timing to define if there was a delay in experimental animals compared to control animals (the regular growth pattern) [100]. Larvae in this experiment were kept in a 25°C incubator, and at first, the staging process was conducted every hour to monitor the number changes. The number of L2 larvae that turned into L3 larva was documented every few hours in the first 48 hrs until no L2 larva was turning into L3. Depending on the genetic background of the experimental groups, different control groups were used. It usually takes 48 hr for WT L2 larvae to develop into the L3 stage [187]; with loss-of-*ppk20* animals, there might be a delay (hours may vary) or arrest in L2 stage (no turning into L3 stage).

2.3 Supplemental rescue experiments

In this study, the regular food or food control refers to “Nutrifly food” from the Bloomington *Drosophila* Stock Center. The recipe is described in 2.1, and more information can be found on the INDIANA UNIVERSITY BLOOMINGTON website (<https://bdsc.indiana.edu/information/recipes/bloomfood.html>).

For different fly phenotype rescue experiments, Nutrifly medium was used as the food control, and other chemical and biological supplements were added with a specific concentration as supplemented fly food. The properties and specific concentrations of all different supplements can be found in Table 2-1. All the concentrations were tested and modified by lab members [188].

Many food supplements use ethanol as a solvent, and the concentrations of different supplements can be found in Table 2-1. This procedure using 0.02 g of cholesterol to make food supplements is described below as an example, and all the other supplements follow the same lab protocol as follows:

An amount of 0.02 g of cholesterol powder was added into a tube containing 48 mL of 100% ethanol and vortexed to dissolve. This cholesterol stock was prepared first and stored in the freezer before being used. Next, 18 g Nutrifly food was added into a flask, and then 100 mL of Milli-Q water was added. The mixture was then boiled for 5 min and cooled. After the food was cooled, 480 μ L of propionic acid was added and mixed well. The following step was to add 6 mL cholesterol stock to make 250 μ g/mL the final concentration. To fill a small Petri dish (30 mm x 15 mm), 3 mL of the supplemented Nutrifly food was required, while 5 mL was required to fill a vial.

2.4 Grape juice plate

The grape juice plates were used to collect embryos. To make 250 mL total volume of grape juice, 6 g of bacto agar, and 200 mL of distilled water were added to a flask before autoclaving. Next, 50 mL grape juice was added to the autoclaved mixture, and then 5 mL of 95% ethanol with 0.5 g methylparaben was added. The final product was mixed well and poured into small-sized Petri dishes to solidify before use.

2.5 Larval tissue immunofluorescence (IF)

(1) Sample preparation

For general validation of the porphyria-like phenotype and protein localization, 42-hr L3 larvae were used for tissue/organ collection in order for consistency. This time point was also used for collecting protein samples from larvae, and L2/L3 moulting larvae were staged to synchronize the larvae to the same age. Approximately 30-40 larvae from each experimental or control group were then dissected in cold PBS, and various tissues/organs were collected and fixed in 4% paraformaldehyde (EMS #15710) in PBS for 20 min at room temperature (RT). Next, the samples were washed with 0.3% PBST (PBS containing 0.3% Triton X-100) 3× 10 min.

(2) Immunostaining

Following the sample preparation, the specimen was blocked with the blocking buffer (5% normal serum and 0.3% Triton-X 100 in 1x PBS) for 60 min at RT. Next, the sample was incubated in different primary antibodies. All the information regarding antibodies used in this study can be found in Table 2-2. For example, mouse anti-HA primary antibodies from Abcam (ab18181) with 1:1,000 dilution were incubated at 4°C overnight to identify the protein with an HA tag. The sample was then washed with 0.3% PBST for 3× 10 min. After the wash, the sample was incubated with secondary goat anti-mouse antibodies at RT for 2 hr (ab18181; 1:2,000 dilution; Alexa Fluor Plus 555). 4',6-diamidino-2-phenylindole (DAPI) was added to the samples and incubated for 15-20 min for nuclear staining. The sample was then washed with 0.3% PBST for 3× 10 min and placed onto a glass slide in mounting solution (50% PBST and 50% glycerol). Subsequently, a coverslip was placed on top of the samples, and nail polish was applied to seal the coverslip. The protocol can be referred to Cell Signaling Technology® Immunofluorescence General Protocol, and some modifications were described above (<https://www.cellsignal.com/contents/resources-protocols/Immunofluorescence-general-protocol/if>). After nail polish was solidified, samples could be examined by fluorescent or confocal microscopy.

2.6 Immunoprecipitation (IP)

The protein samples were immunoprecipitated [189] before proceeding with the Western blot (WB) analysis and mass spectrometry (MS). The following describes the detailed steps, and the reagents used are shown in Tables 2-2 to 2-6.

(1) Sample collection

The fly line that carries a tagged version of the target protein (PPK20 with mVenus and 3x Hemagglutinin (HA) tags, see Table 2-10) was used as the experimental group, and *w¹¹¹⁸* was the negative control. Forty-two hr L3 larvae were collected and washed in PBS for 3 × 5 min. The larvae were then placed in a 1.5 mL microfuge tube containing cold PBS with 0.1% Triton X-100 (0.1% PBST). Next, the larvae were fixed in a freshly prepared 0.2% formaldehyde in PBS for 15 min at RT to crosslink macromolecules [190], and the formaldehyde was removed after the fixation. The quench buffer (0.25 M glycine in 0.1% PBST) was added and incubated on a shaker for 5 min to stop the fixation. Next, the quench solution was removed, and the sample was washed in 0.1% PBST by gently inverting the tube five times. Lastly, the samples were flash-frozen using liquid nitrogen and stored at -80°C until enough samples were collected.

Alternatively, the brain ring gland complexes (BRGC) were collected and used as samples instead of whole-body larvae. All the steps described above to process the sample apply to the BRGC preparation. At least 150 larvae were collected for each sample and 1,000 mg of BRGC was collected as a sample. PPK20 is tagged with mVenus and 3xHA tags, and two different types of beads were used to IP these two different protein tags.

(2) Protein IP using anti-GFP affinity gel

Sample preparation

When enough sample was collected, the sample tubes were removed from the -80°C freezer, thawed on ice, and combined if needed. In the meantime, the lysis buffer was used to rinse the Dounce homogenizer. Next, the sample was homogenized by a pestle motor mixer in the pre-

rinsed and prechilled Dounce homogenizer on ice with 1 mL lysis buffer (Tables 2-3 and 2-4). Homogenization was repeated every 15 min for another three times. After the homogenization, the lysate was transferred to a 1.5 mL centrifuge tube and incubated on ice for 15 min to ensure that the sample was thoroughly lysed. Then, the lysate was centrifuged at 16,000 x g for 30 min at 4°C.

Anti-GFP affinity gel preparation

The anti-GFP affinity gel (Chromotek GFP-Trap® Agarose, lot 009172-02-03) was used to immunoprecipitate proteins with a GFP tag. First, 40 µL anti-GFP affinity gel was transferred into the spin-column. A volume of 300 µL lysis buffer was added to the column to wash the gel, and the supernatant was removed after centrifugation. The washing step was repeated another four times. On the sixth time of the washing, the bottom of the spin-column was plugged, 300 µL lysis buffer was then added into the column, and the mixture was stored on ice until needed. Right before the lysate sample was ready, the bottom of the column was unplugged and placed into a centrifuge for a quick spin to get rid of the supernatant.

Protein IP

After the 30-min centrifugation was finished (sample preparation step), the transparent layer of the supernatant was transferred into the spin-column that was just prepared in the anti-GFP affinity gel preparation; when taking the supernatant from the tube, the layer of fat on top should be avoided. Next, the column was incubated with the lysate on a rotating platform for 2 hr at 4°C for IP. The column was centrifuged at 12,000 x g for 10 s to eliminate the flow-through. Then, the column was washed with 300 µL wash buffer 1 (Table 2-5), and centrifuged at 12,000 x g for 10 s to remove the flow-through. The washing step was repeated three times. A volume of 300 µL wash buffer 2 (Table 2-6) was then added to wash the column by centrifugation at 12,000 x g for 10 s to remove the flow-through. The washing step was repeated three times.

Lastly, 30-40 µL loading buffer (2x loading buffer: 4% SDS, 10% 2-mercaptoethanol, 20% glycerol, 0.004% bromophenol blue, and 0.125 M Tris-HCL, pH 6.8) was added into the sample column, and the mixture was boiled at 95-100°C for 5 min before loading. The column was

centrifuged at 12,000 x g for 1 min, in which the flow-through was collected as the final sample before preceding to experiment further, *i.e.*, SDS-PAGE gel running.

(3) Protein IP using IgG magnetic beads

The sample preparation steps were the same as described in the “Protein IP using anti-GFP affinity gel” section.

Preparation of Dynabeads™ magnetic beads

Anti-HA (rabbit mAb #3724) is used as an example in describing the procedure for simplicity. All the information regarding the antibodies is listed in Table 2-2.

The beads (Invitrogen Dynabeads™ protein G, lot 00571508) were first resuspended well by inverting the tube, and then 80 μ L beads solution (for 2 samples) was transferred to a 1.5 mL microfuge tube. Next, the microfuge tube was placed on the magnet stand for about 1 min to separate the beads and the supernatant. The supernatant was then removed by pipetting, the tube on the magnet stand was removed next, and directly proceeding to the next step.

Antibody binding

A volume of 8 μ L of anti-HA antibody was added to 150 μ L of 0.1% PBST (0.1% tween-20) for dilution. The diluted antibody was then incubated with the beads on a rotating platform for 40 min at RT in order for binding. Next, the tube was placed on the magnet stand for 1 min to separate the beads and the supernatant. Then, the supernatant was removed before the tube was removed from the stand. Lastly, the beads-antibody complex was washed with 1 mL of 0.1% PBST by inverting the tube multiple times.

IP of target antigen

The tube was removed from the stand, and 500-1,000 μ L of the protein sample from “(2) sample preparation” section was added to the tube. Note that the input sample can be taken from

the protein sample before it was added to the beads, in which around 50 μL is enough. Next, the protein and beads-antibody complex mixture was incubated on a rotating platform for 2 hr at 4°C. After the incubation, the tube was placed on the magnet stand for 1 min, and the supernatant was transferred to a new microfuge tube to be analyzed later (the flow-through sample). Then, the beads were washed with 1 mL 0.1% PBST 3 times and 1 mL PBS once. Lastly, 50 μL SDS-PAGE loading buffer was added to the sample and boiled for 5 min at 95-100°C.

2.7 Coomassie Brilliant Blue staining

(1) SDS-PAGE gel preparation

The SDS-PAGE gel was prepared freshly prior to running. The separating and stacking gels were made first (Tables 2-7 and 2-8). For the 1.5 mm-glass plates, a 7 mL separating gel solution was used. To smoothen the top of the separating gel and block it from the air during the polymerization process, 1 mL isopropanol was added to the top of the separating gel. It took about 50 min for the separating gel to polymerize at RT.

After the separating gel solidified, the isopropanol was removed. Next, the stacking gel solution was poured onto the separating gel, and a 1.5 mm 10 lane comb was inserted into the stacking gel. It took about 50 min for the stacking gel to set at RT. After the gel was set, the comb was removed. Then, the apparatus was set up before pouring the running buffer (1 L 10x running buffer: 30 g Tris base, 144 g glycine and 10 g SDS) into the tank to meet the required level line. Depending on the sample, different volumes need to be loaded into the wells, *i.e.*, 5 μL IP sample, and others usually range from 40-60 μL . 5 μL of a prestained protein ladder (PageRuler™ Prestained Protein Ladder, 10 to 180 kDa, catalogue number: 26616) was loaded as the standard to monitor the presence of the interested target proteins.

For MS sample preparation, the protein ladder showed a clear separation on the separating gel and moved past the stacking gel for about 1cm before proceeding to the Coomassie staining.

(2) Coomassie staining

After the SDS-PAGE gel was ready, it was removed from the glass and rinsed once in ddH₂O. Then, the gel was stained with a Coomassie stain by microwaving on high power for 40 s to 1 min to boil and incubated for 5-10 min on a rocking platform. The Coomassie stain was then removed, and the gel was rinsed with ddH₂O twice. Next, the destain solution was added to the gel, microwaved on high power for 40 s to 1 min to boil, and incubated for at least 10 min. The incubation time varied, and the sufficiently destained gel should have visible protein bands. Then the destained gel was sent for analysis at Alberta Proteomics and Mass Spectrometry Facility (4096 Katz Group Centre For Pharmacy and Health Research Building (KGR)).

2.8 Western blot analysis

Western blots were performed according to the Bio-Rad protocol with some modifications. The recipe for different reagents can be found in Tables 2-7, and 2-8 [191], however, the gel percentage was altered, depending on the size of the protein (Table 2-9):

The first step was to make the SDS-PAGE gels (Bio-Rad, Mini-PROTEAN® System): separating and stacking gels as described in the “Coomassie Brilliant Blue staining” section, and electrophoresis conditions for WB gels were 2 hrs at 100 v.

Transfer the protein from the SDS-PAGE gel to the PVDF membrane

Next, the proteins were transferred from the gel onto the PVDF membrane (0.2 µm). The PVDF membrane was incubated in methanol for 15 s to balance, and then it was rinsed with ddH₂O. Next, the membrane was put into the prechilled transfer buffer (10x Tris-glycine: Tris base 30.3 g, glycine 144 g, add ddH₂O to 1 L; 1L 1x transfer buffer: 10x Tris-glycine 100 mL, methanol 200 mL, ddH₂O 700 mL). Then, the transfer stack was prepared in a specific order (Figure 2-1, Bio-Rad, Mini Trans-Blot® Cell) and followed by setting up the protein transferring apparatus (insert a cooling unit into the tank). The transfer process takes around 1.5 hr at 100 v (or 200 mA).

Antibody incubation

After protein transfer, the membrane was first blocked in the blocking buffer (TBS with 0.1% Tween-20 and 5% (w/v) skim milk powder; making 1 L 10x TBS, 80 g NaCl, 2 g KCl and 23 g Tris base) at RT for 1 hr or overnight at 4°C. After blocking, the membrane was incubated with primary antibody (approximately 1:1,000) in the blocking buffer at 4°C overnight (information regarding antibodies used can be found in Table 2-2). Next, the membrane was washed by washing buffer TBST (TBS with 0.5% Tween-20) at RT for 15 min 3 times. Then, the membrane was incubated with a secondary antibody (approximately 1:15,000) in blocking buffer at RT for 1 hr. The TBST washing steps were carried out before imaging.

Imaging

ECL (Enhanced Chemiluminescence) detection technique was used to visualize the target proteins. All procedures can be found in the manufacturer's instructions (Pierce™ ECL Western Blotting Substrate with catalogue number: 32106).

First, the TBST washing buffer was removed. Next, two ECL solutions were mixed, 200 μ L of solution A and 200 μ L of solution B, to add to each membrane, making the surface of the PVDF membrane touch the ECL solution mixture. Then, the membrane was incubated for 15 s, followed by removing the ECL solution from the membrane. Lastly, the membrane was placed into a transparent plastic bag in order for better signal detection. The ChemiDoc imaging system (Bio-Rad) was used to image the blots.

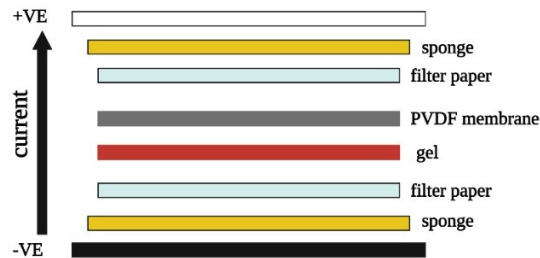


Figure 2-1. Western blot gel transfer stack.

The transfer stack was prepared in a specific order from negative (-VE) to positive (+VE): sponge, filter paper, gel, PVDF membrane, filter paper, and sponge.

2.9 Mass spectrometry (MS)

In this study, *Drosophila* BRGC samples were used for MS, and the procedure to acquire the samples and make the crosslink was described in the “Immunoprecipitation (IP) sample collection” section. The flow-through and input samples were used as controls. The samples were loaded and separated via SDS-PAGE until the loading dye reached about 1cm on the separating gel (100 v, 45 min). Next, the gel was stained with Coomassie reagent as described in Section 2.7. Lastly, the gel samples were sent for analysis at Alberta Proteomics and Mass Spectrometry Facility (4096 Katz Group Centre For Pharmacy and Health Research Building (KGR)). The protocol of MS can be referred to in the papers [192, 193].

2.10 Confocal microscopy

A Nikon C2 Plus confocal microscopy system was used for different signal detections, *i.e.*, porphyria-like PG phenotype and cellular localization of PPK20. The intensity of the lasers and other parameters were kept the same when photos were taken of the specimens from experimental and control groups. Apart from observing the detailed localization of a protein, its whole localization pattern in a tissue can be determined by doing a Z-stack on a 3-dimensional (3D) level. A detailed operating manual can be found on Nikon’s website, and the images were edited with NIS-Elements Viewer.

2.11 RNA-sequencing (RNAseq)

Dr. Nhan Huynh, a former Ph.D. student from Dr. Kirst King-Jones’s lab, conducted the RNAseq experiment, and the information was adapted from his thesis.

Three biological repeat groups were set up, and 75 RGs (18-hr L2 stage *ppk20^{KO}* larvae) were used for each group. RG samples were placed into microfuge tubes containing Trizol (ThermoFisher #15596026), flash-frozen using liquid nitrogen, and stored in a -80°C freezer for long-term preservation. RNA was extracted from the RG samples and analyzed to ensure its concentration and integrity. 100 ng RNA was taken from each sample to create strand-specific RNA-Seq libraries based on the Ovation *Drosophila* RNA-Seq System 1-16 (Nugen #0350-32).

The Complementary DNA (cDNA) quality was analyzed before sending for sequencing along with the controls (Genome Quebec Innovation Center at McGill University) [194].

2.12 Ferric iron staining

(1) Sample preparation

The whole gut of 42-hr L3 larvae was acquired (to keep consistent with the time point of other sample collection). The larvae were first dissected in cold PBS to obtain complete intestines. Then, the intestines were washed with PBS three times to eliminate the hemolymph as much as possible. Next, the intestines were fixed with 4% formaldehyde in PBS for approximately 30 min and washed with 1% PBST (tween 20) for 15 min.

(2) Prussian blue staining and imaging

The intestines were incubated with freshly prepared Prussian blue staining solution, made by adding an equal volume of 2% $K_4[Fe(CN)_6]$ and 2% HCl under dark conditions for 1 hr. Samples were then washed three times with PBS and mounted in mounting buffer [46]. Sample pictures were taken under a light microscope with magnifications set at 3.2x and 8x to ensure the consistency of the scale.

2.13 Larval ferritin injection

The general injection protocol was adapted from “*Drosophila* germline transformation” written by Nicolas Gompel, and Eva Ayla Schröder (<http://gompel.org/wp-content/uploads/2015/12/Drosophila-transformation-with-chorion.pdf>). Several modifications, based on previous larval injections, were made to cater to the needs for larval injection [195]. The iron-loaded ferritin proteins were purchased from Sigma Aldrich: horse spleen (F4503) and human liver ferritin (F6754). The injection concentration for both ferritins was 4.219 pM.

(1) Preparation for injection: larvae collection and setting up the injection system

The parental flies were raised on regular Nutrifly food in a 25°C, 60% humidity incubator, and the L1 larvae from the control and experimental groups were collected for injection. Next, the larvae were washed in PBS (3× 3 min) in a mesh basket (Diamed GEN46-101) and then dried with Kimwipes. Double-sided tape was then placed on one side of the glass slide so that the larvae could be glued to the tape to fix them in place. It is essential to expose the anterior part for injection when aligning the larvae onto the tape. Moreover, the store-bought olive oil was added to the larvae to prevent drying. Next, the glass slides were then placed into a 4°C fridge or on the ice for 3-5 min to slow down larval movement, making it easier for injection. After low-temperature treatment, the glass slides were placed under the objective lens of a microscope connected to the injection system. Pieces of Nutrifly food were placed in front of the larvae to stimulate larvae to elongate their body for easy injection entry.

(2) Larval ferritin injection

Ferritin solution was injected by a capillary glass tube through the larval dorsal side at the second abdominal segment to access the hemolymph while not piercing the major organs. For each injection, time should be controlled to less than 3 min per slide. The needles were prepared before the injection or preserved in the 4°C fridge. Furthermore, the injection system was manually controlled, and for each injection, air pressure should be the same amount to ensure the quantity of the ferritin injected into each larva was the same. After injection, the larvae were immediately put into the Nutrifly food to allow them to recover in the 25°C, 60% humidity incubator. These animals were then carefully transferred and quantified for a survival rate study.

2.14 *Drosophila* whole-body DNA extraction using “DNAzol”

DNA from different fly lines was extracted as the raw material for polymerase chain reaction (PCR). Fifty flies from each fly line were placed into a 1.5 mL microfuge tube, and liquid nitrogen was used for fast freezing. A volume of 200 µL DNAzol was added into the microfuge tube, and a precooled pestle with the mixer was used to grind the frozen flies for 2× 15 s. Next,

400 μL DNAzol was added to the tube, and the mixture was mixed by vortexing for 15 s. This step was repeated another time, making the total volume 1 mL. Then, the sample was incubated for 5 min at RT. After incubation, the sample was centrifuged at 13,000 rpm for 15 min at 4°C, and the green viscous supernatant was transferred into a new tube. An equal amount of chloroform (600-800 μL) of the supernatant was added into that new tube and mixed well by inverting 3-4 times. Then, 500 μL of 100% ethanol was added into the tube, and then the mixture was incubated on a shaker for 3 min at RT. Next, the mixture was centrifuged at 13,000 rpm for 2 min at 4°C. Afterward, the DNA pellet was formed at the bottom of the tube together with polysaccharides and proteins. The supernatant was removed, and 800 μL of 70% ethanol was added to the tube. The mixture was inverted 3-4 times before being centrifuged at 13,000 rpm at 4°C for 1 min. The pellet collected after centrifuge was the DNA product, and it was air-dried at RT for 3 min. 100 μL of nuclease-free water was added to dissolve the pellet.

After pellet resuspension, 200 μL of chloroform was added to the tube and inverted 3-4 times. The tube was then centrifuged at 13,000 rpm for 2 min at 4°C, and the upper phase layer was transferred into a new 1.5 mL tube. Next, 4 μL of 5 M NaCl was added into the tube and mixed by pipetting. 500 μL of 100% ethanol was added to the mixture and incubated on a shaker at RT for 3 min. Followed by centrifugation at 13,000 rpm at 4°C for 2 min, the supernatant was removed, and a pellet of DNA should be visible. Then, 800 μL of 70% ethanol was added into the tube and mixed by inverting 3-4 times. Next, the mixture was centrifuged at 13,000 rpm for 1 min at 4°C, and the supernatant was removed. The DNA pellet was air-dried at RT for 3 min. Lastly, 200 μL of 8 mM NaOH was added into the tube to dissolve the DNA. The concentration of DNA product was measured by a NanoDrop spectrophotometer (Thermo Scientific™ ND-7000).

2.15 High-efficiency transformation

A microfuge tube of competent *E.coli* DH5 α cells (~50 μL) was taken out from -80°C freezer to thaw on ice for 10 min. Plasmid DNA (70 ng) was added to the tube of competent cells. Next, the mixture was mixed by flicking the tube 4-5 times and placed on ice for 30 min to allow DNA to enter the cells. After incubation, the tube was placed into a 42°C water bath for exactly 30 s to induce heat shock, immediately followed by 5-min incubation on ice. A volume of 950 μL

of room temperature LB medium was transferred into the mixture and then incubated at 37°C for 60 min in a shaking incubator. Before inoculation, both control and experimental agar plates need to be prewarmed in a 37°C incubator. Following the incubation, around 100 µL of each prepared transformant was spread onto the antibiotic-containing plates, followed by overnight (14-16 hr) incubation at 37°C. The following day, single colonies with suitable sizes and no satellite colonies could be picked for plasmid DNA extraction.

2.16 Plasmid DNA extraction

Following the *E.coli* transformation steps, “Thermo Scientific GeneJET Plasmid Miniprep Kit” (K0502, K0503) was used to extract plasmid DNA. Several bacterial colonies were selected after transformation and incubated separately for harvesting. The LB culture was centrifuged at 8000 rpm or 6800 x g for 2 min at RT following the incubation. The supernatant was then removed, and the pellet was kept to proceed with the following steps:

(1) Resuspension, lysis and neutralization of bacterial cells

A volume of 250 µL resuspension buffer was added to the pellet and vortexed to resuspend the mixture. Next, 250 µL lysis solution was added to the mixture. For thorough cell lysis, the tube was inverted 4-6 times, followed by adding 350 µL neutralization solution and inverting 4-6 times to mix. Then the tube was centrifuged at $\geq 10,000$ -14,000 rpm (or 12,000 x g) at RT for 5 min.

(2) DNA binding

After centrifugation, the supernatant was transferred to the Thermo Scientific GeneJET Spin Column and centrifuged at $\geq 10,000$ -14,000 rpm at RT for 1 min.

(3) Column washing

A volume of 500 μL wash solution was then added to the column and centrifuged at $\geq 10,000$ -14,000 rpm at RT for 30-60 s. Next, the flow-through was removed, and this washing process was repeated, followed by spinning the empty column at the same rpm for 1 min.

(4) DNA elution

The column was placed into a new centrifuge tube, and 50 μL elution buffer was added to elute the DNA at RT for 2 min. Next, the tube and column were centrifuged at $\geq 10,000$ -14,000 rpm at RT for 2 min, and then the flow-through was collected. The collected flow-through sample was the plasmid DNA. Lastly, a spectrophotometer (NanoDrop) was used to measure the DNA concentration.

2.17 Statistics

The statistical significance was calculated using a two-tailed unpaired t-test in this thesis. Error bars represented the standard deviations. The asterisks suggest the significance levels: $*p < 0.05$ and $**p < 0.01$.

One-way ANOVA test was used to analyze Figures 3-4A and 3-6, where multiple groups were compared to see if the supplements had rescued the adult survival of flies, with the p values set as the same as the t-test: $*p < 0.05$ and $**p < 0.01$.

2.18 Tables

Table 2-1. The concentration of various supplements in Nutrifly food.

Supplement	Experiment	Solvent	Stock concentration	Final concentration
cholesterol	sterol rescue	ethanol	25 mg/ml	250 µg/ml
7-dehydrocholesterol (7dC)	sterol rescue	ethanol	125 mg/ml	125 µg/ml
20-hydroxyecdysone (20E)	sterol rescue	ethanol	250 mg/ml	250 µg/ml
ferric ammonium citrate (FAC)	iron manipulation	nuclease-free water	1 M	1 mM
bathophenanthroline disulfonic acid disodium salt trihydrate (BPS)	iron manipulation	nuclease-free water	100 mM	100 µM
hemin	iron manipulation	NaOH	38 mM	1 mM
zinc protoporphyrin	iron manipulation	DMSO	50 mM	1 mM
equine (horse) ferritin	iron manipulation	NaCl	42.19 nM	42.19 pM
human ferritin	iron manipulation	NaCl	42.19 nM	42.19 pM

Table 2-2. The antibodies used in this study.

Antibody/stain	Source of product	Experiment	Dilution
monoclonal rabbit anti-HA	Cell Signaling #3724S	transgene ^{IF}	1:1,000
		transgene ^{WB}	1:1,000
monoclonal mouse anti-HA	Abcam #18181	transgene ^{IF}	1:1,000
		transgene ^{WB}	1:1,000
monoclonal rabbit anti-GFP	Invitrogen #G10362	transgene ^{IF}	1:500
		transgene ^{WB}	1:1,000
monoclonal mouse anti-GFP	Invitrogen #MA5-15256	transgene ^{IF}	1:1,000
		transgene ^{WB}	1:1,000
goat anti-mouse IgG H&L Alexa Fluor 488	Abcam #150113	transgene ^{IF}	1:2,000
goat anti-mouse IgG H&L Alexa Fluor 555	Abcam #150114	transgene ^{IF}	1:2,000
goat anti-rabbit IgG H&L Alexa Fluor 488	Abcam #1500777	transgene ^{IF}	1:2,000
goat anti-rabbit IgG H&L Alexa Fluor 555	Abcam #1500778	transgene ^{IF}	1:2,000
goat anti-mouse IgG H&L HRP	Abcam #97023	WB	1:15,000
goat anti-rabbit IgG H&L HRP	Abcam #97051	WB	1:15,000
DAPI	Cell Signaling #4083	tissue nuclei	1:50,000

^{IF} Immunofluorescence

^{WB} Western Blot

Table 2-3. The recipe for 2x buffer used in immunoprecipitation (IP).

Component	Stock concentration	Final concentration	Amount to be added
Na-HEPES, pH 7.5	1.0 M	50 mM	5.0 mL
NaCl	5.0 M	150 mM	3.0 mL
EDTA	0.5 M	1 mM	0.2 mL
MiliQ water			To 100 mL

Table 2-4. The recipe for 1x lysis buffer used in immunoprecipitation (IP).

Component	Stock concentration	Final concentration	Amount to be added
2x Buffer G	2x	1x	10.0 mL
Triton X-100		1%	0.2 mL
Glycerol	50%	10%	4.0 mL
Protease Inhibitor cocktail	25x	1x	0.8 mL
MiliQ water			To 20 mL

Table 2-5. The composition of wash buffer 1 used in immunoprecipitation (IP).

Component	Stock concentration	Final concentration	Amount to be added
2x Buffer G	2x	1x	5.0 mL
Triton X-100		0.1%	0.01 mL
Glycerol	50%	5%	1.0 mL
MiliQ water			To 10 mL

Table 2-6. The composition of wash buffer 2 used in immunoprecipitation (IP).

Component	Stock concentration	Final concentration	Amount to be added
2x Buffer G	2x	1x	5.0 mL
Glycerol	50%	5%	1.0 mL
MiliQ water			To 10 mL

Table 2-7. The composition of SDS-PAGE separating gel using 40% acrylamide.

Separating gel	8 mL (one gel)				
Acylamide percentage	6%	8%	10%	12%	15%
ddH ₂ O	4.6 mL	4.2 mL	3.8 mL	3.4 mL	2.8 mL
40% Acrylamide/Bis-acrylamide	1.2 mL	1.6 mL	2 mL	2.4 mL	3 mL
1.5 M Tris(pH=8.8)	2 mL	2 mL	2 mL	2 mL	2 mL
10% SDS	80 μ L	80 μ L	80 μ L	80 μ L	80 μ L
TEMED	8 μ L	8 μ L	8 μ L	8 μ L	8 μ L
10% AP	80 μ L	80 μ L	80 μ L	80 μ L	80 μ L

AP: ammonium persulfate

Table 2-8. The composition of SDS-PAGE stacking gel using 40% acrylamide.

Stacking gel (4%)	5 mL
ddH ₂ O	3.725 mL
40% Acrylamide/Bis-acrylamide	0.5 mL
1 M Tris-HCl, pH 6.8	0.625 mL
10% SDS	50 µL
TEMED	5 µL
10% AP	50 µL

Table 2-9. The SDS-PAGE gel acrylamide percentage in response to the protein size.

Protein size	Gel acrylamide percentage
4–40 kDa	20%
12–45 kDa	15%
10–70 kDa	12.50%
15–100 kDa	10%
25–200 kDa	8%

Table 2-10. List of *Drosophila* stocks used in this study.

Commercially available fly lines were obtained from the Bloomington *Drosophila* stock center (BDSC) or the Vienna *Drosophila* research center (VDRC). Some lines are generous gifts from Michael O'Connor's lab. Other lines were made by Dr. Nhan Huynh in Kirst King-Jones's (KKJ) lab, as indicated.

Genotype	Description	Source	Stock #
<i>w</i> ¹¹¹⁸	Wild type	BDSC	3605
<i>phm22-Gal4</i>	PG-specific driver	Michael O'Connor's lab	N/A
<i>w: tubulin-Gal4/TM3, GFP</i>	Whole-body driver	BDSC	5138
<i>w: actin-Gal4/TM3, GFP</i>	Whole-body driver	BDSC	7408
<i>UAS-hTfR</i> ^{WT} · <i>GFP</i>	hTfR	BDSC	36858
<i>ppk20</i> ^{FCH}	<i>ppk20</i> mutation	KKJ's lab	N/A
<i>ppk20</i> ^{RNAi}	<i>ppk20</i> RNAi	VDRC	36659
<i>ppk20</i> ^{KO} / <i>TM6B, Hu Tb</i>	<i>ppk20</i> mutation	KKJ's lab	N/A
<i>Fer1HCH</i> ⁰⁰⁴⁵¹	<i>ferritin</i> mutation	BDSC	N/A
<i>UAS-ppk20</i> ^{PA.mVenus}	<i>ppk20</i> overexpression tag line with mVenus tagged PPK20 isoform A	KKJ's lab	N/A
<i>UAS-ppk20</i> ^{3H.PA}	<i>ppk20</i> overexpression tag line with 3xHA tagged PPK20 isoform A	KKJ's lab	N/A
<i>UAS-ppk20</i> ^{PC.mVenus}	<i>ppk20</i> overexpression tag line with mVenus tagged PPK20 isoform C	KKJ's lab	N/A
<i>UAS-ppk20</i> ^{3H.PC}	<i>ppk20</i> overexpression tag line with 3xHA tagged PPK20 isoform C	KKJ's lab	N/A
<i>UAS-eGFP</i>	UAS control	BDSC	5430

Chapter 3. The study of how *ppk20* is involved in cellular iron import

3.1 Introduction and rationale

Preliminary two-step screens (see 1.7) demonstrated that the *ppk20* gene might be involved in the heme synthesis pathway. This assumption was based on the presence of developmental defects, and red autofluorescence observed in PGs of *PG>ppk20-RNAi* larvae [194]. The original observation was made in the *ppk20-RNAi* fly line (#36659), which was acquired from the VDRC stock center. PPK20 belongs to the DEG/ENaC family and is predicted to have a membrane sodium channel function that has not yet been elucidated experimentally. More importantly, no previous publication has specifically focused on studying the connection between PPK20 and iron homeostasis.

3.1.1 The primary scenarios by which PPK20 may be involved in cellular iron import

As a putative membrane protein, PPK20 is predicted to localize to the plasma membrane, where it may play a direct role in cellular iron import. A plausible hypothesis is that *ppk20* impairment affects cellular iron import, causing the heme synthesis pathway to halt at the last step. Consequently, heme's immediate precursor, PPIX, would accumulate (Figure 1-4), causing the porphyria-like PG phenotype. Furthermore, ecdysone synthesis requires heme, and the impaired iron import would lower the production of heme, resulting in a decrease in ecdysone level (Figure 1-3B), which causes developmental defects (*i.e.*, developmental delays or larval arrest). If this rationale was valid, there might be two different possibilities for how PPK20 mediates cellular iron import:

- (1) PPK20 directly affects non-transferrin-binding iron (NTBI) cellular import;

(2) PPK20 is the potential receptor for Tsf and/or ferritin or modulates the function of the actual (unknown) receptor and assists indirectly in cellular iron import.

The reason for making these hypotheses is that NTBI, and potential fly systemic iron carriers, Tsf and ferritin, provide cells with iron (refer to Introduction 1.2). Among the two potential iron carriers, Tsf is the primary systemic iron carrier in humans with a known receptor and defined import process. However, the function of Tsf in flies is undetermined, and there is no identified fly TfR [19, 47, 51]. Ferritin is also considered a fly systemic iron carrier candidate due to its high concentration in the hemolymph [44]. In humans, there are several proposed ferritin receptor candidates: i) human TfR can bind and mediate the import of H-ferritin (ferritin heavy chain) [181]; ii) T-cell immunoglobulin and mucin domain 2 (Tim2) might be the H-ferritin receptor on oligodendrocytes [182]; iii) Scara5 mediates serum ferritin import [183]. However, there is no identified ferritin receptor in *Drosophila*.

Although NTBI might not be the primary iron source, it is still a part of systemic iron and can enter cells in humans. Hence, NTBI is considered one of the candidates [87, 88]. One review paper suggested that NTBI might be one way to deliver iron in flies in the proposed fruit fly iron metabolism model [45].

Testing PPK20 function in the heme synthesis pathway

As a first step, I added heme to the diet of loss-of-*ppk20* animals (*PG>ppk20-RNAi* and *ppk20* mutants) to determine whether the heme production pathway was disrupted. The PG phenotype and survival rate were examined to determine if there was a rescue of these animals. A rescue would constitute a wild-type or a mild porphyria-like phenotype in the PG and an increased survival rate, especially in adults. If the addition of heme rescues the phenotypes, it would indicate that the loss of PPK20 function disrupted the heme synthesis pathway; hence, supplementing fly media with heme might compensate for this. Moreover, heme import might provide iron to compensate for the loss, hence the rescue.

Furthermore, I fed fly larvae iron-rich food (food supplemented with ammonium iron (III) citrate (FAC), a form of NTBI) to test whether the PG and developmental phenotypes could be rescued without PPK20 function. In addition, PPIX was added to the diet to test whether heme synthesis was disrupted due to the lack of iron, and if so, PPIX should not rescue the phenotypes. Iron and PPIX rescue experiments could complement each other, and my prediction is that there would be no rescue effect on animal survival, suggesting fly cellular iron import requires PPK20 function.

Testing whether PPK20 functions in Tsf cellular import

While ferric iron (FAC) can be directly added to the diet, iron-binding proteins require different delivery approaches. To perform the rescue experiment, the *human transferrin receptor (hTfR)* cDNA was expressed in the loss-of-*ppk20* genetic background. Although it is uncertain whether fly Tsf is the main systemic iron carrier, adding hTfR might offer an alternative entry, provided that fly Tsf could be imported by it. If fly Tsf is not normally imported as an iron source, adding hTfR would provide a new entry. And if the animal survival could be rescued by importing Tsf, the hypothesis that PPK20 mediates cellular iron import would be supported. However, more experiments need to be conducted to test whether PPK20 is the potential fly Tsf receptor or mediates the function of the unknown receptor.

Testing whether PPK20 functions in ferritin cellular import

As for the ferritin rescue experiment in loss-of-*ppk20* animals, due to the lack of understanding of ferritin import in both humans and flies, feeding, larval hemolymph injection, and *ferritin* overexpression were used to deliver the protein. Consistent with all the other iron delivery approaches above, if ferritin is one of the systemic iron carriers destined for cellular import and PPK20 mediates this process, then little to no phenotype rescue would be observed. However, ferritin might not be the fly systemic iron carrier; thus, the addition of ferritin would not rescue regardless.

3.1.2 Other possibilities of how PPK20 is involved in fly iron and heme homeostasis

Apart from affecting cellular iron import, loss of *ppk20* might disturb the function of enzymes involved in heme synthesis, causing red autofluorescent precursors to accumulate. This is because heme synthesis precursors other than PPIX contain porphyrin rings (Figure 1-4A). Hence, the porphyria-like phenotype might be caused by accumulating a different precursor, whereby the enzyme responsible for synthesizing that precursor is disrupted due to the loss of PPK20. Suppose PPK20 is involved in the pathway by disrupting the synthesis of the different precursors, then loss-of-*ppk20* may lead to the accumulation of aminolaevulinic acid synthase (ALAS) due to the halt of the heme synthesis. ALAS is one of the earliest precursors required in the heme production pathway [126], and the upregulation of *ALAS* could be confirmed by examining the fold change on its transcript level using qPCR.

3.2 Results and discussion

3.2.1 The phenotypes study of other *ppk* loss-of-function animals

There are 31 *ppk* genes in *Drosophila*, and only one gene, *ppk20*, was identified in the two-step screen (see 1.7). It emphasized the importance of *ppk20* and triggered some questions: whether other PPKs have a similar function to PPK20, and perhaps PPK20 requires other PPKs to complete its function. Past research has shown that in the ENaC family, different PPK proteins sometimes form complexes together and function as a unit; for example, PPK11/16 functions with PPK1 as a heterotrimeric ENaC in presynaptic homeostasis [196]. If PPK20 forms a heterotrimeric complex with other PPK proteins, one would expect that the KD of putative *ppk* partner proteins phenocopy *ppk20* loss-of-function phenotypes.

Therefore, at least two fly RNAi lines acquired from VDRC and Bloomington stock centers of all 31 *ppk* genes were used to determine if knocking down another *ppk* gene had a phenotype similar to *ppk20*. Of all 30 genes, *ppk2* (also known as *ripped pocket*, *rpk*) Bloomington RNAi line had a red RG and L3 arrest phenotype, but the same phenotypes were not seen using the VDRC line. The inconsistent phenotypes might be caused by the RNAi off-target effect, which needs further validation, such as creating gene KO by CRISPR/Cas9. Due to the rarity of the porphyria-

like PG phenotype, *ppk2* is considered one of the candidates that could form hetero-complexes with *ppk20*, and there was no other *ppk* gene KD line that showed a similar trait. In addition, apart from the possibility of forming the heteromeric complex with PPK20, PPK2 might be playing a similar role to PPK20.

Furthermore, knocking down *ppk* genes 1, 3, 5, 6, 9, 14, 15, 18 and 27 demonstrated various levels of developmental delays: genes 1, 3, 5, 9 and 27 had 4-6 hour delay of L2/L3 larval moulting in fly lines acquired from Bloomington but not from VDRC; *ppk* genes 14 and 18 had a 1-day delay of L2/L3 larval moulting, and these fly lines were acquired from Bloomington, not VDRC; as for *ppk15*, the RNAi line acquired from VDRC showed an L2 larval arrest phenotype, while the line acquired from Bloomington showed 5-day delay phenotype (Table 3-1). The inconsistent phenotypes of these flies from different stock centers might be that different RNAi lines might have target sites and a possible RNAi off-target effect.

Although developmental defects were observed, none of the RNAi lines above had a consistent porphyria-like PG phenotype. Only *ppk20* displayed a consistent red PG phenotype when its function was disrupted in the RNAi and mutant lines (see 3.2.1). More importantly, the result also indicated that the porphyria-like PG was not a common trait shared among the loss-of-*ppk* animals, but specific to *ppk20*. However, without the function of other *ppk* genes, animals might have defective phenotypes in their growth due to undetermined reasons. According to past studies on *ppk* gene functions, one reason could be that defective sodium channel function might cause stress in epithelial salt transport and sensory processes [197], resulting in larval developmental defects. Overall, the results suggested that PPK20 may form homomeric protein complexes by itself instead of heteromeric complexes.

3.2.2 Characterization of PG phenotype and survival rate of the loss-of-*ppk20* animals

I wanted to ensure that the phenotypes observed from the 2-step screen, porphyria-like PG phenotype and L2/L3 larval stage arrest, were accurate. Therefore, I first dissected the *PG>ppk20*-RNAi animals and examined their PGs under the confocal microscope to see if there was any red signal compared to the WT larval PG. And next, the survival rate of the *PG>ppk20*-RNAi animals was quantified to see if the loss of *ppk20* would be lethal to the animals.

As mentioned previously, the porphyria-like phenotype in the PG can be observed when *ppk20* was knocked down by RNAi. Showing the red PG would suggest the accumulation of the red-fluorescing precursors made in the heme production pathway, causing the decreased heme production level. It would follow that the CYPs required in the ecdysone production pathway cannot catalyze ecdysone synthesis without their cofactor heme. Steroid hormones regulate all developmental stages of a fly; thus, a significant reduction in the production of ecdysone results in flies that cannot go through all developmental stages, thus causing developmental defects; depending on the level of ecdysone, larval arrest at specific stages, or are delayed through certain stages.

ppk20-RNAi animals were obtained from VDRC Stock Center (#36659). Dr. Huynh generated two mutant lines to avoid RNAi's off-target effect. *ppk20^{KO}* is a whole-body KO line, and it is a CRISPR-mediated mutant line in which endogenous *ppk20* was removed entirely (Figure 3-1A). *ppk20^{FRT}* is a tissue-specific conditional KO line (Figure 3-1B), in which the endogenous *ppk20* allele was replaced by another allele flanked by FRT sequences. Therefore, the *ppk20* transcription unit can be effectively excised from the genome by expressing the flippase specifically in PG cells.

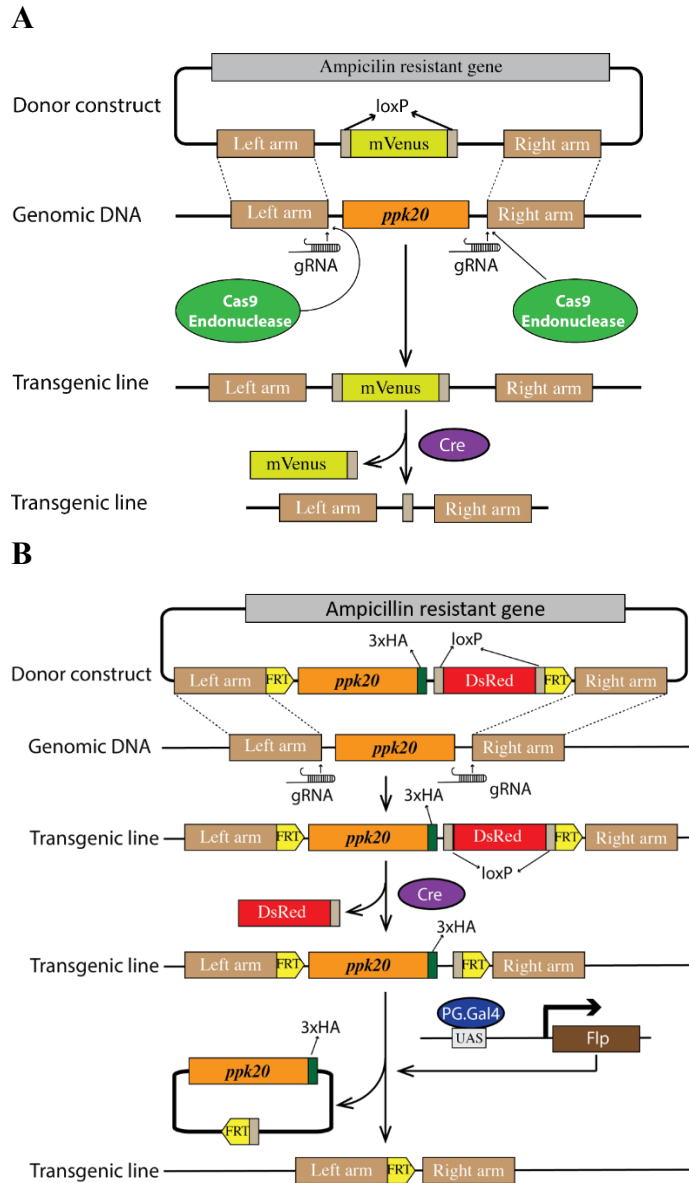


Figure 3-1. The constructs of the two *ppk20* mutant lines.

A[#]. CRISPR/Cas9 mediated generation of a *ppk20* null mutation, where the endogenous *ppk20* was replaced by mVenus and then removed by Cre-LoxP. B[#]. The conditional *ppk20* KO line. The endogenous *ppk20* allele was replaced by another allele flanked by FRT sequences. By expressing the flippase specifically in the PG, *ppk20* can be removed from the tissue. [#]indicates from “Characterizing new players involved in iron homeostasis during *Drosophila* larval development: Shifting the classic paradigm of iron metabolism” by Nhan Huynh, 2020, Doctor of Philosophy Thesis, 173, Copyright (2020) by the University of Alberta. Reprinted with permission.

(1) Porphyria-like phenotype in larval PG

To assess the PG phenotype of the *PG>ppk20-RNAi* and *ppk20^{KO}* animals compared to the WT control, I dissected around 20 larvae from the respective fly strains. These larvae were staged at the L2/L3 moult to minimize biological variation during the dissection time window (42-hr L3 larvae). Compared to the WT control, the experimental animals, *PG>ppk20-RNAi* and *ppk20^{KO}*, both showed a robust red signal in the PG (Figure 3-2) when analyzed with a confocal microscope. All the PG samples from the loss-of-*ppk20* animals had porphyria-like phenotypes. No significant size difference in RG was observed in loss-of-*ppk20* animals compared to the control, which suggests that the larvae were not old enough to develop the pronounced size enlargement. When the control animals were pupated and became adults, loss-of-*ppk20* animals still stayed at the larval stage. By then, the enlarged red RG can be observed even through the cuticle layer, indicating the abnormal growth of PG and the further accumulation of the precursors when loss-of-*ppk20* larvae were much older than 42 hours.

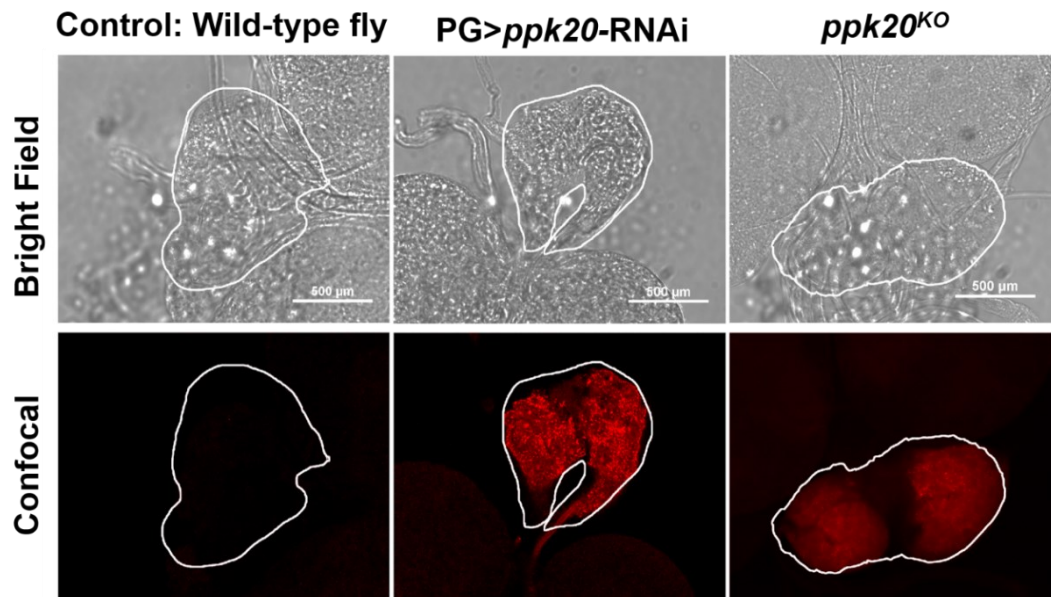


Figure 3-2. The PG phenotypes in different loss-of-*ppk20* and wild-type animals.

PG>ppk20-RNAi and *ppk20^{KO}* show porphyria-like PG under confocal microscopy compared to WT control (n>20, more than 20 larval PG were examined for each group).

(2) Survival rate quantification

Next, the L2/L3 larval stage arrest phenotype observed in *PG>ppk20-RNAi* animals in the secondary screen was confirmed by conducting a fly larval developmental study. I used regular Nutrifly food that contained none of the supplements as the food control, which means no other chemicals or biological supplements were added for specific rescue purposes. Fifty embryos were collected from each biological replicate (x3), and the survival rate at each stage was normalized to the embryo number (see 2.1.3).

The result showed that *PG>ppk20-RNAi* animals had a significant developmental defect compared with WT control animals (Figure 3-3A). Most *PG>ppk20-RNAi* embryos hatched, but arrested later in development at the L2 and L3 larval. In total, less than 10% pupated, and none reached adulthood. The result indicates that ecdysone concentration might be decreased, causing the larvae to be unable to go through all developmental transitions. The reason that these embryos made it to early larval stages might be that the requirement for ecdysone concentration is lower for early-stage transitions. These phenotypes were similar to those associated with decreased ecdysone production, consistent with the idea that *ppk20* could indirectly be involved in this biochemical pathway [132, 198, 199].

I also quantified the survival rate of whole-body KO animals (*ppk20^{KO}*), in which there was less than 25% of pupation rate (Figure 3-3B). In theory, the whole-body KO might have a more severe phenotype than tissue-specific KD (*PG>ppk20-RNAi*). However, this was not the observation since the pupal survival of *ppk20^{KO}* animals was higher than that of *ppk20^{RNAi-KD}* (Figure 3-3AB).

The possible explanation is that the quantification of the survival rates of these two different lines (*PG>ppk20-RNAi* and *ppk20^{KO}*) started at different stages; therefore, they cannot be directly compared. The quantification of *ppk20^{KO}* survival rate started at the L2 stage because it is impossible to distinguish between the homozygous *ppk20^{KO}* and heterozygotes with a Tb balancer at the embryonic stage (see 2.1.3). Starting quantification at the L2 stage means healthier larvae were selected since they had already turned into L2, and thus they survived the L1 stage, eliminating weaker individuals. Moreover, the *ppk20^{KO}* “pupae” all showed a very unhealthy phenotype (Figure 3-3C).

ppk20^{FRT} animals (PG-specific *ppk20* KO) had a similar survival phenotype as the *PG>ppk20-RNAi* animals, where there was an L2/L3 arrest phenotype with approximately 40% of animals reaching L3 stages and less than 10% pupation rate (Figure 3-3D).

The results above suggested that the initial screening data was accurate. When *ppk20* is knocked down or mutated, the animals display larval developmental arrest and porphyria-like PG phenotype. Based on the rationales stated in the introduction (see 3.1), there are several possibilities by which PPK20 may be involved in heme synthesis regulation, and the following experiments were designed to test the possibilities.

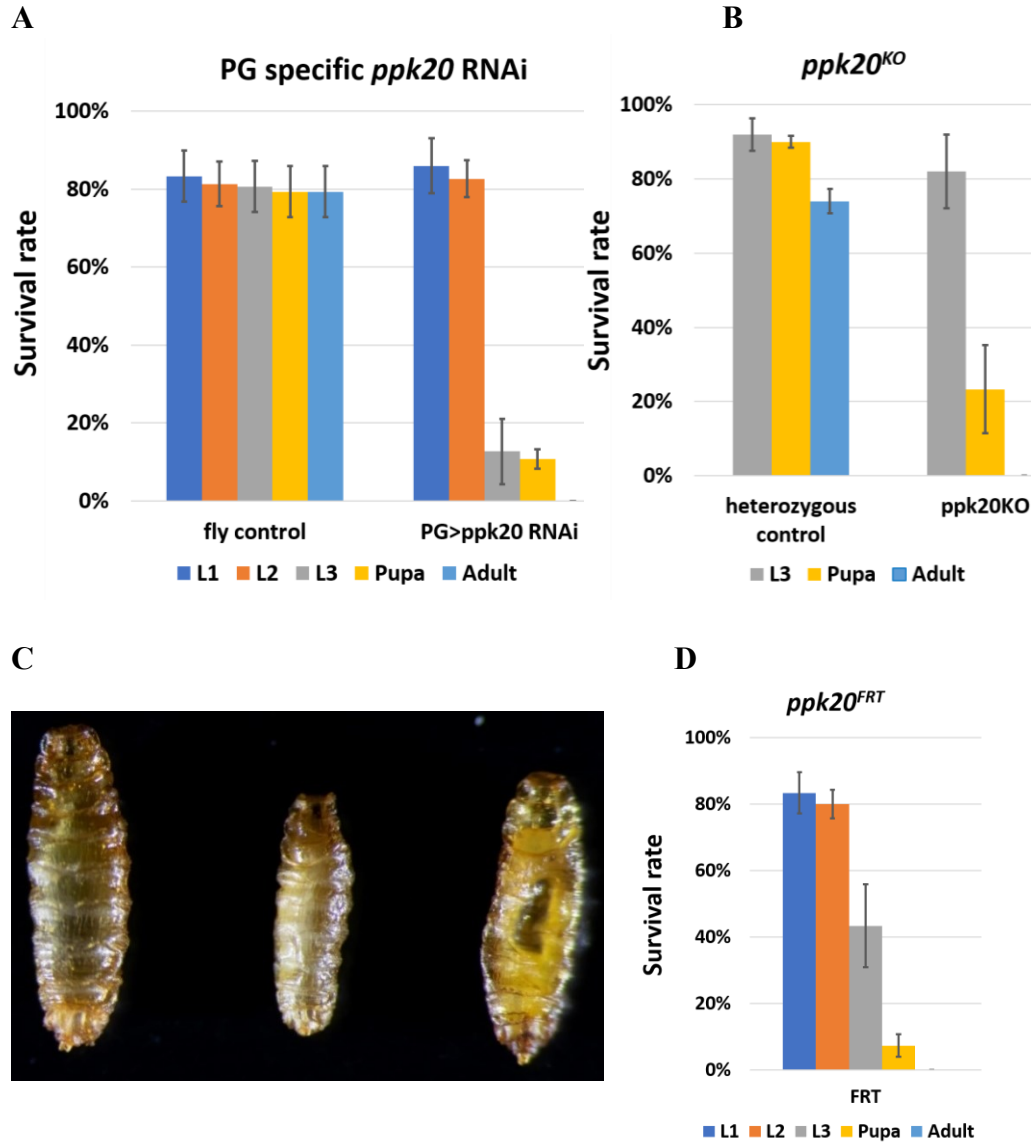


Figure 3-3. The survival rate study of the loss-of-*ppk20* animals.

A. *PG>ppk20*-RNAi animals show an L2/L3 larval arrest phenotype compared to the control, most animals arrested at L2 and L3 stages, none made it to adulthood. B. The *ppk20*^{KO} animals showed a developmental defect. 50 Tb heterozygous and 50 non-Tb homozygous L2 larvae were obtained for quantification. Heterozygous controls showed no defect in development, while homozygotes showed only a 10% pupation rate and no adult survival. C. The unhealthy *ppk20*^{KO} pupae ($n > 5$, more than 5 pupae were examined). D. *ppk20*^{FRT} animals had an L2/L3 larval arrest phenotype. (error bar represents stand deviation, the survival rate of three biological replicates was measured for each group)

3.2.2 Supplement food rescue experiment of *PG>ppk20-RNAi* and *ppk20^{KO}* animals

Various supplements were added to the regular fly food with a specific concentration (see Table 2-1) to test whether this would improve survival rates and rescue the PG phenotype of different loss-of-*ppk20* animals. The possible involvement of *ppk20* in heme and ecdysone production pathways was tested via specific supplement feeding. In addition, this series of experiments examined the possibility that *ppk20* plays a role in cellular iron import.

(1) Iron enrichment, iron depletion, Zinc protoporphyrin IX (PPIX) precursor and hemin food rescue (heme synthesis pathway)

It has been tested that the loss of *ppk20* could lead to the porphyria-like PG phenotype and developmental defects (see 3.2.1). The next question was whether the red colour observed in the PG was caused by the interruption of the heme synthesis pathway. This question was tested by adding hemin to the animals' diet to rescue the phenotypes. Another variable that could influence heme production is the availability of the cofactor iron. Iron is required at the last step of the heme production pathway, during which Fe^{2+} is incorporated into PPIX to form heme (Figure 1-4A). The addition of iron and PPIX to the diet would test whether a low cellular iron level was the cause to impair heme synthesis.

Hemin (heme), iron and PPIX feeding

Hemin (Sigma #51280) was used as an alternative to heme in this study because the only difference between hemin and heme is that the ferrous iron in the heme moiety is replaced by ferric iron in hemin (Figure 3-4).

In this experiment, *ppox* mutant flies were used as a positive control because we had previously shown that these animals could be rescued via hemin feeding. PPOX is one of the enzymes required for heme synthesis; when *ppox* function is compromised, the heme production pathway is impaired, and heme synthesis is reduced or abrogated due to a reduction in PPIX synthesis. The hemin feeding of *ppox* mutant ensures that the compound is intact, which is critical in this case since hemin is light-sensitive and can easily degrade during the food preparation

process (Figure 3-4B). Consequently, in theory, by adding hemin to the diet, the survival of *ppox* mutant animals should be rescued, provided that hemin is delivered to the PG. As stated above, this rescue has been indeed observed in our lab, indicating that hemin provided in the diet can be transported to and utilized by target tissues, such as the PG. This result also suggested that the PPIX structure remained intact and made it from diet to the PG.

When hemin was added to the diet of *PG>ppk20-RNAi* animals, the survival rates of L3 larvae, pupae, and adults all significantly increased (Figure 3-4A). The adult survival rate increase was a unique trait amongst all rescue experiments, in which around 10% of embryos survived to the adult stage. This result indicates that ecdysone synthesis might be restored with the presence of heme as a cofactor for the CYPs, leading to the recovery of developmental transitions. The hemin feeding experiment confirmed that the PG porphyria-like phenotype was caused by disruption of the heme production pathway.

In order to determine which step was interrupted specifically by the loss of PPK20, an iron and PPIX feeding experiment was performed. In the iron-enriched diet supplemented by FAC, *PG>ppk20-RNAi* animals could be rescued partially. Specifically, the L3 larval survival rate significantly increased from 10% in controls to almost 80% (Figure 3-4A). However, the adult survival rate was not increased significantly. The reason for using this iron-enriched food (FAC) is that this iron-supplemented diet has rescued the loss of 1,4-Alpha-Glucan Branching Enzyme (AGBE) animals' survival rate from almost no adult to around 40%-60% [96]. Therefore, no iron rescue of *PG>ppk20-RNAi* animals might indicate that free iron importation requires the presence of PPK20, and the porphyria-like PG might be caused by the lack of iron in the heme synthesis.

PPIX is the immediate precursor to heme [126]; when the iron is incorporated into the molecule catalyzed by FECH, heme is formed, which does not fluoresce (Figure 1-4). In this experiment, Zinc-PPIX (Zn-PPIX), was added to the diet, of which the only difference between hemin and Zn-PPIX is the metal in its center (*i.e.*, hemin is identical to Fe^{3+} -PPIX). If the addition of PPIX resulted in a rescue of the loss-of-PPK20 animals, one would conclude that there is sufficient intracellular iron in *PG>ppk20-RNAi* PG, but that the process of making PPIX was affected. When the food was supplemented with Zn-PPIX, there was a significant increase in *PG>ppk20-RNAi* L3 larval survival rate from 10% to 50%, but not in pupal or adult stage survival (Figure 3-4A).

Therefore, the accumulation of red autofluorescent precursors might be caused by the halt of heme synthesis, hence causing the red PG phenotype. Ecdysone production might be affected due to the lack of heme as a cofactor, hence causing developmental defects. Partial rescue of *PG>PPIX-RNAi* animals by dietary supplementation with hemin (or ZnPPIX) showed that hemin was delivered intact (as opposed to be broken down in the gut) to target cells and imported into these cells. However, the lack of complete rescue suggested that the effects caused by losing PPK20 function were not wholly counteracted.

Overall, the partial rescue of survival rate from hemin to the loss-of-*ppk20* flies demonstrated that heme as a cofactor of CYPs, the addition of heme might restore CYPs' enzymatic functions by bypassing the heme synthesis. Consequently, ecdysone was produced, which enabled the developmental transitions to take place. When dissected, some larvae had porphyria-like PG phenotypes (more than 50%, data not shown), which triggers the suspicion that these larvae could not make it to later stages. The reasons that hemin did not have a better rescue effect on *PG>ppk20-RNAi* animals could be: i) the concentration of heme was not high enough, and maybe a higher concentration would have resulted in a more substantial rescue; however, a higher concentration might be toxic to the larvae; ii) the loss of PPK20 not only affected the heme production but had some severe effect on tracheal development, water clearance and other mechanisms, that are essential for larval survival; thus, hemin cannot completely rescue the phenotype. These possibilities are discussed later in chapter 5.

In short, the results above showed that dietary iron and PPIX had no rescue in adult survival, but that hemin partially rescued. Therefore, these results indicated that *ppk20* could play a role in the delivery and/or availability of iron to tissues and cells involved in the production of heme.

Iron-depleted food feeding

Iron-depleted food was used to feed the *PG>ppk20-RNAi* animals to see if there was any worsened phenotype since less iron in the diet might cause more problems. The Iron chelator bathophenanthrolinedisulfonic acid disodium salt trihydrate (BPS), was used to chelate iron from regular Nutrifly food, thus reducing the bioavailability of dietary iron (hereafter referred to as “iron-depleted food”).

After feeding the animals with the iron-depleted food for one generation, there was no apparent adverse effect on the survival rate compared to the control group (Figure 3-4A). A more pronounced result might be observed if flies were fed on iron-chelated food for a few more generations until the iron stored in embryos is not enough to support animal survival; then, a more severe survival phenotype defect might be seen. Based on previous experiments performed by others in the lab, iron should start to become limiting after 4-6 generations, depending on the genes they studied.

This series of feeding experiments was also carried out in the *ppk20^{KO}* mutant line. The results above showed no rescue in adult survival of *PG>ppk20-RNAi* animals with iron-enriched food (Figure 3-4A), and consequently, a very similar result was observed in *ppk20^{KO}* animals. In contrast to *PG>ppk20-RNAi* animals, *ppk20^{KO}* animals could not be rescued by hemin (Figure 3-5A), which is different from the *PG>ppk20-RNAi* feeding result where there was a significant rescue using hemin. The PG phenotype was consistent; the red remained when hemin was added to the diet (Figure 3-5B). The reason for this discrepancy might be that *ppk20^{KO}* line is a mutant line, which suggests a more severe effect due to the ubiquitous loss of PPK20; whereas the RNAi was only triggered in the PG. Therefore, even when hemin was added, the non-iron-related issues could be hindering the rescue by hemin, for instance, the defect in water clearance and tracheal necrosis (see chapter 5). Another possibility is that if PPK20 was involved in the larval intestinal iron import, then different forms of iron, *i.e.*, free iron, heme, and iron-binding proteins, cannot be absorbed into the larvae; therefore, lack of overall iron uptake could lead to a more severe phenotype that may not be rescued by hemin feeding.

(2) Cholesterol, 7-dehydrocholesterol (7dC), and 20-hydroxyecdysone (20E) food rescue (ecdysone synthesis pathway)

Apart from the apparent relevance of iron and heme homeostasis to PPK20, the developmental defect might be directly related to the production of ecdysone. In this study, various components required at different steps were added to investigate whether the synthesis of a specific precursor was directly affected by the loss of PPK20 via examining if there was any rescue of

survival in *PG>ppk20*-RNAi animals. 20-hydroxyecdysone (20E), the active form of ecdysone, was added to the food diet to compensate for the possibly lowered concentration.

The results showed that cholesterol, 7dC and 20E all had various degrees of rescue in *PG>ppk20*-RNAi animals' survival (Figure 3-6). Cholesterol feeding showed an increase in the percentages of L3, pupa, and adult survival, in which the survival rates of L3 larva and pupa increased significantly from 35% and 15% to 75% and 25%. 7dC feeding only showed a significant increase in the pupa's survival from 15% to 40%. Interestingly, some L2 larvae skipped the L3 stage and formed pupae directly when fed with 7dC. Lastly, the 20E feeding showed a similar rescue result as cholesterol, not as many adults, but a higher percentage of pupa survival which was around 50%.

Although there was no significant rescue of the adult survival with these three different supplements, more flies surviving to later stages might suggest that a better diet may increase the chances for animals to live longer. Low adult survival rates were also observed in all the feeding groups (cholesterol, 7dC and 20E), the reason might be that these adults are the fly escapers since the animals were kept in the food for a long time, and other lab members have also observed this phenomenon. The reason for this remains unclear.

Interestingly, the addition of 7dC made some L2 larvae skip the L3 stage and become pupae directly. The reason that led to the results was undetermined, but this phenomenon has been previously documented [132]. One observation was that these L2 pupae were smaller than the control.

20E, as the active form of ecdysone, was added to the food to supplement the possible loss of ecdysone production because the ecdysone concentration was increased in the food in order to restore sufficient levels of the hormone, hence triggering the developmental transitions. The results suggested that even with the addition of 20E, there was no significant rescue for the adult survival, suggesting that although the pulses were restored, loss of PPK20 leads to larval lethality.

In addition, these three supplements were also used to feed *ppk20^{KO}* animals to test whether this would improve survival rates. The result showed that cholesterol feeding did not rescue; 7dC showed an increase in the pupa's survival, whereas 20E did not show a good rescue effect (Figure

3-5A). These results were consistent with that of *PG>ppk20-RNAi*, indicating that the loss of PPK20 causes developmental defects.

In summary, it became more evident that without PPK20, the heme synthesis pathway is likely disrupted due to the lack or reduction of intracellular iron. Next, the possibilities of how PPK20 might be involved in heme synthesis pathway and iron import were investigated.

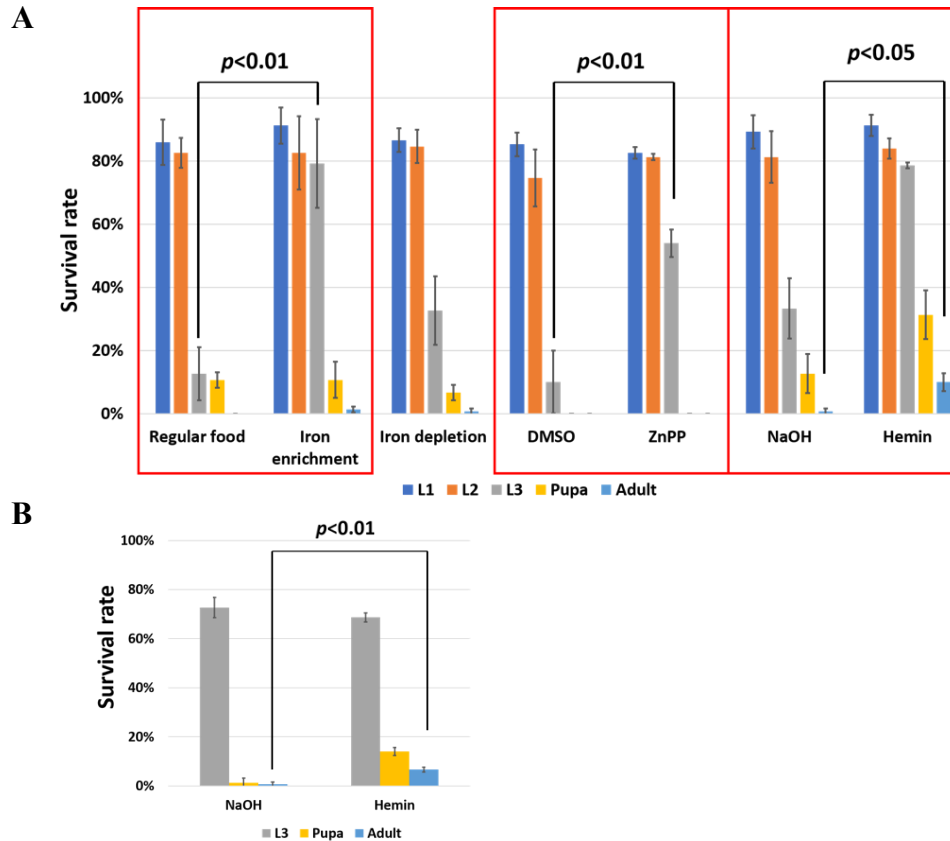


Figure 3-4. Food supplement rescue experiment of *ppk20*-RNAi animals (heme synthesis pathway).

A. The survival rate of *PG>ppk20*-RNAi animals in different supplemented foods. Control food is regularly Nutrifly made with water, and it is the control for iron-enrichment (FAC), and iron-depletion (BPS) supplemented food. DMSO-food is the control for PPIX and NaOH-food is the control for hemin. With the addition of FAC, PPIX and hemin, *PG>ppk20*-RNAi animals were partially rescued at different stages to various degrees. Only hemin feeding partially rescued *PG>ppk20*-RNAi adult animal survival by increasing the survival rate from 0% to 10%. (with the one-way Anova test, the hemin feeding significantly rescued the adult survival, and the p-value is 0.00012). B. The survival rate of *ppox* mutant animals in hemin-supplemented food. The *ppox* mutant animals could be partially rescued by hemin feeding, in which, compared to the NaOH-food control, the addition of hemin rescued the adult survival from 0% to almost 10%. This result indicates that the hemin was active. (error bar represents standard deviation, *: p value < 0.05; **: p value < 0.01, the survival rate of three biological replicates was measured for each group)

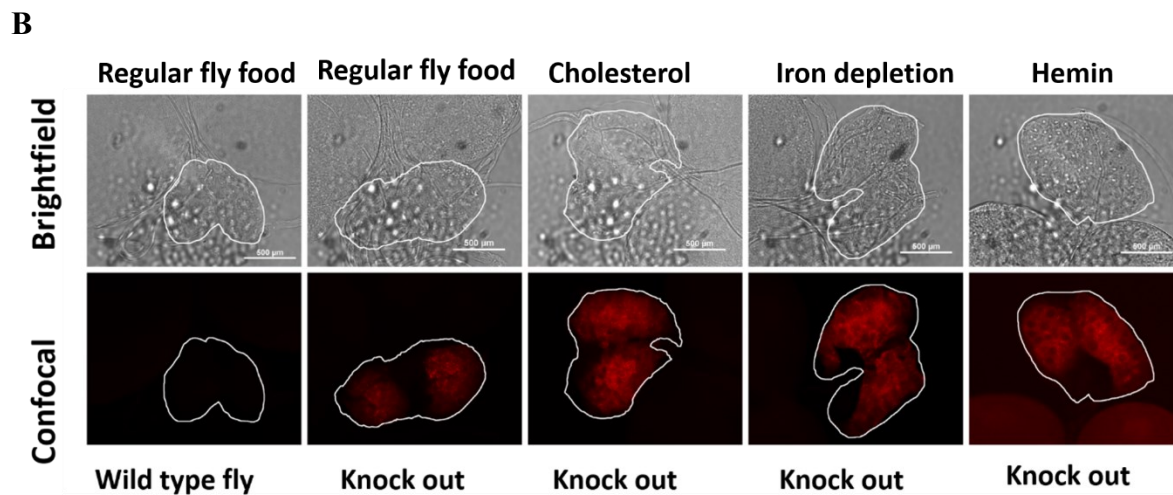
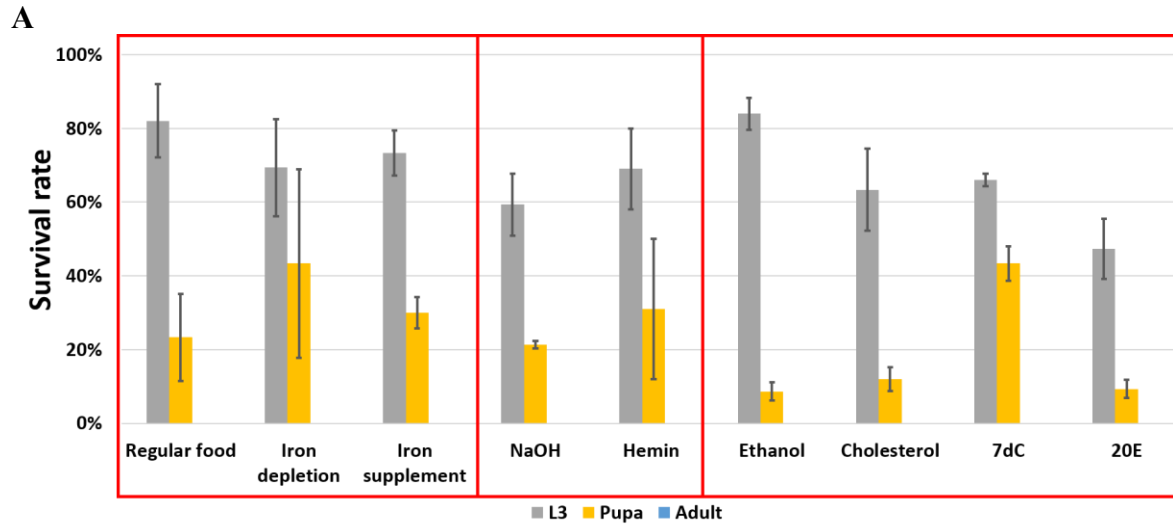


Figure 3-5. The survival rate and the PG phenotype of $ppk20^{KO}$ animals in different supplemented foods.

A. The survival rate of $ppk20^{KO}$ animals in different supplemented foods, including FAC, cholesterol, 7dC, 20E and hemin. The increased survival rate of the adult was not observed using different supplements. B. The PG phenotype of $ppk20^{KO}$ animals reared on different supplemented foods, including cholesterol, FAC and hemin. Compared to the PG of wild-type flies fed with regular food, all the other PGs of $ppk20^{KO}$ in different supplements showed a porphyria-like phenotype. (error bar represents standard deviation, the survival rate of three biological replicates was measured for each group; $n > 20$, more than 20 larval PGs were examined for each group)

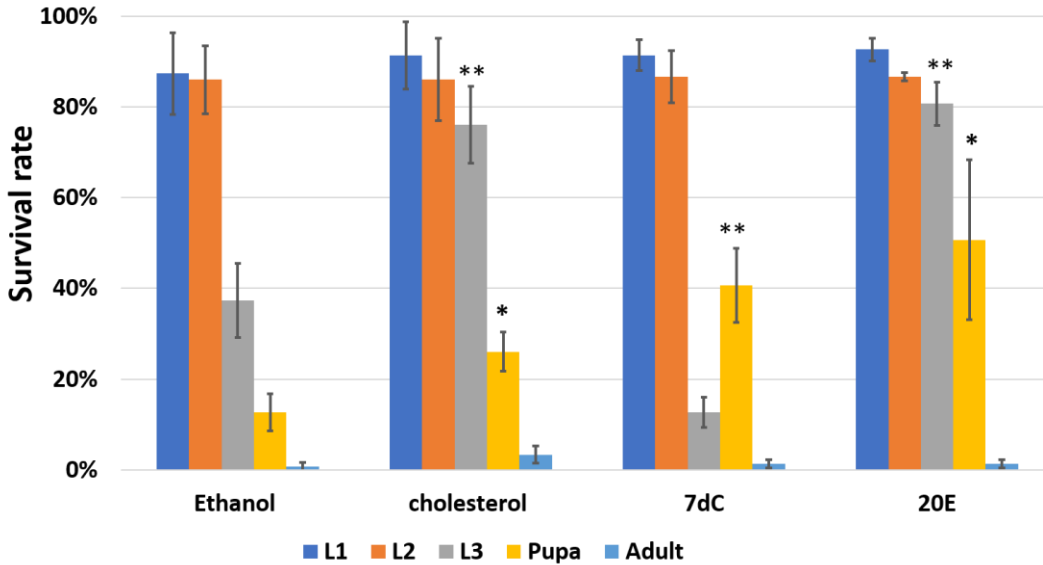


Figure 3-6. Food supplement rescue experiment of *ppk20*-RNAi animals (ecdysone synthesis pathway).

A. The survival rate of *PG>ppk20*-RNAi animals in different supplemented foods. The ethanol food is the control for cholesterol, 7dC and 20E. With the addition of cholesterol, 7dC and 20E, *PG>ppk20*-RNAi animals were partially rescued at different stages with various degrees. (with the one-way Anova test, none of the supplement feeding significantly rescued the adult survival, and the p-value is 0.24; error bar represents standard deviation, *: p value < 0.05; **: p value < 0.01, the survival rate of three biological replicates was measured for each group)

3.2.3 Loss of *ppk20* may disturb the function of enzymes involved in the heme synthesis pathway

Hitherto, the direct effect caused by losing *ppk20* function was suggested, which is the low cellular iron level. However, the mechanism of PPK20 mediates the iron import remains undetermined.

If the cellular iron import was indeed affected by the loss of PPK20, it might suggest that the accumulated precursor should be the immediate precursor to heme, PPIX. On the other hand, PPK20 function might be related to the expression and function of the enzymes involved in the heme production process. For example, when a certain gene encoding an enzyme involved in heme synthesis is not appropriately expressed (Figure 1-4A), such as *ppox*, PG will have a porphyria-like phenotype [96]. The same consequence might occur when the enzyme does not function as it should in the heme synthesis pathway. In both scenarios, the first enzyme, ALAS, will accumulate due to the suspension of the heme synthesis theoretically.

The qPCR data showed that ALAS is upregulated in the loss-of-*ppk20* animals (Figure 3-7), suggesting that *ppk20* was required for protoporphyrin ring synthesis via its involvement in cellular iron import. The data showed that once *ppk20* was knocked down (*PG>ppk20-RNAi*) and conditionally knocked out (PG-specific *ppk20^{FRT}*), heme synthesis was disrupted by showing the transcriptional induction of ALAS, which encodes the enzyme acting in the first step of heme biosynthesis. However, the result was not conclusive since a halt at different steps after ALAS might also cause it to accumulate, possibly due to the low cellular iron level caused by loss of PPK20 or PPK20's involvement in the production of other enzymes. Therefore, it needs to be further elucidated by performing the qPCR experiment to analyze if the expression of other enzymes required in heme synthesis was upregulated.

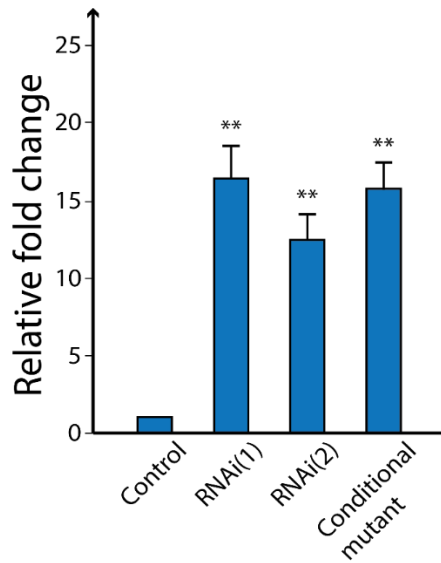


Figure 3-7[#]. The transcript level of ALAS was significantly upregulated by knocking down or knocking out *ppk20*.

When *ppk20* was knocked down (two RNAi lines) or knocked out (*ppk20^{FRT}*) in PG of the animals, the transcript level of *ALAS* showed a 10-fold upregulation compared to the WT control. The transcript level change was analyzed by qPCR. Two *ppk20*-RNAi lines: RNAi (1) is V36659 from VDRC, and RNAi (2) is BL25897 from BDSC. (error bar represents standard deviation, *: p value < 0.05; **: p value < 0.01, three replicates were done for each group) [#]indicates Nhan Huynh collected the data, reprinted with permission.

3.2.4 The possibilities of how *ppk20* mediates cellular iron import: (1) PPK20 directly affects non-transferrin-binding iron (NTBI) cellular import

One possibility of how *ppk20* mediates cellular iron import is through regulating NTBI import. As a member of ENaC family, PPK20 might regulate NTBI importing on the plasma membrane.

Based on a previous paper [46], the iron uptake level can be visualized through gut ferric iron staining. This approach could help elucidate the role that PPK20 plays in free iron uptake and is not disrupted by other forms of iron imported from the gut; because the gut is the primary iron uptake site, any iron-combined proteins need to be broken down before they can get absorbed. *Drosophila* iron intake is primarily through the midgut iron cell region and then accumulated in the anterior midgut [68, 69]. Prussian blue staining method was used to stain the ferric iron stored in the ferritin of the enterocytes in the iron cell region [200]. The mechanism regarding iron being accumulated in the anterior midgut region remains unclear [68]. The predicted outcome of this experiment is that when *ppk20* is not expressed in the gut, the ferric iron staining might be lighter or not exist compared to the control animals with intact PPK20 function in the gut due to the reduced ferritin incorporation of the imported iron.

The ferric iron staining experiment was carried out using PG-specific and gut-specific Gal4 drivers in *ppk20*-RNAi animals, *ppk20*^{KO} mutants and WT controls (Figure 3-8). Regular Nutrifly fly food, iron-rich (FAC-supplemented) and iron-depleted food (BPS-supplemented) were used to feed the animals. The intestine ferric iron stain results in the regular fly food were not that pronounced, while iron-rich and iron-deplete feeding showed better contrast in staining (Figure 3-8C).

In the FAC-supplemented food, the intestines from each group showed a stronger staining pattern than in BPS-supplemented food, especially in the midgut iron uptake region. *ppk20*^{KO} intestine had a very faint ferric iron stain in both food supplements compared to WT control, PG-specific and gut-specific *ppk20*-RNAi animals. Moreover, in the FAC-supplemented food, the midgut region stain of *ppk20*^{KO} animal was less extended and fainter, indicating that the loss of *ppk20* disrupts the free iron uptake (Figure 3-8A panel c). Consistently, *ppk20*^{KO} anterior midgut iron accumulation region also showed less extended and fainter staining, suggesting that not as

much iron was being accumulated as in the other groups. However, the difference between the control and the two tissue-specific lines, *PG>ppk20-RNAi* and *gut>ppk20-RNAi*, was almost undetectable (Figure 3-8A panels a and b). The reason might be that the excessive amount of ferric iron from the food accumulated on the gut lumen, making it impossible to distinguish between the absorbed iron and the iron remaining in the lumen of the gut when stained.

The difference between *ppk20^{KO}* larval gut stain and the gut staining of all other groups was more pronounced in the BPS-supplemented food (Figure 3-8B panel c). When the iron was chelated in the food, the midgut was the only region with visible iron staining; the anterior midgut staining was faint in all groups, indicating that the accumulation might not occur without iron uptake. *ppk20^{KO}* larval gut has the least amount of stain, which was almost undetectable compared to the control. The iron uptake in *PG>ppk20-RNAi* animal guts was not affected (Figure 3-8B panel a), whereas *gut>ppk20-RNAi* larval gut seemed to be affected because of the lighter staining phenotype (Figure 3-8B panel b).

This result suggested that if the PPK20 function in the PG was disrupted, its gut function might remain normal. In contrast, without PPK20 in the gut, iron storage in the gut appears to be compromised. The reason that guts isolated from *ppk20^{KO}* mutant larvae showed very faint to no stain might be that gene KO caused a more severe phenotype, whereas the Gal4 driver only switched on in certain regions, and RNAi only knocked down the gene. Thus, RNAi knocking down the gene in *PG>ppk20-RNAi* and *gut>ppk20-RNAi* animals might not be as efficient as knocking out the gene in *ppk20^{KO}* mutant larvae.

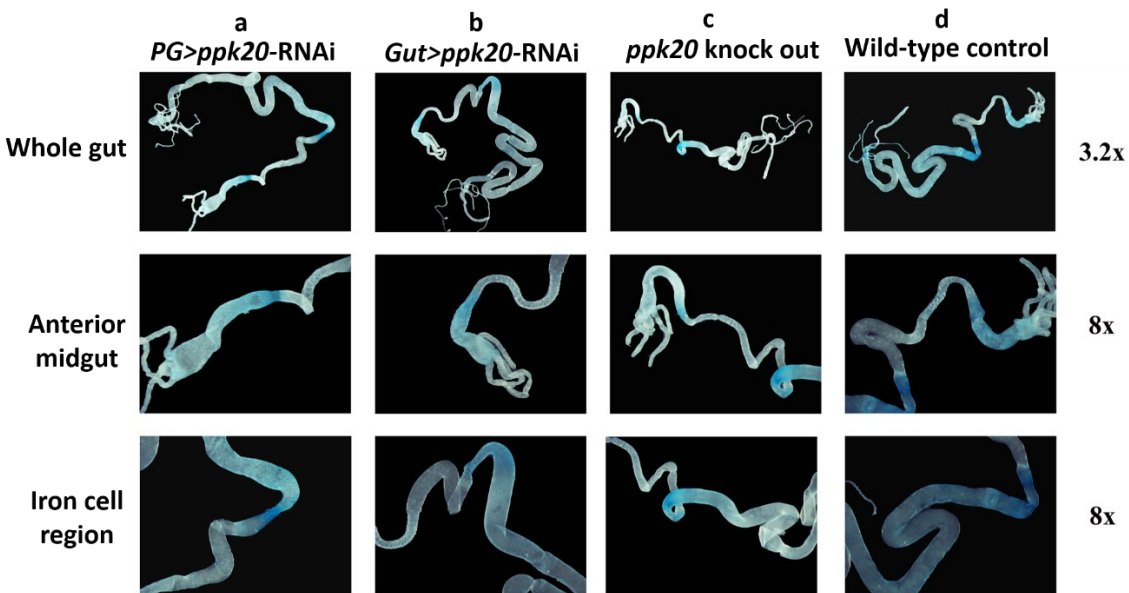
Overall, the larval intestinal ferric iron staining result suggested that PPK20 plays a role in dietary iron uptake into the larval gut, as evidenced by the reduced staining in *ppk20^{KO}* larval guts (panel c of Figure 3-8 A and B). Furthermore, the relation between protein-bound iron import, *i.e.*, Tsf and ferritin iron, and PPK20 still need to be investigated.

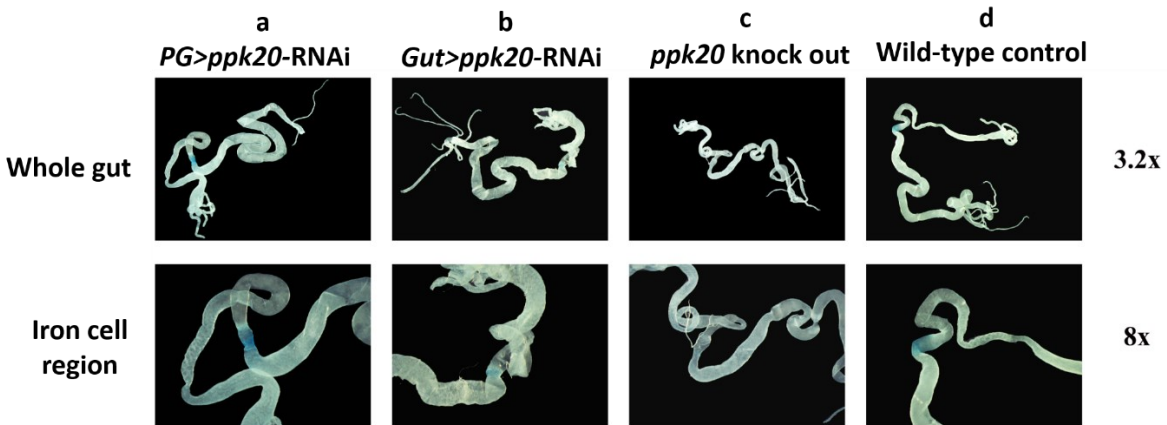
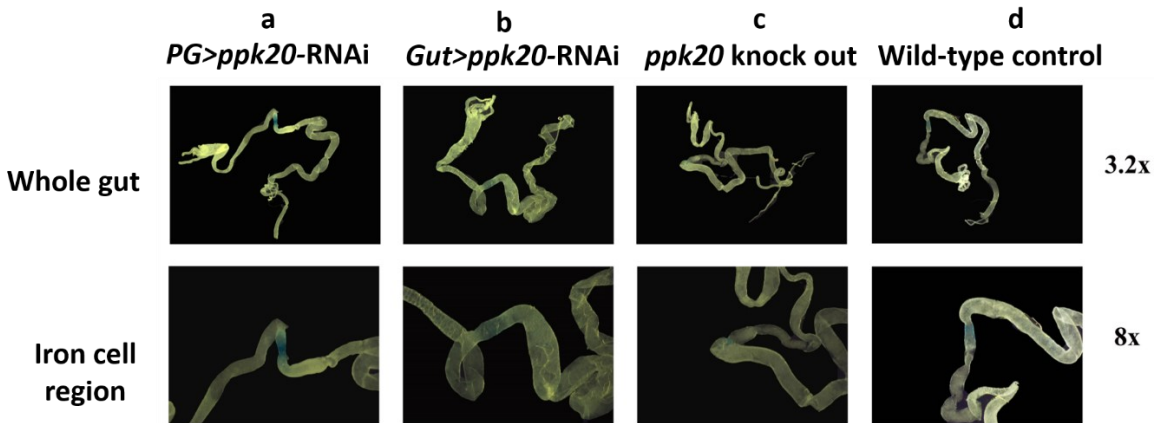
While I was conducting the gut ferric iron staining experiment, some PG tissues were also separated and stained to observe the ferric iron level; however, the results were not as expected. After several washes, the blue stain started to fade before I was able to take images. Due to the size of the tissue, PGs cannot be stained well, and the stains were even harder to be distinguished

among different groups. Therefore, ferric iron staining is not the best approach to quantify the iron levels in the PG.

Interestingly, one unique trait of the *ppk20^{KO}* in BPS-supplemented and FAC-supplemented food was that the *ppk20^{KO}* larvae appeared to have a less extended tracheal network throughout their body compared to all the other groups. In addition, the size of the *ppk20^{KO}* larval whole gut was significantly smaller in all food supplements compared to both WT control and other loss-of-*ppk20* animals (Figure 3-8 *ppk20^{KO}* larvae showed small intestine compared to all the groups). This trait might be related to the observed tracheal necrosis phenotype (see chapter 5), and is consistent with a possible role for PPK20 in larval tracheal development and function [101, 160].

A



B**C****Figure 3-8. Larval gut ferric iron staining.**

A. In FAC-supplemented food, all different groups, including *PG>ppk20-RNAi*, *gut>ppk20-RNAi*, *ppk20^{KO}* and WT control, showed the staining at the iron uptake midgut regions and the iron accumulation anterior midgut region [68, 69] by Prussian blue staining. *ppk20^{KO}* larval gut showed the lightest staining, while the staining pattern of *PG>ppk20-RNAi* and *gut>ppk20-RNAi* larval guts did not significantly differ from WT animals. B. In BPS-supplemented food, *gut>ppk20-RNAi* and *ppk20^{KO}* larval guts had fainter staining than the WT and *PG>ppk20-RNAi* animals in both midgut and anterior midgut regions. C. In regular fly food, there are no pronounced differences in staining in all different groups. (magnifications: 3.2x and 8x; n>10, more than 10 larval guts were examined for each group)

3.2.5 The possibilities of how *ppk20* mediates cellular iron import: (2) *ppk20* is the potential receptor for Tsf/ferritin or affects their receptor (unknown) function in cellular iron import

As mentioned in the introduction (see 3.1), it is unclear in *Drosophila* how exactly iron is transported into the target tissue cells (excluding enterocytes) or which vehicle carries iron. Compared to humans, two promising candidates, Tsf and ferritin, could be considered the systemic iron carriers that are subsequently imported into cells, acting as the primary iron source. PPK20 function in the putative Tsf/ferritin import pathway was examined as follows.

(1) Human transferrin receptor (*hTfR*) cDNA overexpression rescue study

Tsf is the known systemic iron carrier found in human blood plasma and is used to carry iron to target tissues and organs as a stable iron source (Figures 1-1 and 1-6). The dietary iron is absorbed through enterocytes, released in the blood, and picked by Tsf [89]. TfR-mediated endocytosis recruits clathrin as coat protein [50, 51] to import Tsf as a primary way to supply the cells with iron [19, 45, 47]. Although there is a fly Tsf1, the TfR is unidentified [45]; therefore, it is unclear whether or not Tsf1 plays the role of fly Tsf or whether the Tsf-TfR endocytosis is conserved in flies. Even without *ppk20* function, flies should produce Tsf1. The evidence was that when *ppk20* was knocked out, *Tsf1* was upregulated based on the RANseq result (see 4.2.6). Thus, supplementing the loss-of-*ppk20* animals with hTfR might be more feasible to examine the rescue effect because hTfR might be able to provide a novel entry for fly Tsf or substitute for the interrupted unidentified fly TfR function.

PG-specific overexpression of a GFP-tagged human transferrin receptor (*hTfR*) cDNA partially rescued *PG>ppk20-RNAi* animals (Figure 3-9), in which the adult survival rate increased from 0% to approximately 45%. The control group used in this experiment was the GFP-tagged Gal4 line without hTfR, and it showed no rescue of the *PG>ppk20-RNAi* animals, suggesting the rescue was due to the overexpression of *hTfR* cDNA. The improved adult survival rate was likely caused by an increased cellular iron level, in which hTfR provided accessibility for Tsf to be endocytosed as an iron source to compensate for the low intracellular iron level caused by the loss of PPK20.

The results suggested two main possibilities for how PPK20 might be involved in Tsf import: i) PPK20 is the fly equivalent of the hTfR; ii) the unknown fly TfR cannot function normally without PPK20. These possibilities are based on the assumption that Tsf is the primary systemic iron carrier in flies, and the canonical iron importation is through Tsf-TfR endocytosis.

If the PPK20 is the fly transferrin receptor, then without its function, Tsf cannot enter the cell and provide iron; hence when an alternative human receptor was added, Tsf was recognized and imported by hTfR, restoring the iron import pathway.

On the other hand, PPK20 might not be the fly TfR, but it mediates Tsf import via interacting with the putative fly TfR. Without the PPK20 function, the fly TfR fails to carry out its function to import Tsf. Therefore, the ectopically expressed hTfR in this experiment might substitute for the functional loss of the unknown fly TfR.

Last but not least, there is another scenario in which fly Tsf does not play the same role as in humans, meaning it might not be the primary systemic iron carrier. Consequently, the reason for not having a *hTfR* ortholog might be that fly Tsf does not enter the cells. Hence, *hTfR* cDNA expression provided a new entry for the fly Tsf, suggesting that without PPK20, cellular iron is low and can be supplemented through a novel way of importing iron. Therefore, further experiments need to be conducted to examine whether Tsf is the primary iron carrier and how PPK20 might mediate its uptake.

(2) Larval ferritin injection rescue study

Ferritin is an iron-binding protein complex and is a promising candidate for carrying systemic iron. Human ferritin is mostly found intracellularly and acts as a storage protein, while serum ferritin can be found in the blood with a possible novel function in delivering iron to the brain and other organs [44]. Ferritin concentration is about 1,000 times higher in the hemolymph of *Drosophila* larvae compared to human blood [201, 202]; therefore, ferritin might function as one of the primary fly systemic iron carriers candidates. However, whether it can be imported into the cell or how it can be imported needs to be investigated. There are several proposed ferritin

receptors in humans, namely hTfR, Tim2 and Scara5 (see 3.1.1), but the *Drosophila* ferritin receptor remains unidentified.

In addition, there were no available *Tim2* and *Scara5* cDNA containing lines, so it was difficult to use a known ferritin receptor to perform the rescue experiment. Consequently, dietary feeding, injection and overexpression of ferritin were performed to rescue the *ppk20^{KO}* animals' survival.

A ferritin mutant *Fer1HCH* (*Fer1HCH⁰⁰⁴⁵¹*) fly line with abolished ferritin expression was used as the control in this experiment. The rescue of the mutant's survival would confirm that dietary or injected ferritin protein remains active, hence could be used to rescue *ppk20^{KO}* flies. Moreover, the extracted horse-origin ferritin^{ho} and human-origin ferritin^{hu} were used as food supplements and injected into larvae.

First, as a dietary supplement, neither horse nor human ferritin had any rescue effect on *Fer1HCH⁰⁰⁴⁵¹* or *ppk20^{KO}* larvae (Figure 3-10AB). Ferritin is a protein complex; hence, high temperatures used during the food preparation process might break its structure (one needs to add compounds when the food is still liquid to allow for mixing). Additionally, the digestive system may not absorb ferritin directly, and in this case, it would have to be broken down before being taken in by the intestines. Due to these factors, ferritin feeding might not be the best approach for survival rate rescue experiments. Thus, no apparent rescue was observed in either *Fer1HCH⁰⁰⁴⁵¹* or *ppk20^{KO}* animals.

Next, when ferritin was injected directly into the larvae, both *Fer1HCH⁰⁰⁴⁵¹* and *ppk20^{KO}* animals were partially rescued by horse and human ferritin. Human ferritin had a better rescue in both genotypes, in which the survival rate of *Fer1HCH⁰⁰⁴⁵¹* adult went from 0% to just above 40%, while *ppk20^{KO}* adult survival rate increased from 0% to almost 40%. Lastly, overexpression of ferritin transgenes (a single P-element harboring cDNAs for both the ferritin light and the heavy chain), originated from horse, and human was able to rescue both *Fer1HCH⁰⁰⁴⁵¹* and *ppk20^{KO}* animals. A more substantial rescue effect of *Fer1HCH⁰⁰⁴⁵¹* animals was observed (Figure 3-10A), in which the survival rate of adult flies went from 0% to approximately 50% with either horse or human ferritin expression. However, overexpression of neither horse nor human *ferritin* cDNAs had rescued adult survival of *ppk20^{KO}* animals (Figure 3-10B).

Compared to dietary feeding, the direct ferritin injection might be a better approach to deliver the protein, especially with larval hemolymph injection, because it simulates the scenario that ferritin carries systemic iron in the blood. The results showed that *Fer1HCH⁰⁰⁴⁵¹* animals could not survive past the L2 stage, and when human or horse ferritin was injected into L1 larvae, almost 50% of the population progressed to adulthood (Figure 3-10A). This injection rescue suggested that the ferritin used was active and could supplement the larvae with iron by possibly being imported into the cells. As a ferritin mutation line, *Fer1HCH⁰⁰⁴⁵¹* animals are incapable of making ferritin; hence the cellular iron cannot be appropriately stored, which might cause cytotoxic, leading to premature death at early larval stages. Ferritin injection rescue might indicate that ferritin could be imported into the cells and used as an iron storage unit. However, there is no identified fly ferritin receptor; thus, more evidence is needed to support the hypothesis above.

Since the injection strategy worked in controls and thus was feasible, the next question was whether *ppk20^{KO}* animals could be rescued by the same approach (Figure 3-10B). Indeed the *ppk20^{KO}* adult survival rate increased from 0% to almost 40% with the ferritin injection, indicating that without PPK20 function, ferritin could be imported intracellularly and rescue the animals. Therefore, the results suggest that ferritin import might not require PPK20 function, and a lack of PPK20 function does lead to a low cellular iron level; hence when more ferritin was delivered through injection, and more ferritin was imported into cells, the iron carried by ferritin could supplement the cells' needs. However, more experiments need to be conducted to confirm the conclusion above.

Another critical result observed in this experiment was that, when ferritin was overexpressed in *ppk20^{KO}* animals, there was no rescue in adult survival, which suggested that the rescue effect was due to the presence of iron in the injected ferritin, rather than ferritin protein alone. These results are significant because they provided evidence that ferritin might play a role in fly systemic iron transport, which has a similar role to human Tsf.

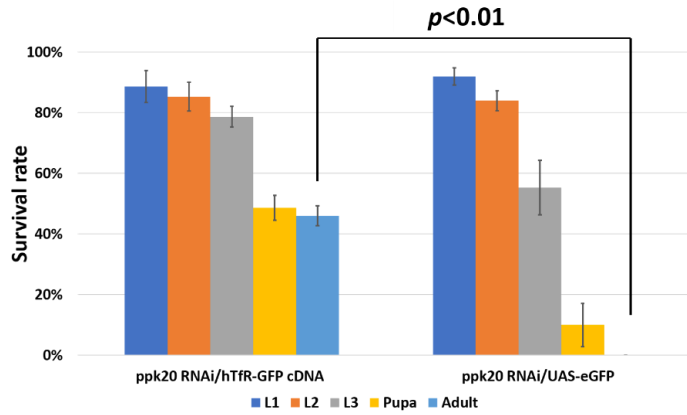


Figure 3-9. *hTfR* cDNA could partially rescue *ppk20* RNAi animals.

When *hTfR* cDNA was expressed in the genetic background of *PG>ppk20-RNAi*, the adult survival of these animals could be partially rescued. Compared to the control, almost 50% of the embryos survived to the pupal stage, and around 45% made it to the adult stage. (error bar represents standard deviation, $**p < 0.01$, three biological replicates were tested for each group)

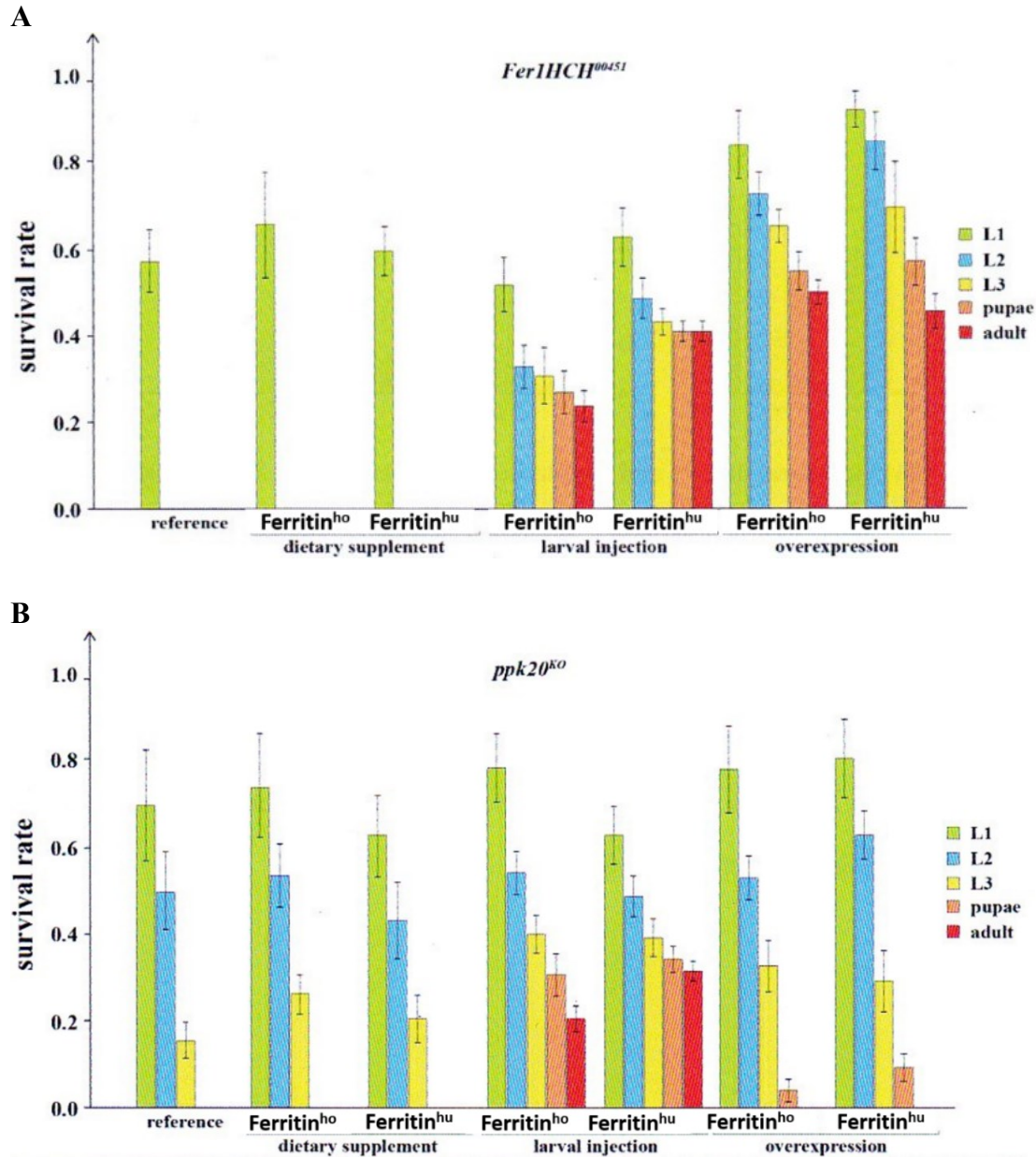


Figure 3-10[#]. Larval ferritin dietary feeding, injection and overexpression in *ppk20^{KO}* and *Fer1HCH⁰⁰⁴⁵¹* animals.

A. *Fer1HCH⁰⁰⁴⁵¹* is a ferritin mutant that cannot make intact ferritin protein, and it was used as the animal control for the ferritin feed, injection and overexpression experiment. The mutant animals cannot survive to the L2 stage, and when horse and human ferritin were added to the food, the survival rate stayed the same. When the ferritin was injected and expressed in those animals (both horse and human ferritin), the adult survival rate improved greatly from 0% to 25% (horse ferritin)

and 40% (human ferritin). Overexpression of human and horse *ferritin* cDNA in the mutant animals improved the survival rate more significantly than ferritin injection, in which the adult survival rates increased from 0% to more than 50%. B. The dietary feeding of *ppk20^{KO}* animals with ferritin did not rescue the survival rate, and a similar result was observed in the ferritin expression. When ferritin was injected into the animals (both horse and human ferritin), the adult survival rate improved from 0% to almost 30-40%. (error bar represents stand deviation, three biological replicates were tested for each group) #indicates from “Characterizing new players involved in iron homeostasis during *Drosophila* larval development: Shifting the classic paradigm of iron metabolism” by Nhan Huynh, 2020, Doctor of Philosophy Thesis, 176, Copyright (2020) by the University of Alberta. Reprinted with permission.

3.3 Discussion

In summary, the loss of PPK20 function disrupted the heme synthetic pathway, due to insufficient iron uptake. This caused the accumulation of red autofluorescent precursors in the larval PG. L2/L3 larva arrest phenotype showed that most larvae had defects in developmental transitions, indicating the possible disruption in ecdysone pulses. Heme is a cofactor for the CYPs involved in the ecdysone synthesis pathway. Without PPK20, heme production is interrupted, CYPs' function is impaired due to the lack of heme, which ultimately leads to abnormal ecdysone production. When ecdysone concentration is not reached to trigger developmental transitions, animals cannot transition to different stages.

The larval intestinal iron ferric iron staining results showed the direct involvement of PPK20 in intestinal free iron import. *hTfR* cDNA overexpression could partially rescue the *PG>ppk20-RNAi* animals, suggesting that PPK20 might mediate Tsf import. Since ferritin injection showed partial rescue of *ppk20^{KO}* animals, it suggests that PPK20 may not be involved in ferritin import. The reason for the ferritin injection rescue might be that under normal iron conditions, the ferritin import pathway is not maxed out, which means there are still receptors not utilized. Therefore, when there was more ferritin injected, so more got through. However, the possibility that PPK20 mediates ferritin cannot be ruled out.

Overall, all the evidence indicated that the loss of PPK20 might lead to a low cellular iron level via interrupting the uptake of NTBI, Tsf or ferritin; therefore, it is crucial to proceed with the experiments on tracking the iron movement and quantifying the iron level in loss-of-*ppk20* animals compared to WT animals. In addition, ferritin and Tsf might be the systemic iron-carrying vehicles in *Drosophila*. Several experiments are proposed to address the questions mentioned previously (see chapter 6).

3.4 Tables

Table 3-1[#]. Validation of PG-specific RNAi phenotypes of all 31 *ppk* genes.

Only *ppk20* displayed the red PG phenotype in two independent RNAi lines. *ppk2(rpik)* displays a red PG phenotype in the Bloomington RNAi line. *ppk* genes 1-3, 5, 6, 9, 14, 15, 18 and 27 demonstrate various levels of developmental delay.

SYMBOL	Stock(s)			
	VDRC		Bloomington	
	No.	Phenotype	No.	Phenotype
<i>ppk (ppk1)</i>	V108683 V330392	No	BL29571	4- to 6-hour delay
<i>rpik (ppk2)</i>	V105463 V8549	No	BL25847	Delay (duration unknown)
			BL39053	L3 arrested
<i>ppk3</i>	V104593	No	BL61995	4-hour delay
<i>Nach (ppk4)</i>	V106647 V45921	No	BL27262 BL62894	No
<i>ppk5</i>	V101664 V48290 V48289	No	BL25816	6-hour delay
<i>ppk6</i>	V101091	No	BL53010	1-day delay
			BL25880	No
<i>ppk7</i>	V100643 V7900	No	BL25922	No
<i>ppk8</i>	V47047 V47048	No	BL25814	No
<i>ppk9</i>	V109685 V104952 V23391 V17213	No	BL25892	4-hour delay

<i>ppk10</i>	V330625	No	BL27256	No
<i>ppk11</i>	V107741 V330319	No	BL23781	No
<i>ppk12</i>	V105131	No	BL27092	No
<i>ppk13</i>	V110084 V9494	No	BL25817	No
<i>ppk14</i>	V110258 V7903 V7904	No	BL27091	1-day delay
<i>ppk15</i>	V109855 V42523	L2 arrested	BL28012	5-day delay
<i>ppk16</i>	V22989 V22990	No	BL25890	No
<i>ppk17</i>	V109927 V8595 V8596	No	BL58557	No
<i>ppk18</i>	V105199 V13211 V13209	No	BL61949	1-day delay
			BL27240	1-day delay
			BL25883	1-day delay
<i>ppk19</i>	V107638 V36660	No	BL58203	No
			BL25887	No
<i>ppk20</i>	V36659	L2 arrested	BL25897	50% L2 arrested, L3 arrested
<i>ppk21</i>	V107892 V1345 V1346	No	BL25849	No
			BL62487	No
<i>ppk22</i>	V106384 V47946	No	BL28706	No
			BL61821	No

<i>ppk23</i>	V106873 V39581 V39580	No	BL28350	No
<i>ppk24</i>	V102923 V30196	No	BL26006	No
<i>ppk25</i>	V101808 V7343	No	BL27088	No
<i>ppk26</i>	V100834 V5110 V5109	No	BL25825	No
<i>ppk27</i>	V330515	No	BL27239	6-hour delay
<i>ppk28</i>	V100946 V44412	No	BL31878	No
<i>ppk29</i>	V106888 V330294	No	BL27241	No
<i>ppk30</i>	V105896 V1349 V1351	No	BL25810	No
<i>ppk31</i>	V106385 V1269	No	BL27087 BL44013	No

Key:

No RG phenotype
Big RG but not red
Red RG

#i indicates from “Characterizing new players involved in iron homeostasis during *Drosophila* larval development: Shifting the classic paradigm of iron metabolism” by Nhan Huynh, 2020, Doctor of Philosophy Thesis, 185, Copyright (2020) by the University of Alberta. Reprinted with permission.

Chapter 4. Characterization of PPK20 protein and its interaction with other proteins

4.1 Introduction and rationale

Protein functions are often closely related to their location; for example, the human TfR can be found on the plasma membrane, and its function is to import Tsf into the cell. In contrast, human ferritin is mostly found intracellularly and functions in iron storage [203]. PPK20 localization may reveal tissues that rely heavily on PPK20 function, and its subcellular localization might also reveal important insights into the mechanism of action for PPK20 [204]. Based on the observations in chapter 3, many detailed questions still need to be answered regarding the function of PPK20 protein. Therefore, detailed proteomic and transcriptomic studies might better illuminate the role of PPK20.

4.1.1 PPK20 expression pattern study

First, I examined the localization of PPK20. The study of human DEG/ENaC proteins discovered that these proteins commonly localize on the liquid and gas exchange surfaces where the sodium balance must be maintained. Organs that contain these exchange surfaces include the kidney, lung and colon [146, 205].

PPK20 belongs to the DEG/ENaC family and might have a sodium channel function, but the localization of the PPK20 protein is currently unknown. Multiple online gene expression prediction resources, including FlyAtlas (<http://flyatlas.org/atlas.cgi>), and modENCODE (<http://intermine.modencode.org/release-33/report.do?id=1022763>), PPK20 had a low to an undetectable amount of expression (Figure 4-1). In theory, the traditional approach to examining a protein's presence and its localization would be to create a knock-in construct where a tagged target gene replaces the endogenous gene, and the construct is then injected into the embryos to

create a new fly line. Consequently, the protein can be detected using the knock-in tagged fly line, and it should more accurately be compared to overexpression protein tag lines to reflect the localization and expression level of that protein. However, low-expression proteins cannot be accurately detected using these knock-in animals with tagged proteins, so overexpression constructs need to be created to determine the protein expression pattern.

In this study, several overexpression lines with different tags on either terminus of different isoforms of the PPK20 were made by Dr. Huynh to study the expression pattern and function of PPK20; information regarding the genotypes of these fly lines can be found in Table 4-1. As mentioned in the introduction (see 1.8), modification at different termini might cause the protein properties to change because the C terminus of mammalian ENaC proteins contains a “PY” motif [156]. Although fly PPK20 does not contain the “PY” motif, its different termini might still have different functions, and adding a tag may alter protein location and function. Thus, tags were added to each terminus to examine whether the localization remained the same, and significant differences might suggest that the addition of tags may alter protein localization. In addition, different PPK20 isoforms (isoforms A and C) might have different roles; therefore, the combination of tags (3xHA and mVenus tags), termini and isoforms likely gives a complete picture of how PPK20 localizes and functions (Table 4-1).

Transgenic protein overexpression has its merit compared to a knock-in construct, which is that even the low expression level protein can be characterized. However, the overexpression construct might cause possible artifacts, *i.e.*, protein complexes formed inaccurately, ectopic subcellular localizations and others [206, 207]. Therefore, to avoid the potential overexpression artifact effect that might be observed under the microscope when examining the protein expression, different *Gal4* drivers were used to induce the different levels of expression of *ppk20*. This experiment used two whole-body drivers, *tubulin* and *actin-Gal4* and PG-specific driver *phm-Gal4*. Moreover, it was important to determine the PPK20 localization in each organ/tissue, since no research has specifically investigated this, and its function in different organs and tissues is unknown.

This study primarily focuses on the PPK20 function in iron import in the PG; therefore, based on the results of chapter 3, PPK20 is predicted to localize to the plasma membrane of the PG. In addition, *ppk20* expression in other tissues and organs is worth examining, especially in the

trachea. A study showed that PPK4 and PPK11 localize and function in the larval tracheal network, and they might play a role in tracheal water clearance and sodium exchange [160]. Organs like the intestine and salivary gland (SG) are ideal candidates for observing PPK20 localization patterns because their surfaces need to carry out large quantities of ion exchange [208]. Additionally, the fly intestine is the iron uptake site, and PPK20 distribution could correspond to iron uptake regions.

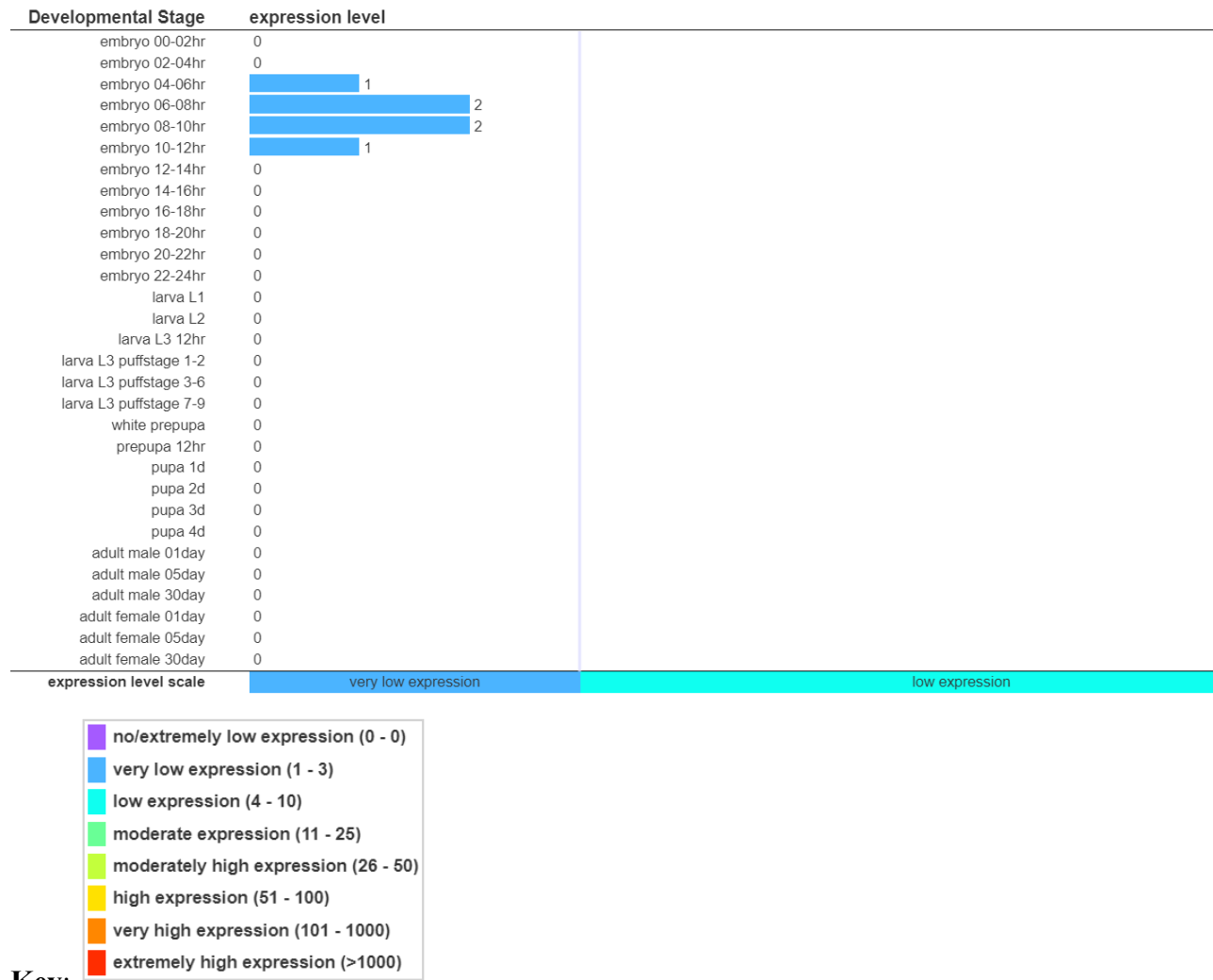


Figure 4-1. ModENCODE predicted temporal expression data of *ppk20*.

The expression level of *ppk20* at different stages from embryo to adult is consistently low. The ModENCODE predicted result showed that *ppk20* has low to no expression across different stages(<http://intermine.modencode.org/release-33/report.do?id=1022763>).

4.1.2 Proteins that may interact with PPK20

This study used proteomic analysis to identify the potential candidate proteins interacting with PPK20. Different proteins may interact with PPK20 at different sites at various stages. If a plasma membrane protein interacts with PPK20, it could be hypothesized that such a protein likely functions directly with PPK20. In addition, the intracellular protein-protein interaction may indicate that the channel function of PPK20 regulates intracellular protein directly. After identifying the proteins interacting with PPK20, its potential functional network could be mapped out. Therefore, the mechanism of PPK20 mediates iron import, and the connection between tracheal necrosis and the porphyria-like PG phenotype might be elucidated.

From a transcriptome point of view, as a gene of the ENaC family, the expression or absence of *ppk20* might affect other genes at the transcriptional level due to the presence or lack of PPK20 channel function that affects the normal function of different pathways. An RNAseq experiment was carried out using RG tissues of *ppk20^{ko}* animals (18-hour L2 larvae) by Dr. Huynh (see 2.11). The purpose of the RNAseq was to identify the genes with significant transcriptional level changes in the absence of *ppk20*. Genes that were significantly upregulated in their transcriptional levels might be complementing the functional loss of *ppk20* via increased expression. On the contrary, the downregulated genes might require *ppk20* to function; without it, downregulated genes cannot perform their functions, leading to the porphyria-like PG and developmental defect phenotypes. Therefore, the RNAseq result might help map out the functional network of *ppk20*.

4.2 Results and discussion

4.2.1 Localization of PPK20 in the larval PG using various Gal4 drivers

I used ectopically expressed PPK20 protein fused to different tags to detect the location of PPK20 because its endogenous expression levels are deficient. Late L3 stage larvae (~42 hr) were collected from the overexpression lines (Table 4-1) for dissection and proceeded with IF preparation steps (see 2.5). The *tubulin* and *actin-Gal4* ubiquitous drivers were used to induce the

larval whole-body expression of *ppk20*, and different tissues were separated and stained for confocal microscopic examination.

PPK20 isoforms A and C (PA and PC) were mainly localized to the PG plasma membrane, which was similar to the positive control, a known plasma membrane protein, hTfR. PPK20 could also be seen inside the cytoplasm but not in the nucleus (Figure 4-2AB). The localization of PPK20 in the PG was consistent among different samples using different drivers, indicating that there was no difference in PPK20 expression of the two isoforms (Figure 4-2A). In addition, tags at different termini did not show a significant localization difference (Figure 4-2B). However, the signal of the sample is very robust, suggesting that overexpression might cause the artifact effect, and it could be mitigated by using a weaker PG-specific Gal4 driver, *i.e.*, *spookier-Gal4*.

In short, the results showed that the expression of *ppk20* in the PG was mainly on the plasma membrane, which supported the prediction that PPK20 might play a role in cellular iron import. Thus, without PPK20 function, the porphyria-like phenotype PG was likely caused by a lack of cellular iron. Additionally, the subcellular localization might give more details about the role of PPK20; for example, if PPK20 co-localizes with mitochondria, it might indicate that PPK20 functions in mitochondrial iron import. However, due to the small size of the PG cells, the expression pattern of PPK20 in the cytoplasm was not very clear. The size of the salivary gland cell is much bigger; therefore, it was an excellent candidate for determining the subcellular localization of PPK20.

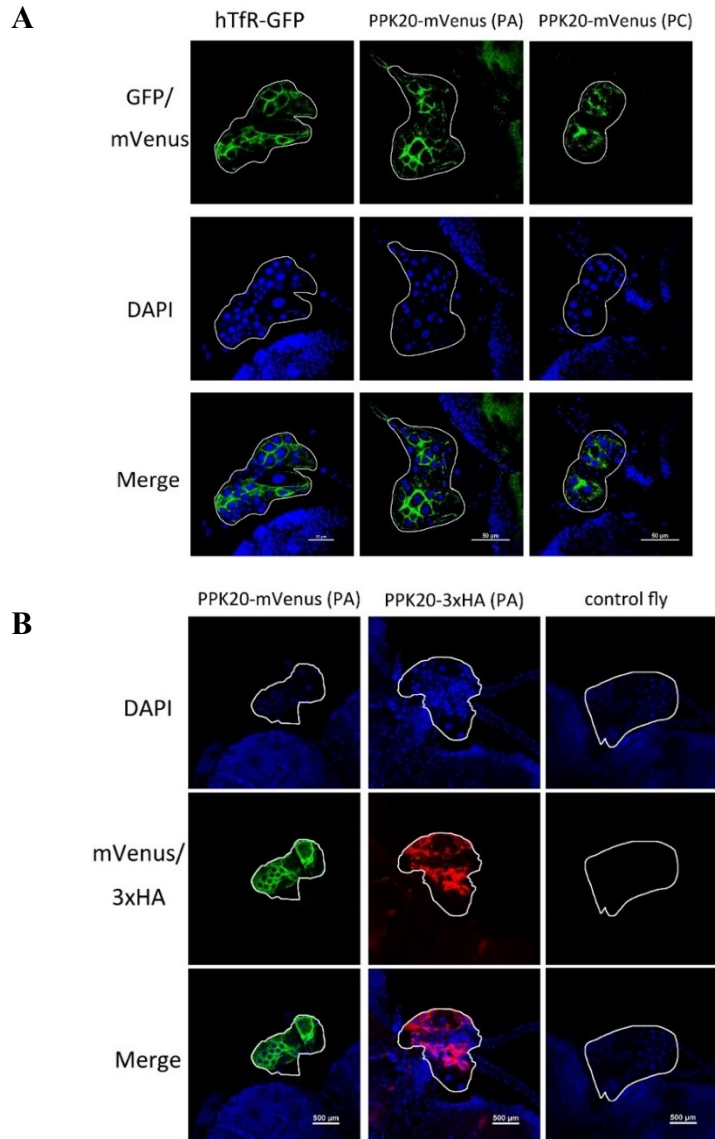


Figure 4-2. Localization of PPK20 in larval PG.

A. PPK20 isoforms A and C (PA and PC) showed robust expression on the plasma membrane and faint expression inside the cytoplasm. hTfR-GFP was used as the positive control to show the localization of a plasma membrane protein, and *actin-Gal4* ubiquitous driver was used to induce the larval whole-body expression of *ppk20*. B. PPK20 isoform A tagged at different termini mVenus (C terminus), and 3xHA (N terminus) showed robust expression on the plasma membrane and faint expression inside the cytoplasm. *w¹¹¹⁸* larvae were used as the negative control, and *tubulin-Gal4* (*αTub84B-Gal4*) ubiquitous driver was used to induce the larval whole-body expression of *ppk20*. (n>10, more than 10 larval PGs were examined for each group)

4.2.2 Localization of PPK20 in various larval tissues using *actin-Gal4* driver

Various tissues were collected, prepared and analyzed to determine the PPK20 localization in these tissues using the same approach described in 4.2.1. These tissues include the salivary gland, gut, trachea, and fat body. The *tubulin-Gal4* and *actin-Gal4* drivers were used to induce the whole-body overexpression of *ppk20* in larvae.

In general, the expression pattern of PPK20 was consistent among different tissues, which was mainly on the plasma membrane and some unknown subcellular compartments resembling vesicle-like structures. Based on many trial experiments and the staining results shown in the PG, PPK20 with 3xHA tag (PPK20-HA) did not have the ideal outcome since it requires a more prolonged staining process than PPK20-mVenus animals. Moreover, the prolonged staining process caused tissues to deteriorate, which compromised their integrity, and no ideal intact tissues could be observed. Therefore, most staining experiments were conducted using mVenus tagged PPK20 lines to achieve better results because the mVenus tag can autofluoresce and does not need the antibody staining process.

(1) PPK20 expression pattern in the fat body

In *Drosophila*, the fat body plays a similar role to the human liver, which controls energy storage and utilization. In terms of their differences, the human liver has a solid structure, whereas the fly fat body is made of loose tissues [209].

The expression of *ppk20* was mainly on the plasma membrane and inside cells of the fat body tissue (Figure 4-3A). After the staining process, the cells became looser; as shown in the figure, the integrity of the plasma membrane was compromised, and the outline of the cell membrane could barely be seen. Although the fat body cells appeared larger than PG cells, the subcellular structures were still very blurry. The substantial subcellular distribution might represent the route of PPK20 being transported to the plasma membrane, suggesting that the fat body could be used as a target site to synthesize PPK20. This finding would be used for a proposed future experiment on expressing iron-containing proteins (see chapter 6). The intracellular

distribution could also be the co-localization of PPK20 with organelles, and this possibility needs further experiment to validate.

(2) PPK20 expression pattern in the tracheal system

Previous literature [210, 211] suggested that it is not feasible to detect subcellular protein localization in the *Drosophila* tracheal system because the epithelial layer is extremely thin, and the light microscope cannot distinguish the subcellular structures. However, it is possible to track protein localization across different tracheal branches, including dorsal trunks, primary, secondary, and terminal branches.

The results showed that the expression of *ppk20* outlined the tracheal branches without overlapping with nuclei (Figure 4-3B). The outline was the epithelial layer of the trachea, and the hollow interior was the lumen; thus, there was no distribution of PPK20 in the lumen. In addition, since the epithelial layer was too thin, it was impossible to distinguish between the membrane and cytosolic layers; therefore, the distribution of PPK20 might overlap in these two layers. Apart from the expression on the central trachea, the distribution was spread around the smaller branches. The distribution pattern suggests that PPK20 could play a role in water clearance and sodium exchange on the epithelial layer of the tracheal network due to its sodium channel function. However, further experiments need to be done to test this hypothesis (see chapter 6).

(3) PPK20 expression pattern on the salivary gland (SG)

In the SG, PPK20 had a robust expression on the plasma membrane, some unknown intracellular localization, and no expression in the nuclei (Figure 4-3C). The SG cells are involved in glue secretion during different developmental stages. PPK20 might have a role in maintaining the electrolyte balance during SG cells' high secretory activity [212, 213]. Due to the considerable size of the SG cells, it is evident that the intracellular distribution of PPK20 had a vesicle-like structure.

Before the subcellular localization of PPK20 is determined, there are several possibilities of what the vesicle-shaped structures could be: i) the vesicles are derived from the Golgi and

transport PPK20 to the plasma membrane, which maps out the protein synthesis pathway; ii) based on the hypothesis discussed in chapter 3, PPK20 might be the potential receptor for importing Tsf; hence, these vesicles could be the endocytosed structures containing clathrin for transporting Tsf; iii) the PPK20 distribution might co-localize with other organelles and carry out other functions in that specific organelle.

(4) PPK20 expression pattern on the intestine

PPK20 expression was mainly on the plasma membrane with scattered distribution in the cytoplasm at the intestinal region (Figure 4-3D). The mid-gut is the iron uptake region, and the anterior midgut is where iron accumulates. PPK20 was distributed in both intestinal regions, suggesting its potential role in free iron import in the gut (see 3.2.4).

Overall, the expression pattern of different PPK20 isoforms in different organs and tissues was consistent with the protein tags in either terminus using different Gal4 drivers, suggesting the localization of PPK20 might be mainly on the plasma membrane. The scattered distribution needs further experiments to analyze. So far, with the protein localization data, it is clear that the function of PPK20 could be related to its localization on the plasma membrane, in which it might regulate cellular iron import directly or indirectly. The intracellular distribution of PPK20 remains undetermined, and the structure resembles intracellular vesicles. If PPK20 were the potential fly receptor for Tsf, the Tsf import process could be mediated by PPK20 through recruiting clathrin as the coat protein forming endocytosis vesicles.

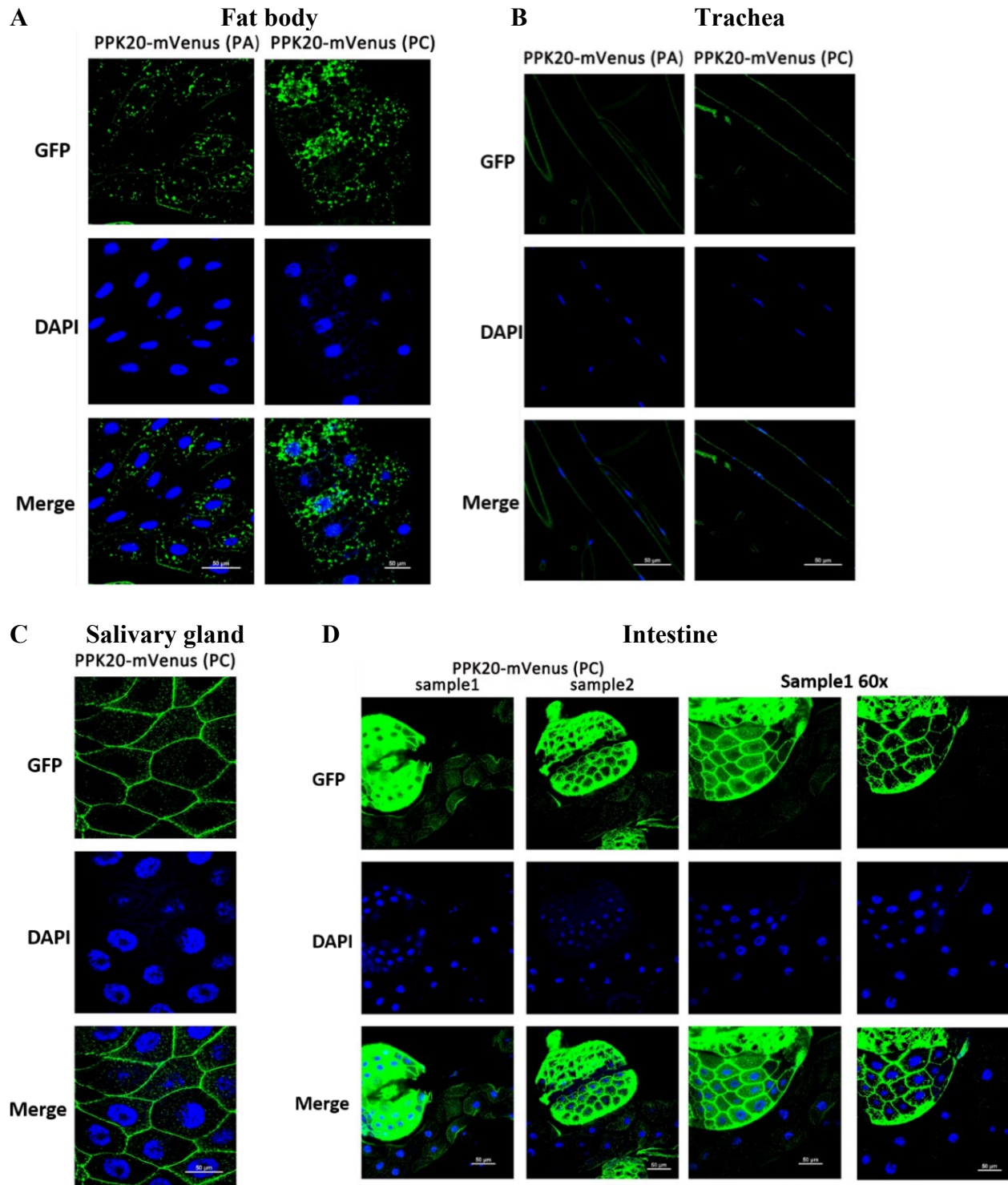


Figure 4-3. Localization of PPK20 in various larval tissues using the *actin-Gal4* driver.

A. PPK20 expression on the fat body. PPK20 isoforms PA and PC are expressed on the plasma membrane and inside fat body cells. B. PPK20 expression in the trachea. PA and PC are expressed

on the plasma membrane of epithelial cells, which outline the tracheal lining. C. PPK20 expression in the SG. PC is expressed on the plasma membrane and inside SG cells. D. PPK20 expression in the intestine. PC is found on the plasma membrane and inside the intestinal cells. (PA: PPK20 isoform A; PC: PPK20 isoform C; n>10, more than 10 larval tissues were examined for each group)

4.2.3 Immunoprecipitation and Western blot analysis of PPK20 expression

After the localization of PPK20 was determined, proteins that interact with PPK20 were to be identified next. The potential protein candidates might give clues to the functional network of PPK20. PPK20 was immunoprecipitated first, during which 4% formaldehyde was added to crosslink proteins, and WB was then carried out to ensure the protein quantity was detectable. The sample was sent for MS for a more detailed analysis to identify the proteins interacting with PPK20. According to UniProt, the size of PPK20 is approximately 67 kDa. The size of 3xHA and mVenus tags are 9 kDa and 26.9 kDa, respectively, making the sizes of PPK20-3xHA and PPK20-mVenus approximately 76 kDa and 94 kDa.

Late L3 larvae and BRGCs of late L3 larvae from different tag lines (Table 4-1) were collected separately for protein extraction and IP. For protein detection, WB was then carried out. The tagged PPK20 lines were used as the experimental groups, whereas the non-tagged wild-type animals were the negative control. The input samples were collected before the IP process, and flow-through samples were collected during IP, and they were both used as references (see 2.6).

The PPK20-3xHA sample was not very clearly detected on the blot, whereas the PPK20-mVenus sample was likely detected but with some nonspecific bands (Figure 4-4). Several reasons might cause the PPK20 to be undetected: i) the amount of PPK20 was too low to be detected by WB due to the unsuccessful IP process; ii) during the protein extraction process, PPK20 was digested by enzymes because of inappropriate temperature control, which also might be the reason for having the unspecific bands; iii) another possibility of not having the ideal result is that PPK20 might be a membrane protein which is known to be difficult to be extracted and separated. Thus, better positive controls and an optimized experimental process are needed to troubleshoot and improve the quality of results. In addition, sending the samples for MS can help determine if the WB result was accurate, and the protein candidate interacting with PPK20 may be recognized.

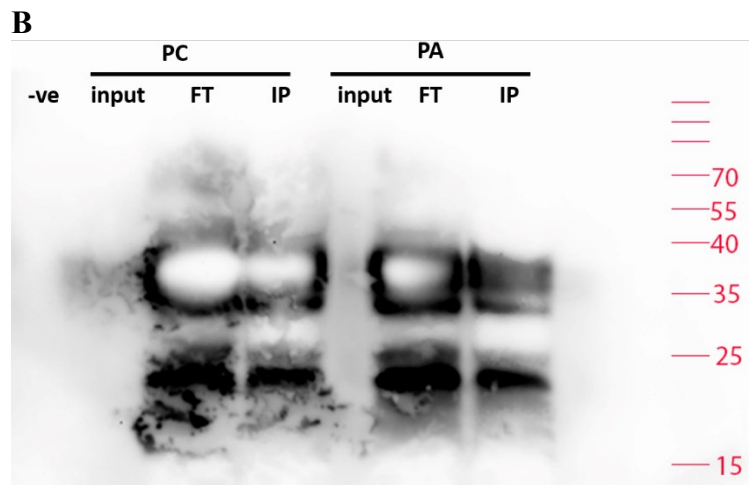


Figure 4-4. Validation of *ppk20* expression induced by the *tubulin-Gal4* driver using Western blot analysis.

A. The validation of PPK20-mVenus expression. The size of PPK20-mVenus is about 94 kDa, and it was detected in both IP samples of isoforms A and C. B. The validation of PPK20-3xHA expression. The size of PPK20-3xHA is about 76 kDa, and it was not detected in IP, input or FT samples of isoforms A or C. (IP: immunoprecipitation; FT: flow-through)

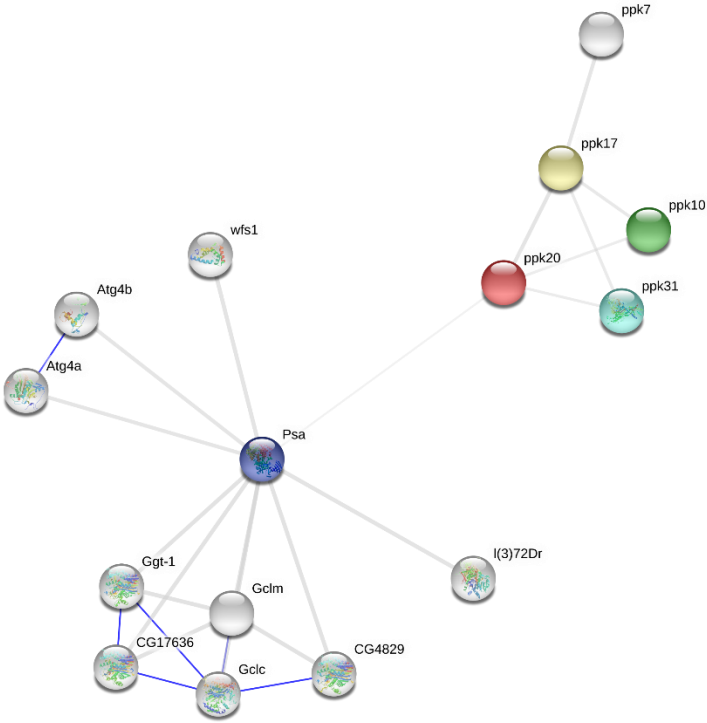
4.2.4 Mass spectrometry analysis

The Coomassie-stained protein-containing SDS-PAGE gels were sent for MS analysis to detect the proteins that might interact with PPK20. The detection was based on the protein-protein physical proximity established by the crosslink made by formaldehyde.

The result of MS turned out to be negative, meaning MS did not detect PPK20. Therefore, it was impossible to identify the protein candidates. Several possibilities might explain why this experiment did not have the desired results: i) the WB result was not accurate: the protein bands that had a similar size to PPK20 were not the target protein but nonspecific binding; ii) although WB was able to detect PPK20, the amount of PPK20 was too low for MS detection. Perhaps a higher concentration of PPK20 and a different approach to extracting membrane protein are required. Even if PPK20 could be detected, the crosslink might not be strong enough for finding the candidate proteins. Therefore, a better approach, TurboID, was proposed for a more accurate detection (see chapter 6).

4.2.5 Predicted PPK20 functional network


Thus far, proteins that interact with PPK20 have not been identified due to the negative results of WB and MS analyses, but there are tools available to predict the protein functional network. According to the predictions of String (<https://string-db.org/cgi/network.pl?taskId=15yez6yZSWfR>) [214], *ppk10*, *17*, *31* and *puromycin sensitive aminopeptidase (psa)* genes are in proximity with PPK20 (Figure 4-5). These *ppk* genes might be the candidates that form hetero-complexes with PPK20 and carry out activity together as a channel in sodium or iron import. Although these three genes had no distinctive features when screened for developmental and PG phenotypes (Table 3-1), they might come in proximity with PPK20, and more evidence is needed to confirm their interaction. As for *psa*, there is no evidence showing that PPK20 has a role in the peptide catabolic process [215], but this possibility could be explored. Although these could be gene candidates, the predictions made by String are not based on experimental evidence. They are solely based on computational analyses since no literature focuses on the study of *ppk20*. Therefore, this predicted PPK20 protein function network needs to be verified by co-IP and MS.




Nodes:


Network nodes represent proteins
splice isoforms or post-translational modifications are collapsed, i.e. each node represents all the proteins produced by a single, protein-coding gene locus.


Node Color

 *colored nodes:*
query proteins and first shell of interactors

 *white nodes:*
second shell of interactors

Node Content


 *empty nodes:*
proteins of unknown 3D structure


 *filled nodes:*
some 3D structure is known or predicted

Edges:


Edges represent protein-protein associations
associations are meant to be specific and meaningful, i.e. proteins jointly contribute to a shared function; this does not necessarily mean they are physically binding to each other.


Known Interactions


 *from curated databases*

 *experimentally determined*


Predicted Interactions


 *gene neighborhood*

 *gene fusions*

 *gene co-occurrence*

Others

 *textmining*

 *co-expression*


 *protein homology*

Figure 4-5. PPK20 protein interaction network based on the prediction of String.

The String prediction of PPK20's functional network: *ppk10*, *17*, *31* and *psa* genes may function in proximity with *ppk20* ([https://string db.org/cgi/network.pl?taskId=l5yez6yZSWfR](https://string-db.org/cgi/network.pl?taskId=l5yez6yZSWfR)). This prediction is based on computational analysis but not experimental evidence.

4.2.6 RNAseq result

A transcriptomic study was carried out to map out the functional network of *ppk20*. RNAseq is a powerful tool to identify the transcriptional changes of different genes. In this study, 18-hr L2 larval RG tissues collected from *ppk20^{KO}* animals were used in RNAseq. Consequently, significantly up- and down-regulated genes caused by knocking out *ppk20* were identified after analysis. The expression levels of genes that encode the enzymes involved in ecdysone synthesis were examined. The most relevant genes with at least a 2-fold change in transcript level compared to control were as follows:

(1) Downregulated genes: *Osiris (Osi)*, *spookier (spo)*, and *shade (shd)*

All 24 *Osi* genes were downregulated when *ppk20* was knocked out (Table 4-2). This gene cluster can be found at the *Drosophila Triplo-lethal* locus, and its synteny is well conserved in flies [216, 217]. *Osi* family was predicted to have endo-lysosomal signals and transmembrane domains. Moreover, the *Osi* proteins are highly expressed in vesicle-like structures at and near the apical membrane, and seven *osi* genes showed expression in the embryonic trachea (*osi* genes 9, 15, 17, 18, 19, 20 and 24) [218, 219]. Although the function of *Osi* is not determined, their localization in the tracheal system and cell membrane seems to overlap with PPK20, indicating their possible functional link: the loss of *ppk20* has led to the downregulation of all *osi* genes, which might disturb *Osi* function in the tracheal system, hence, causing tracheal necrosis (see chapter 5).

The *spo* and *shd* are two genes that encode the enzymes involved in the ecdysone synthesis. These two genes were downregulated by more than 10-fold and around 3-fold when *ppk20* was knocked down (Table 4-2), suggesting the synthetic pathway of ecdysone might be interrupted, which leads to decreased ecdysone production. A low concentration of ecdysone at certain stages of *Drosophila* growth can lead to developmental defects (see 1.5), which is consistent with the larval stage arrest phenotype observed in loss-of-*ppk20* animals, including *PG>ppk20-RNAi*, *ppk20^{KO}* and *ppk20^{FRT}* animals (see chapter 3).

(2) Upregulated genes: *Larval serum protein one (Lsp1) alpha/beta/gamma, Tsf1, Alas, phm, disembodied (dib) and shadow (sad)*

Lsp1 belongs to the hemocyanin superfamily [220, 221] and is one of the components that form hemolymph of L3 larva and pupa, emphasizing its importance in metamorphosis [222-224]. *Lsp1* genes were upregulated by more than 10-fold when *ppk20* was knocked out (Table 4-2), indicating that even with sufficient Lsp1, lack of ecdysone could still lead to the inability to initiate pupation (due to the lack of heme for CYPs). The result suggested that upregulated Lsp1 expression might prepare the larval to transition from the L2 to the L3 stage, but due to insufficient iron uptake in loss-of-*ppk20* animals, ecdysone pulses were disrupted; hence, most larvae stayed in the larval stage and were unable to metamorphose.

Tsf1 was upregulated more than 10-fold in the absence of *ppk20*, which indicates their functional link: perhaps without *ppk20*, Tsf1 cannot be imported; therefore, more is produced for compensation. This result is consistent with the observation in chapter 3 (see 3.2.5).

ALAS was also upregulated by 4-fold, which is consistent with the data observed in chapter 3 (see 3.2.3), suggesting that the heme synthesis pathway was disrupted.

Genes *phm*, *dib* and *sad* were upregulated by 2-3 folds, indicating that the ecdysone synthesis pathway was disrupted, hence causing the developmental phenotype in loss-of-*ppk20* animals.

4.3 Discussion

In summary, compared to the plasma membrane protein control hTfR, PPK20 localizes mainly to the membrane but can also be detected inside the cytoplasm in various tissues, including fat body, trachea, SG and intestine, using various overexpression tagged lines (Table 4-1). The results supported the previous prediction about PPK20 function, which is that PPK20 might be involved in cellular iron import on the plasma membrane. Although the subcellular localization of PPK20 is undetermined, the vesicle-shaped structures could be promising candidates as the PPK20-Tsf-clathrin vesicles that enter the cell through endocytosis. Further experiments and analyses were done to seek potential protein candidates that interact with PPK20.

4.4 Tables

Table 4-1[#]. The overexpression constructs of *ppk20* and their properties.

Transgene	Description
UAS-3xHA- <i>ppk20</i> ^{PA}	expresses wild type N terminal 3xHA-tagged <i>ppk20</i> PA cDNA under Gal4/UAS control
UAS- <i>ppk20</i> ^{PA} -mVenus	expresses wild type C terminal mVenus-tagged <i>ppk20</i> PA cDNA under Gal4/UAS control
UAS- <i>ppk20</i> ^{PC} -3xHA	expresses wild type C terminal 3xHA-tagged <i>ppk20</i> PC cDNA under Gal4/UAS control
UAS-mVenus- <i>ppk20</i> ^{PC}	expresses wild type N terminal mVenus-tagged <i>ppk20</i> PC cDNA under Gal4/UAS control

[#]indicates from “Characterizing new players involved in iron homeostasis during *Drosophila* larval development: Shifting the classic paradigm of iron metabolism” by Nhan Huynh, 2020, Doctor of Philosophy Thesis, 179, Copyright (2020) by the University of Alberta. Reprinted with permission with modification.

Table 4-2[#]. Genes identified in RNAseq.

Name	FBgn (Arraystar)	CG (Arraystar)	FC PPK:C	P value
<i>Osi9</i>	FBgn0037416	CG15592	-3401.24811	0.09
<i>Osi18</i>	FBgn0037428	CG1169	-2226.51332	0.101
<i>Osi19</i>	FBgn0037429	CG15189	-1647.35193	0.0413
<i>Osi15</i>	FBgn0037424	CG1157	-1507.18151	0.00382
<i>Osi20</i>	FBgn0037430	CG15188	-1308.35248	0.00334
<i>Osi7</i>	FBgn0037414	CG1153	-771.130191	0.0266
<i>Osi16</i>	FBgn0051561	CG31561	-520.127677	0.0114
<i>Osi8</i>	FBgn0037415	CG15591	-420.199274	0.00431
<i>Osi2</i>	FBgn0037410	CG1148	-267.207138	0.047
<i>Osi6</i>	FBgn0027527	CG1151	-234.964936	0.00133
<i>Osi4</i>	FBgn0037412	CG10303	-46.334301	0.183
<i>Osi17</i>	FBgn0037427	CG15598	-27.7371649	0.0298
<i>Osi5</i>	FBgn0037413	CG15590	-25.0213694	0.423
<i>Osi23</i>	FBgn0039771	CG15538	-19.4843694	0.423
<i>Osi13</i>	FBgn0037422	CG15595	-18.8231989	0.423
<i>Osi14</i>	FBgn0040279	CG1155	-18.6696733	0.0134
<i>Osi1</i>	FBgn0037406	CG15585	-13.9123472	0.423
<i>Osi3</i>	FBgn0037411	CG1150	-4.65199326	0.11
<i>Osi24</i>	FBgn0037409	CG15589	-4.2731288	0.0338
<i>Osi10</i>	FBgn0037417	CG15593	-4.20210231	0.0809
<i>Osi21</i>	FBgn0283678	CG14925	-3.80870845	0.0678
<i>Osi11</i>	FBgn0037418	CG15596	-2.34406791	0.839
<i>Osi22</i>	FBgn0038133	CG8644	-1.898912	0.886
<i>Osi12</i>	FBgn0037419	CG1154	-1.43544258	0.9
<i>spo</i>	FBgn0003486	CG10594	-10.73	0.143
<i>shd</i>	FBgn0003388	CG13478	-2.77	0.364
<i>Lsplgamma</i>	FBgn0002564	CG6821	56.11	0.033
<i>Lsplalpha</i>	FBgn0002562	CG2559	44.63	0.0121
<i>Lsplbeta</i>	FBgn0002563	CG4178	14.9	0.0692
<i>Tsfl</i>	FBgn0022355	CG6186	12.83	0.00175
<i>Alas</i>	FBgn0020764	CG3017	4.56	0.00176
<i>phm</i>	FBgn0004959	CG6578	3.80	0.0466
<i>dib</i>	FBgn0000449	CG12028	3.72	0.0897
<i>sad</i>	FBgn0003312	CG14728	2.58	0.0886

[#]indicates Nhan Huynh collected the data, analyzed by me, and reprinted with permission.

Chapter 5. PPK20 may be involved in larval tracheal liquid clearance

5.1 Introduction and rationale

While I was collecting the data for *PG>ppk20*-RNAi and *ppk20^{KO}* animal survival rate, I made an intriguing observation concerning the larval trachea in these animals. I found that the primary tracheal branches of some late L2 and L3 larvae (around 20-30%) showed a necrotic phenotype [225], while the WT control animals all had normal trachea. The observation was consistent in *PG>ppk20*-RNAi and *ppk20^{KO}* animals and was not seen in other RNAi lines disrupting other members of the *ppk* gene family (data not shown). Therefore, this phenotype was unique to loss-of-*ppk20* animals, which also might be related to the porphyria-like PG and developmental arrest phenotypes observed so far.

Interestingly, a study regarding RG-Specific transcripts analysis showed that genes *hs6st*, *esg*, *form3*, *torso*, *warts*, and *snail* might be involved in tube formation [101], suggesting that a similar regulatory process underlies the development of both the RG and the trachea. *PG>ppk20*-RNAi and *ppk20^{KO}* animals both had the porphyria-like PG phenotype, suggesting that tracheal tubing formation might be interrupted caused by the impaired PG function; hence the tracheal function might be affected.

In addition, another study has shown the expression of *ppk4* and *ppk11* in the fly tracheal system. Without PPK4 and PPK11 function, larval tracheal liquid clearance was affected [160]. The protein localization study has suggested that the PPK20 expression was mainly distributed on the plasma membrane of different tissues, especially on the tracheal epithelial layer (Figure 4-3B). Therefore, the tracheal necrotic phenotype was caused by the loss of PPK20.

So far, there was no evidence to show that the porphyria-like PG phenotype and the developmental defect were directly related to tracheal function. However, in the survival study, hemin dietary feeding, ferritin injection and *hTfR* cDNA expression only partially rescued animal

survival (see chapter 3), suggesting that a lack of iron was not the only consequence of PPK20 loss. Thus, it was possible that tracheal dysfunction might impact animal survival. Hence even when iron was supplemented, an ideal rescue effect for animals' survival could not be achieved.

The necrotic trachea was likely caused by the larvae's inability to perform the liquid clearance, and gradually, the trachea became more damaged due to O₂ deprivation, leading to cell death. Consequently, the damaged trachea might lose its integrity and collapse, resulting in blockage in O₂ transportation to the target areas. Additionally, the HIF pathway might be induced due to the low O₂ absorption [226] (see 1.9); hence, critical weight cannot be reached, causing the animals' developmental transitioning to be disrupted. Here, the tracheal necrosis phenotype will be studied to make further connections to the loss function of PPK20.

5.2 Results and discussion

5.2.1 Tracheal necrosis in *PG>ppk20-RNAi* and *ppk20^{KO}* animals

Two *Drosophila* PPK proteins, PPK4 and PPK11, had confirmed localization in the tracheal system. When *ppk4* and *ppk11* RNAi were injected into the larvae, they showed defects in tracheal liquid clearance [160]. Trachea necrosis in *PG>ppk20-RNAi* and *ppk20^{KO}* animals might indicate their functional defect to clear the liquid in the trachea (Figure 5-1). The primary tracheal branches were the main area with darkened tube necrotic phenotype, while the secondary and terminal branches had no apparent necrosis. Moreover, the necrotic phenotype was more severe when the larvae were kept in the food longer. It is worth noting that *ppk20^{KO}* animals had a more pronounced tracheal necrotic phenotype than *PG>ppk20-RNAi* animals, of which the necrotic region of *ppk20^{KO}* was more extended from the anterior part of the body to the posterior. In contrast, in *PG>ppk20-RNAi* animals, the necrotic region was only restricted to the anterior part of the body.

It was difficult to determine whether the tracheal necrosis was caused by PG malfunction in *PG>ppk20-RNAi* animals or the leaky expression driven by the *phm-Gal4* at the anterior part of the trachea [185], which is directly connected to the PG and the brain. Whereas in the *ppk20^{KO}* animals, the necrosis was likely caused by the collective loss of PPK20 in the whole-body larva.

Hence, the alternative PG-specific Gal4 driver, *spookier*, will be used to knock down PPK20 to determine whether the leaky expression was only limited to *phm-Gal4* driven expression.

The extensive larval tracheal network helps deliver O₂ to every part of the body, and this effective system is essential for larval survival [227]. Larvae raised in the lab spend a significant amount of time feeding in the food, suggesting they constantly live in an O₂ deprivation condition. When the tracheal system is damaged, it will cause the failure to deliver O₂ to the target tissues, resulting in larvae death. One of the reasons that could lead to tracheal function defects is its inability to clear water out of the tube to give way to O₂. Morphological development failure and inappropriate balance of epithelial ion exchange can lead to tracheal liquid clearance issues [160]. If PPK20 functions as the sodium channel on the tracheal epithelial layer, loss of PPK20 might disrupt sodium balance, causing the water to accumulate and not be cleared out. Consequently, the accumulated water might cause damage to the trachea and lead to insufficient oxygen delivery.

Moreover, the defective PG function caused by loss of PPK20 might lead to abnormal tracheal formation, which might be the second contributor to the necrotic phenotype. When the tube formation was disrupted, immature or damaged trachea could not satisfy the needs for O₂ of a growing larva, which might lead to suffocation hence causing cell death. The morphological under-development tracheal phenotype was observed in dissected larvae while conducting the ferric iron staining experiment, which will be discussed in 5.2.3.

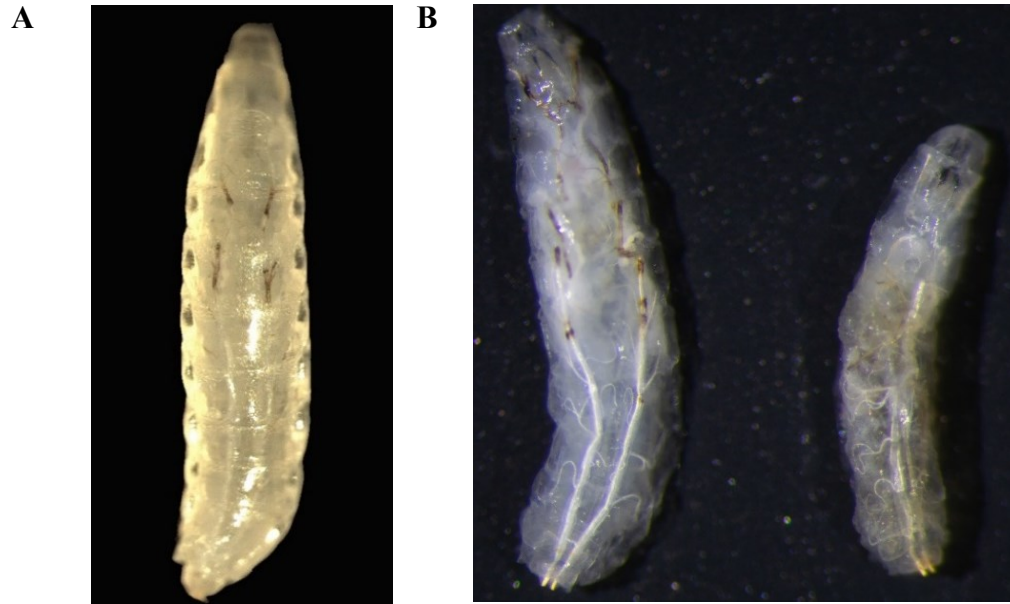


Figure 5-1. Loss of PPK20 causes larval trachea necrosis phenotype.

A. *PG>ppk20-RNAi* larvae had a necrotic tracheal phenotype. In the whole-body larva, the damaged trachea could be observed in the anterior part of the body. B. *ppk20^{KO}* larvae had a necrotic tracheal phenotype. The damaged trachea could be observed in the whole-body larva at the anterior to the posterior part.

5.2.2 Expression of *ppk20* in larval trachea

As described in 4.2.2, PPK20 expression in the tracheal system was observed, outlining the branches' epithelial layer without overlapping with the nuclei (Figure 4-3B). The strong expression of *ppk20* might indicate its function in the tracheal system; however, there are several pitfalls with using the transgenic overexpression constructs, which were discussed (see chapter 4). Although the function of PPK20 in the trachea is undetermined, the evidence of the PPK20 expression on the trachea and the necrotic tracheal phenotype observed in loss-of-*ppk20* animals suggest that PPK20 is needed for normal tracheal function, likely via its putative sodium channel function.

5.2.3 Loss-of-*ppk20* animals had less extensive tracheal branching

Apart from having the necrotic trachea, another unique trait of the *ppk20^{KO}* larval trachea was that these animals had a less extended tracheal network than the WT control. This feature could only be observed when the larvae were dissected, and it was difficult to be photographed under a light microscope (Figure 3-8). Only the intestines could be seen in ferric iron staining images, but not the tracheal. When conducting the whole larval intestine ferric iron staining experiment, it was noted that *ppk20^{KO}* larval gut was much easier to be separated from the tracheal network and cleaned than all the other groups (see 3.2.4). The major similarity that all the groups shared is that the primary trachea throughout the whole larval body had normal morphology, while the distinct difference of *ppk20^{KO}* larval trachea to others was that the sub-branches entering into the extremities of the larvae were less extended. These branches appeared to be very scarce in the intestinal region since they were convoluted and twisted together with the intestines, thus making it easy to separate.

ppk20^{KO} animals' less extended tracheal network might be caused by the function loss of PPK20 in the whole body, including the tracheal network. In comparison, *PG>ppk20-RNAi* or *gut>ppk20-RNAi* animals suffered from the loss of PPK20 in the PG and gut regions, respectively, but not in the tracheal region. Hence, the loss of PPK20 in the trachea of *ppk20^{KO}* animals had the most severe defect, resulting in impaired growth of the tracheal tubing system. Consequently, the reduced expansion of the branching tube system throughout the entire larval body may lead to

insufficient O₂ supply. Thus, constant exposure to hypoxia might lead to developmental defects and other problems for larvae, as O₂ is essential for animal survival by being involved in many biological processes [228], *i.e.*, participating in cellular aerobic respiration and regulating *Drosophila* airway branching [227]. In addition, the functional impairment of PG might affect tracheal morphology, causing the necrotic phenotype. In terms of tracheal growth, dysfunction of PG had a less noticeable effect.

5.3 Discussion

In summary, evidence showed that the loss of PPK20 function affected larval development and iron import, and it also caused the death of some tracheal cells leading to the tracheal necrotic phenotype. Damaged trachea could cause a defect in liquid clearance, which blocks air transport, leading to cellular hypoxia and larval death. The hypoxia might trigger the HIF pathway, which regulates iron bioavailability. Therefore, *PG>ppk20-RNAi* animals could only be partially rescued by hemin feeding, *hTfR* cDNA overexpression and ferritin injection since the supplement iron might not be sufficient to rescue the lethality caused by insufficient O₂ supply.

Interrupted PG function might also contribute to the impaired tracheal formation [101], thus causing the necrotic trachea in *PG>ppk20-RNAi* and *ppk20^{KO}* larvae. The more severely damaged tracheal phenotype and less extended tracheal network were observed in *ppk20^{KO}* larvae, suggesting PPK20 might function as a sodium channel directly on the tracheal to perhaps maintain the ion balance on the tracheal epithelial layer. Thus, when the tracheal epithelial ion balance could not be maintained due to the loss of PPK20, larval tracheal functions were disrupted, causing subsequent damage to its formation and development.

Therefore, PPK20 might mediate not only cellular iron import, but also the tracheal liquid clearance. The necrosis trachea phenotype could be caused by loss of PPK20, and is independent of the impaired iron import. However, the impaired tracheal function might be solely caused by cellular iron deficiency, not the loss of PPK20' putative channel function on the tracheal epithelial layer. Thus, how PPK20 might affect the tracheal function need to be investigated.

Chapter 6. Future directions and Conclusion

6.1 Future directions

Drosophila is ideal for studying iron and heme homeostasis, with its many tools available for genetic modification. From the two-step RNAi screen, our lab identified many genes that might be involved in heme synthesis. *ppk20* was one of the genes that were identified from the screen. As a potential membrane protein, PPK20 belongs to the DEG/ENaC family and is predicted to have sodium channel function. Loss-of-PPK20 animals showed developmental defects and porphyria-like PG phenotypes. Hemin partially rescued the survival rate while iron and PPIX feeding had no rescue, confirming that the heme synthesis pathway was disrupted when PPK20 was absent.

The partial rescue of the animal survival rate from *hTfR* cDNA expression and intestinal ferric iron staining suggested that PPK20 mediates cellular iron import. The PPK20 location mainly on the plasma membrane also suggested that it might function in cellular iron importing. Furthermore, the tracheal necrosis phenotype suggested that PPK20 might play a role in water clearance on the tracheal epithelial layer.

6.1.1 PPK20 mediates cellular iron import

The preliminary data showed that loss-of-PPK20 animals could not be rescued by dietary iron supplementation, but could be rescued by hemin feeding, *hTfR* cDNA expression and ferritin injection (Figures 3-4, 3-9 and 3-10), suggesting that if the animals were supplied with sufficient iron, they could survive to later stages. However, no direct results showed that the cellular iron import was responsible for the phenotypic rescue. Thus, it is critical to determine if PPK20 directly affects iron importing. Therefore, it is essential to quantify the iron level inside the RG cells with the presence and absence of PPK20. Once the iron level is measured inside the RG of *ppk20*-RNAi and *ppk20*^{KO} animals compared to the WT control animal, it will be apparent if the loss of *ppk20*

affects cellular iron import. If the PG iron level of *PG>ppk20* RNAi is lower than control animals, then it probably suggests that without PPK20, cellular iron import is impaired. In *ppk20^{KO}* animals, the iron staining in all tissues and organs is expected to be low since the ferric iron staining data showed the possibility that iron might not be imported or accumulated in different regions of the intestine (Figure 3-8). Apart from the intestine, even if enough iron is circulating, other tissues and organs cannot take in iron without PPK20 function resulting in faint staining compared to the control.

Is Tsf or ferritin the primary fly systemic iron carrier?

Another intriguing piece of evidence linking PPK20 function with the cellular iron import was that *hTfR* cDNA expression partially rescued the survival rate of *PG>ppk20*-RNAi animals. The most likely explanation for the survival rescue is that Tsf cannot enter the cells without PPK20, but there is no evidence showing that Tsf was imported when hTfR was expressed. Moreover, in *Drosophila*, it is unclear whether Tsf is the systemic iron carrier, based on literature [46] and the injection data (Figure 3-10), ferritin could be another candidate. Therefore, the localization of Tsf and ferritin associated with the loss of PPK20 needs to be characterized. Many aspects of Tsf and ferritin function are undetermined in *Drosophila*, including whether either protein is the iron carrier that delivers systemic iron to cells. The absence of an identified fly TfR could indicate that the Tsf/TfR pathway may not be the primary cellular iron import process in insects. Interestingly, the hemolymph ferritin concentration in flies is around 1,000-fold higher than that of human serum, suggesting it may be necessary for systemic iron delivery [201, 202, 229] and ferritin injection partially rescued *ppk20^{KO}* animal survival.

In this proposed experiment, fat bodies will be used to overexpress tagged Tsf (Tsf-Flag) and ferritin (Fer1HCH-GFP) individually to track their intracellular and hemolymph localization. Whether tagged Tsf and ferritin could be transported into PGs and other tissues of the WT and *ppk20*-depleted larvae (*ppk20^{KO}*) will be tested. If Tsf and ferritin could be transported into other tissues and organs of the WT animals, suggesting the proteins could be the systemic iron carrier and imported into cells. Consequently, if in the *ppk20^{KO}* animals, these two proteins could not be

imported into other tissues and organs from fat bodies, it would indicate that loss-of-PPK20 impairs the Tsf or ferritin import pathway.

WB analysis and confocal microscopy will be conducted to confirm Tsf and ferritin uptake into target cells. Major tissues and organs will be dissected and examined under the confocal microscope to determine the localization of the proteins of interest. WB will validate confocal microscopy results because the transgenically expressed proteins can be identified by detecting their respective tags. WB will also be used to analyze larval hemolymph to confirm whether ferritin or Tsf is secreted into the hemolymph. If fat body-produced Tsf or ferritin can be detected in hemolymph and other tissues, this would suggest that Tsf or ferritin could be used to transport iron to target tissues as a systemic iron carrier, indicating Tsf or ferritin is the fly equivalent of human Tsf.

To examine whether elemental iron, holo-ferritin, or apo-ferritin injection can rescue the *PG>ppk20*-RNAi phenotypes

Under *ppk20*^{KO} genetic background, the survival rate was partially rescued when ferritin^{hu/ho} was injected into the larval hemolymph. The result suggested that the import of ferritin might not require the PPK20 function. And if the iron import is compromised due to the lack of *ppk20* expression, then flooding the system with more ferritin might compensate for that loss. Ferritin^{hu/ho} overexpression can partially rescue the pupal survival but not that of adult, indicating that ferritin heavy and light chains might not be able to form ferritin complex with *Drosophila* heavy/light chains. Thus, no usable ferritin was made to carry iron and circulate hemolymph.

Further examination will be done in *PG>ppk20*-RNAi animals. If ferritin injection could rescue the survival rate of *PG>ppk20*-RNAi animals, which might suggest that the iron import to the PG might be disrupted due to the loss of PPK20; with an excessive amount of ferritin, iron could be successfully imported into PG tissues without PPK20 function. On the contrary, if injection cannot rescue, animals may have enough ferritin but cannot be utilized in the PG, likely due to the interrupted ferritin import pathway caused by losing PPK20.

Another experiment will be carried out to test whether the rescue of ferritin injection was due to the bound iron (*i.e.*, holo-ferritin) or the ferritin protein itself (without iron, namely the apo-ferritin). For this approach, BPS (an iron chelator) will be added to commercial ferritin before injection to get rid of the iron, and commercially available apo-ferritin can also be used. Furthermore, the ferritin will be boiled to denature the protein leaving the iron by itself. If there is a rescue with BPS-treated or holo ferritin, it could only be originated from ferritin protein. On the other hand, if boiled ferritin injection could rescue, this would suggest that iron was the component that rescued the survival.

6.1.2 PPK20 functional network

Validation of the RNAseq data

After performing the experiments above, the relation between PPK20 and cellular iron import should become more evident. Next, it is necessary to map out the network of how PPK20 mediates the iron import, and the genes identified from the RNAseq data are excellent candidates. qPCR will first be used to validate and quantify the up-and down-regulation of the candidate genes. The downregulated candidate genes will be used to rescue *ppk20^{KO}* animals, and if there is a rescue effect, then it might suggest that the genes may be associated with the *ppk20* gene function. In contrast, the upregulated genes might have a compensatory effect on the loss of function of *ppk20*.

However, the whole-body RNAseq experiment might not be accurate enough to determine PPK20 function in different tissues or organs, as it is evident now that PPK20 functions specifically in PG, gut and trachea. Therefore, a tissue-specific RNAseq will be conducted to determine how the loss of *ppk20* affects the expression of gene candidates more accurately in different tissues. As previously mentioned, PG and tracheal function might be related; comparing the data may reveal the connection between PG and the tracheal system because knocking out/down *ppk20* gene in the PG causes tracheal necrosis.

Subcellular localization of PPK20

Based on the observation of the protein localization study in chapter 4, many remaining questions could be answered through further experiments. First, the subcellular localization of PPK20 needs to be determined to characterize its function better. Specific organelle trackers could be used to determine the subcellular localization of PPK20 at various organelles, *e.g.*, ER, mitochondrion and Golgi. In such ways, it will help demonstrate the temporal and spatial localization of PPK20 expression. The co-localization of PPK20 with a specific organelle tracker might indicate its localization in that organelle. For example, if PPK20 shows robust localization on the mitochondrial membrane, which might suggest that PPK20 might be regulating the iron intake of mitochondria. However, it is possible that the protein synthesis pathway will be tracked, which means that cytoplasmic localization does not represent the functional site of PPK20 but only the synthetic pathway.

Identifying the protein candidates that interact with PPK20

It is crucial to identify the proteins that interact with PPK20 in proximity because PPK20 might directly or indirectly work with potential Tsf/ferritin receptors. Tagged PPK20 will be used for IP and sent for MS analysis (Table 4-1). If the proteins interact closely with PPK20, they would be expected to be pulled down together by IP and recognized by MS, and they could be the protein candidates as Tsf/ferritin receptors. Suppose Tsf or ferritin is the systemic iron carrier and could be imported through receptor-mediated endocytosis by recruiting clathrin as a co-protein; in this case, the co-IP pull-down experiment of PPK20 could validate the association of receptor candidates, clathrin and Tsf/ferritin.

As mentioned in chapter 3, apart from being co-localized with different organelles, the undefined intracellular PPK20-containing vesicle-shaped structures could be the vesicles derived from the receptor-mediated endocytosis. Hence these structures might consist of the cargo (Tsf/ferritin), clathrin and receptor. The co-IP experiment will test whether PPK20/clathrin/Tsf and PPK20/clathrin/ferritin interact closely. If Tsf or ferritin can be imported through receptor-mediated endocytosis associated with clathrin, they should be pulled down by using clathrin as bait. Whether PPK20 would be pulled should determine if it could act as the receptor for either protein. If PPK20 only interacts with clathrin might indicate that the vesicle structures only

transport PPK20 to the plasma membrane after being synthesized, and it is not the receptor for ferritin/Tsf import.

In terms of the approach for identifying candidate proteins that interact with PPK20, MS is the standard procedure used in our lab. The larval whole-body and tissue-specific MS will be conducted to identify the proteins interacting with PPK20. Once the protein candidates are recognized, a co-IP experiment will be conducted to validate their interaction. However, this approach is not accurate enough to recognize proteins that interact closest to PPK20, and the reason is that the crosslink made between different proteins is transient; a better approach will be applied.

For a more precise protein-protein interaction (PPI) recognition, a more specific, reliable, and advanced TurboID system will be performed to identify proteins interacting with PPK20. TurboID utilizes the enzyme-catalyzed proximity labelling (PL) method to label the proteins that come in close contact with PPK20 in living cells [230, 231]. This new and improved TurboID technique avoids the disadvantages of crosslinks made by formaldehyde, which is temporary and resembles taking a snapshot of the protein interaction. After the biotin labelling, the samples will be sent for MS analysis, and candidate proteins could be identified. Proteins identified by MS in combination with TurboID will be the potential candidates interacting with PPK20. Those candidate proteins might map out the PPK20 functional network.

6.1.3 PPK20 function in the tracheal system

In chapter 5, the possibility that PPK20 might be involved in tracheal formation and function was discussed. Further experiments will explore how exactly PPK20 might function in the tracheal system.

Whether loss of PPK20 causes impaired tracheal gas filling and liquid clearance

Based on previous literature [232], a test on the tracheal gas filling experiment can be conducted to score gas filling levels of *PG>ppk20-RNAi* and *ppk20^{KO}* animals. Another approach that could test the functional integrity of the trachea is the fluid filling experiment: the larvae will

be put into the coloured food to track if the liquid can be cleared through the whole tracheal system; a blind test will be used to score the trachea's damage.

The predicted outcome is that loss-of-PPK20 animals would suggest the defects in tracheal liquid clearance and gas filling, causing them to suffer from hypoxia. If the same result can be observed in *PG>ppk20-RNAi*, that might suggest the functional link between PG and trachea.

O₂ rescue experiment

If the damaged trachea cannot deliver enough oxygen to larval tissue under normal oxygen conditions, supplying the larvae with extra oxygen may rescue their survival. Wild-type animals supplied with enough oxygen can be used as the control; another control can be added to test if a low oxygen supply will reduce WT animals' survival rate.

ppk20^{KO} animals with necrotic and normal trachea will be tested for oxygen rescue; the larvae with normal trachea are expected to have a better survival rate than the necrotic tracheal larvae since they have the normal tubing morphology to deliver oxygen. However, the problem with this experiment is that most hypoxia or hyperoxia studies were conducted using adult flies by changing the O₂ in particular apparatus [233]. It is more difficult to change the O₂ gradient for larvae because they live in a semi-solid food environment that lacks O₂ supply.

The function of PPK20 in tracheal formation

To study how PPK20 affects tracheal development, the characteristics of the WT, *PG>ppk20-RNAi* and *ppk20^{KO}* larval trachea need to be examined, *i.e.*, measuring tracheal length and width [234]. From the embryonic to L3 larval stage, the length and width of the animal trachea can be measured for comparison. The result might directly show whether tracheal development is affected by the loss of PPK20. If there is a significant reduction in length and width of the trachea in *ppk20^{KO}* larvae than in the WT control larvae, it might suggest that loss of PPK20 in the trachea could lead to its abnormal development. Consequently, if the same abnormal tracheal growth pattern could be observed in *PG>ppk20-RNAi* animals, it might indicate the functional link between PG and trachea.

6.1.4 The putative sodium channel function of PPK20

Last but not least, the possibility that PPK20 might have sodium channel activity can be explored by restoring and inhibiting its putative channel function. The phenotypes observed in loss-of-PPK20 animals, *i.e.*, developmental defect, porphyria-like PG, and tracheal necrosis, may be caused by the loss of PPK20 channel function, leading to inappropriate sodium balance on the cell membrane. Therefore, the sodium channel function of PPK20 can be studied as follow:

The restoring of possible sodium channel function

Iron import might happen concurrently with sodium import [161], which means there will be no iron import if there is no sodium transport. Additional sodium ions (NaCl, with different concentration gradients) will be added to the food to restore the Na⁺ import, presumably by recruiting other PPK proteins in the absence of PPK20. The experiment will first be conducted in the *PG>ppk20*-RNAi animals since their other organs should function normally. Thus, the extra Na⁺ should get into the hemolymph through feeding, reach the PG cell surface, and restore the Na⁺ influx. If the adult survival rate can be improved significantly, it might indicate that PPK20 works as a sodium channel and iron import depends on the normal concurrent Na⁺ influx. Consequently, the cellular iron import might recover with the balance restored on the plasma membrane. On the contrary, no phenotypic rescue could indicate that PPK20 does not function in sodium import, or its role in iron import is independent of its channel function, or other PPK proteins could not substitute PPK20 channel function.

The inhibition of possible sodium channel function

Amiloride is a sodium channel inhibitor that can disrupt all PPK channel functions. The addition of amiloride might be detrimental to larvae because Na⁺ is essential for survival. Therefore, amiloride will be added to the food after WT fly larvae turn into the L3 stage in order to observe better results. The survival rate and the PG phenotype will be examined. Preliminary data showed that only loss of *ppk20* had larval stage arrest and porphyria-like PG phenotypes in all 31 *ppk* gene PG-specific RNAi knockout lines (Table 3-1). With the addition of amiloride to

late L3 WT animals, if they show the porphyria-like PG phenotype, it is most likely caused by lacking PPK20 function.

Based on the experiment above, if the porphyria-like PG phenotype could be induced by adding amiloride, another experiment could be conducted to validate and complement the result. Amiloride will be added to *ppk20* cDNA overexpression animals' diet to determine if more *ppk20* expression could rescue the animals (Table 4-1). However, this prediction is based on the assumption that the expression of *ppk20* out titrates the added compound.

The gut-specific ferric iron staining will be conducted to test whether these animals' gut iron uptake is interrupted. If amiloride feeding could lead to larval iron uptake deficit by demonstrating no or less ferric iron staining in the gut, then loss of sodium channel function might be affecting the iron import.

6.2 The summary of the study

ppk20, as one of 31 *ppk* genes in the DEG/ENaC family, was the only *ppk* gene that has shown a consistent red PG phenotype and developmental defects when its expression was lost. All the results presented in this thesis revealed the involvement of PPK20 in *Drosophila* cellular iron import, as iron is needed for heme synthesis and other vital biological processes. Although the specific function of PPK20 remains unclear, it has potential roles in mediating cellular iron import via interaction with the hTfR-like protein on the plasma membrane or acting as the free iron/Tsf transporter. As the data showed, the localization of PPK20 on the plasma membrane might be related to its role in regulating iron import. Although it has not been determined yet, this subcellular localization of PPK20 might indicate a role in regulating iron transport into the mitochondrion, which may explain its involvement in the heme synthesis pathway. Moreover, the tracheal necrosis phenotype suggested a potential role for PPK20 in tracheal formation and function. Lack of tracheal function may lead to oxygen deprivation, which ultimately causes larval death. Since iron, oxygen, and a tracheal system for oxygen delivery, are all essential in *Drosophila*, mapping out the regulation network of *ppk20* will improve the current understanding of the iron transport model and possibly its connection to other regulatory pathways.

In summary, the cellular iron import remains poorly understood in *Drosophila* compared to the human model, despite the critical role of iron in organism survival. The study of PPK20 function in cellular level iron uptake may help elucidate the process and reveal whether it is evolutionary conserved.

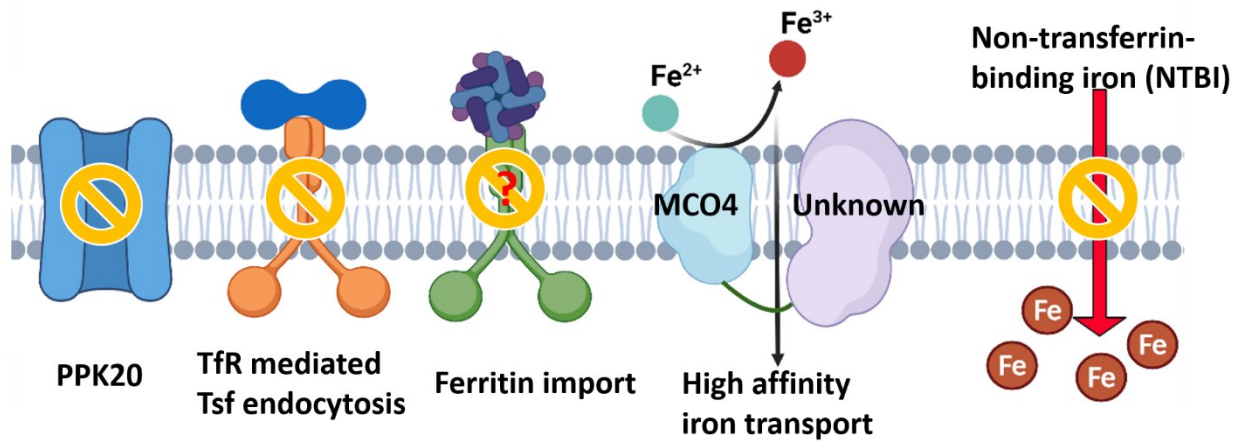


Figure 6-1. The overall summary of PPK20 might mediate Tsf, NTBI and ferritin import.

With PPK20 function, there will be a normal cellular iron import. On the other hand, without *ppk20* expression, the cellular iron level may be low due to the lack of import of the non-protein-binding iron and iron carrier proteins (Tsf and/or ferritin).

Literature cited

1. Klinge, S., et al., *An iron-sulfur domain of the eukaryotic primase is essential for RNA primer synthesis*. Nat Struct Mol Biol, 2007. **14**(9): p. 875-7.
2. Rudolf, J., et al., *The DNA Repair Helicases XPD and FancJ Have Essential Iron-Sulfur Domains*. Molecular Cell, 2006. **23**(6): p. 801-808.
3. Gari, K., et al., *MMS19 links cytoplasmic iron-sulfur cluster assembly to DNA metabolism*. Science, 2012. **337**(6091): p. 243-5.
4. Abbaspour, N., R. Hurrell, and R. Kelishadi, *Review on iron and its importance for human health*. Journal of research in medical sciences : the official journal of Isfahan University of Medical Sciences, 2014. **19**(2): p. 164-174.
5. Lakhali-Littleton, S. and P.A. Robbins, *The interplay between iron and oxygen homeostasis with a particular focus on the heart*. J Appl Physiol (1985), 2017. **123**(4): p. 967-973.
6. Hentze, M.W., et al., *Two to tango: regulation of Mammalian iron metabolism*. Cell, 2010. **142**(1): p. 24-38.
7. Shi, R., et al., *Biogenesis of Iron-Sulfur Clusters and Their Role in DNA Metabolism*. Front Cell Dev Biol, 2021. **9**: p. 735678.
8. Cook, J.D., et al., *Estimates of iron sufficiency in the US population*. 1986.
9. Layrisse, M., et al., *Food Iron Absorption: A Comparison of Vegetable and Animal Foods*. Blood, 1969. **33**(3): p. 430-443.
10. McDowell, L.R., *Minerals in animal and human nutrition*. 2003: Elsevier Science BV.
11. Weiss, J.J., *NATURE OF THE IRON-OXYGEN BOND IN OXYHAEMOGLOBIN*. Nature, 1964. **202**: p. 83-4.

12. Ordway, G.A. and D.J. Garry, *Myoglobin: an essential hemoprotein in striated muscle*. J Exp Biol, 2004. **207**(Pt 20): p. 3441-6.
13. Longeville, S. and L.R. Stingaciu, *Hemoglobin diffusion and the dynamics of oxygen capture by red blood cells*. Sci Rep, 2017. **7**(1): p. 10448.
14. Poulos, T.L., *Heme enzyme structure and function*. Chem Rev, 2014. **114**(7): p. 3919-62.
15. Efimov, I., et al., *Structure and reaction mechanism in the heme dioxygenases*. Biochemistry, 2011. **50**(14): p. 2717-24.
16. Munro, H.N., et al., *The Ferritin Genes: Structure, Expression, and Regulation*. Annals of the New York Academy of Sciences, 1988. **526**(1): p. 113-123.
17. Ponka, P., C. Beaumont, and D.R. Richardson, *Function and regulation of transferrin and ferritin*. Semin Hematol, 1998. **35**(1): p. 35-54.
18. Ford, G.C., et al., *Ferritin: design and formation of an iron-storage molecule*. Philos Trans R Soc Lond B Biol Sci, 1984. **304**(1121): p. 551-65.
19. Fletcher, J. and E.R. Huehns, *Function of Transferrin*. Nature, 1968. **218**(5148): p. 1211-1214.
20. Rouault, T.A. and R.D. Klausner, *Iron-sulfur clusters as biosensors of oxidants and iron*. Trends in biochemical sciences, 1996. **21**(5): p. 174-177.
21. Jordan, S.F., et al., *Spontaneous assembly of redox-active iron-sulfur clusters at low concentrations of cysteine*. Nat Commun, 2021. **12**(1): p. 5925.
22. Yiannikourides, A. and G.O. Latunde-Dada, *A Short Review of Iron Metabolism and Pathophysiology of Iron Disorders*. Medicines (Basel), 2019. **6**(3).
23. Fleming, R.E. and P. Ponka, *Iron Overload in Human Disease*. New England Journal of Medicine, 2012. **366**(4): p. 348-359.
24. Makker, J., et al., *Dysmetabolic hyperferritinemia: all iron overload is not hemochromatosis*. Case Rep Gastroenterol, 2015. **9**(1): p. 7-14.

25. Feng, Q., et al., *Uptake, distribution, clearance, and toxicity of iron oxide nanoparticles with different sizes and coatings*. Sci Rep, 2018. **8**(1): p. 2082.
26. Parmar, J.H., et al., *Modeling the dynamics of mouse iron body distribution: hepcidin is necessary but not sufficient*. BMC Syst Biol, 2017. **11**(1): p. 57.
27. Papanikolaou, G. and K. Pantopoulos, *Systemic iron homeostasis and erythropoiesis*. IUBMB Life, 2017. **69**(6): p. 399-413.
28. Rodgers, G.M. and J.A. Gilreath, *The Role of Intravenous Iron in the Treatment of Anemia Associated with Cancer and Chemotherapy*. Acta Haematol, 2019. **142**(1): p. 13-20.
29. Gomez-Ramirez, S., et al., *Management of Perioperative Iron Deficiency Anemia*. Acta Haematol, 2019. **142**(1): p. 21-29.
30. Gafter-Gvili, A., A. Schechter, and B. Rozen-Zvi, *Iron Deficiency Anemia in Chronic Kidney Disease*. Acta Haematol, 2019. **142**(1): p. 44-50.
31. Pasricha, S.-R., et al., *Iron deficiency*. The Lancet, 2021. **397**(10270): p. 233-248.
32. McLean, E., et al., *Worldwide prevalence of anaemia, WHO Vitamin and Mineral Nutrition Information System, 1993-2005*. Public Health Nutr, 2009. **12**(4): p. 444-54.
33. Camaschella, C., *Iron-deficiency anemia*. N Engl J Med, 2015. **372**(19): p. 1832-43.
34. Elstrott, B., et al., *The role of iron repletion in adult iron deficiency anemia and other diseases*. Eur J Haematol, 2020. **104**(3): p. 153-161.
35. Ning, S. and M.P. Zeller, *Management of iron deficiency*. Hematology Am Soc Hematol Educ Program, 2019. **2019**(1): p. 315-322.
36. Yu, Y., et al., *Hepatic transferrin plays a role in systemic iron homeostasis and liver ferroptosis*. Blood, 2020. **136**(6): p. 726-739.
37. Knovich, M.A., et al., *Ferritin for the clinician*. Blood Rev, 2009. **23**(3): p. 95-104.
38. Georgieva, B.C.D.a.T., *Organization of the Ferritin Genes in Drosophila melanogaster*. DNA and Cell Biology, 1999. **18**(12): p. 937-944.

39. Gonzalez-Morales, N., et al., *Ferritin Is Required in Multiple Tissues during Drosophila melanogaster Development*. PLoS One, 2015. **10**(7): p. e0133499.
40. Hamburger, A.E., et al., *Crystal Structure of a Secreted Insect Ferritin Reveals a Symmetrical Arrangement of Heavy and Light Chains*. Journal of Molecular Biology, 2005. **349**(3): p. 558-569.
41. Jacobs, A. and M. Worwood, *Ferritin in Serum*. New England Journal of Medicine, 1975. **292**(18): p. 951-956.
42. Wang, W., et al., *Serum ferritin: Past, present and future*. Biochim Biophys Acta, 2010. **1800**(8): p. 760-9.
43. Cohen, L.A., et al., *Serum ferritin is derived primarily from macrophages through a nonclassical secretory pathway*. Blood, 2010. **116**(9): p. 1574-84.
44. Fisher, J., et al., *Ferritin: a novel mechanism for delivery of iron to the brain and other organs*. Am J Physiol Cell Physiol, 2007. **293**(2): p. C641-9.
45. Tang, X. and B. Zhou, *Iron homeostasis in insects: Insights from Drosophila studies*. IUBMB Life, 2013. **65**(10): p. 863-72.
46. Xiao, G., et al., *Transferrin 1 Functions in Iron Trafficking and Genetically Interacts with Ferritin in Drosophila melanogaster*. Cell Rep, 2019. **26**(3): p. 748-758 e5.
47. Yang, F., et al., *Human transferrin: cDNA characterization and chromosomal localization*. Proceedings of the National Academy of Sciences, 1984. **81**(9): p. 2752-2756.
48. Lane, R.S., *Transferrin Synthesis in the Rat: A Study Using the Fluorescent Antibody Technique*. British Journal of Haematology, 1968. **15**(4): p. 355-364.
49. Lane, R.S., *Localization of Transferrin in Human and Rat Liver by Fluorescent Antibody Technique*. Nature, 1967. **215**(5097): p. 161-162.
50. Pearse, B.M. and M.S. Robinson, *Clathrin, adaptors, and sorting*. Annu Rev Cell Biol, 1990. **6**: p. 151-71.

51. Parmley, R.T., J.C. Barton, and M.E. Conrad, *Ultrastructural localization of transferrin, transferrin receptor, and iron-binding sites on human placental and duodenal microvilli*. British Journal of Haematology, 1985. **60**(1): p. 81-89.
52. Zhang, D., et al., *Characterization of transferrin receptor-mediated endocytosis and cellular iron delivery of recombinant human serum transferrin from rice (*Oryza sativa* L.)*. BMC Biotechnol, 2012. **12**: p. 92.
53. Kawabata, H., et al., *Molecular cloning of transferrin receptor 2. A new member of the transferrin receptor-like family*. J Biol Chem, 1999. **274**(30): p. 20826-32.
54. Kawabata, H., et al., *Expression of transferrin receptor 2 in normal and neoplastic hematopoietic cells*. Blood, 2001. **98**(9): p. 2714-2719.
55. Fleming, R.E., et al., *Transferrin receptor 2: continued expression in mouse liver in the face of iron overload and in hereditary hemochromatosis*. Proc Natl Acad Sci U S A, 2000. **97**(5): p. 2214-9.
56. Camaschella, C., et al., *The gene TFR2 is mutated in a new type of haemochromatosis mapping to 7q22*. Nat Genet, 2000. **25**(1): p. 14-5.
57. Mayle, K.M., A.M. Le, and D.T. Kamei, *The intracellular trafficking pathway of transferrin*. Biochim Biophys Acta, 2012. **1820**(3): p. 264-81.
58. Nichol, H., J.H. Law, and J.J. Winzerling, *Iron metabolism in insects*. Annu Rev Entomol, 2002. **47**: p. 535-59.
59. Gunshin, H., et al., *Cloning and characterization of a mammalian proton-coupled metal-ion transporter*. Nature, 1997. **388**(6641): p. 482-8.
60. Shawki, A., et al., *Intestinal DMT1 is critical for iron absorption in the mouse but is not required for the absorption of copper or manganese*. American journal of physiology. Gastrointestinal and liver physiology, 2015. **309**(8): p. G635-G647.
61. Rodrigues, V., et al., *malvolio, the Drosophila homologue of mouse NRAMP-1 (Bcg), is expressed in macrophages and in the nervous system and is required for normal taste behaviour*. The EMBO journal, 1995. **14**(13): p. 3007-3020.

62. Betti, L., et al., *Iron depletion in the intestines of Malvolio mutant flies does not occur in the absence of a multicopper oxidase*. Journal of Experimental Biology, 2011. **214**(6): p. 971-978.
63. Latunde-Dada, G.O., et al., *Molecular and Functional Roles of Duodenal Cytochrome B (Dcytb) in Iron Metabolism*. Blood Cells, Molecules, and Diseases, 2002. **29**(3): p. 356-360.
64. Lane, D.J., et al., *Duodenal cytochrome b (DCYTB) in iron metabolism: an update on function and regulation*. Nutrients, 2015. **7**(4): p. 2274-96.
65. Verelst, W. and H. Asard, *A phylogenetic study of cytochrome b561 proteins*. Genome Biology, 2003. **4**(6): p. R38.
66. Iliadi, K.G., et al., *nemy encodes a cytochrome b561 that is required for Drosophila learning and memory*. Proc Natl Acad Sci U S A, 2008. **105**(50): p. 19986-91.
67. Kamyshev, N.G., et al., *Novel memory mutants in Drosophila: behavioral characteristics of the mutant nemyP153*. BMC neuroscience, 2002. **3**: p. 9-9.
68. Mandilaras, K., T. Pathmanathan, and F. Missirlis, *Iron absorption in Drosophila melanogaster*. Nutrients, 2013. **5**(5): p. 1622-47.
69. Naikhwah, W. and M.J. O'Donnell, *Phenotypic plasticity in response to dietary salt stress: Na⁺ and K⁺ transport by the gut of Drosophila melanogaster larvae*. J Exp Biol, 2012. **215**(Pt 3): p. 461-70.
70. McKie, A.T., et al., *A novel duodenal iron-regulated transporter, IREG1, implicated in the basolateral transfer of iron to the circulation*. Mol Cell, 2000. **5**(2): p. 299-309.
71. Sharp, P. and S.-K. Srani, *Molecular mechanisms involved in intestinal iron absorption*. World journal of gastroenterology, 2007. **13**(35): p. 4716-4724.
72. Ganz, T., *Cellular iron: ferroportin is the only way out*. Cell Metab, 2005. **1**(3): p. 155-7.
73. Schimanski, L.M., et al., *In vitro functional analysis of human ferroportin (FPN) and hemochromatosis-associated FPN mutations*. Blood, 2005. **105**(10): p. 4096-102.

74. Griffiths, T.A.M., A.G. Mauk, and R.T.A. MacGillivray, *Recombinant Expression and Functional Characterization of Human Hephaestin: A Multicopper Oxidase with Ferroxidase Activity*. *Biochemistry*, 2005. **44**(45): p. 14725-14731.
75. Syed, B.A., et al., *Analysis of the human hephaestin gene and protein: comparative modelling of the N-terminus ecto-domain based upon ceruloplasmin*. *Protein Engineering, Design and Selection*, 2002. **15**(3): p. 205-214.
76. Dittmer, N.T. and M.R. Kanost, *Insect multicopper oxidases: Diversity, properties, and physiological roles*. *Insect Biochemistry and Molecular Biology*, 2010. **40**(3): p. 179-188.
77. Lang, M., et al., *Multicopper oxidase-1 is a ferroxidase essential for iron homeostasis in Drosophila melanogaster*. *Proc Natl Acad Sci U S A*, 2012. **109**(33): p. 13337-42.
78. Wu, S., S. Yin, and B. Zhou, *Molecular physiology of iron trafficking in Drosophila melanogaster*. *Current Opinion in Insect Science*, 2022. **50**: p. 100888.
79. Wang, X., et al., *Drosophila multicopper oxidase 3 is a potential ferroxidase involved in iron homeostasis*. *Biochimica et Biophysica Acta (BBA) - General Subjects*, 2018. **1862**(8): p. 1826-1834.
80. Park, C.H., et al., *Hepcidin, a urinary antimicrobial peptide synthesized in the liver*. *J Biol Chem*, 2001. **276**(11): p. 7806-10.
81. Zhang, D.-L., et al., *Hepcidin regulates ferroportin expression and intracellular iron homeostasis of erythroblasts*. *Blood*, 2011. **118**(10): p. 2868-2877.
82. Sangkhae, V. and E. Nemeth, *Regulation of the Iron Homeostatic Hormone Hepcidin*. *Adv Nutr*, 2017. **8**(1): p. 126-136.
83. Ganz, T. and E. Nemeth, *Regulation of iron acquisition and iron distribution in mammals*. *Biochim Biophys Acta*, 2006. **1763**(7): p. 690-9.
84. Paffetti, P., et al., *Non-protein-bound iron detection in small samples of biological fluids and tissues*. *Biological Trace Element Research*, 2006. **112**(3): p. 221-232.

85. Patel, M. and D.V. Ramavataram, *Non transferrin bound iron: nature, manifestations and analytical approaches for estimation*. Indian J Clin Biochem, 2012. **27**(4): p. 322-32.
86. Auten, R.L. and J.M. Davis, *Oxygen Toxicity and Reactive Oxygen Species: The Devil Is in the Details*. Pediatric Research, 2009. **66**(2): p. 121-127.
87. Turi, J.L., et al., *The iron cycle and oxidative stress in the lung*. Free Radic Biol Med, 2004. **36**(7): p. 850-7.
88. Arezes, J., et al., *Non-transferrin-bound iron (NTBI) uptake by T lymphocytes: evidence for the selective acquisition of oligomeric ferric citrate species*. PLoS One, 2013. **8**(11): p. e79870.
89. Dasa, F. and T. Abera, *Factors affecting iron absorption and mitigation mechanisms: a review*. International Journal of Agricultural Science and Food Technology, 2018. **4**(2): p. 024-030.
90. Wilkinson, N. and K. Pantopoulos, *The IRP/IRE system in vivo: insights from mouse models*. Front Pharmacol, 2014. **5**: p. 176.
91. Anderson, C.P., et al., *Mammalian iron metabolism and its control by iron regulatory proteins*. Biochim Biophys Acta, 2012. **1823**(9): p. 1468-83.
92. Schalinske, K.L., et al., *The Iron-Sulfur Cluster of Iron Regulatory Protein 1 Modulates the Accessibility of RNA Binding and Phosphorylation Sites*. Biochemistry, 1997. **36**(13): p. 3950-3958.
93. Guo, B., et al., *Iron regulates the intracellular degradation of iron regulatory protein 2 by the proteasome*. J Biol Chem, 1995. **270**(37): p. 21645-51.
94. Iwai, K., R.D. Klausner, and T.A. Rouault, *Requirements for iron-regulated degradation of the RNA binding protein, iron regulatory protein 2*. The EMBO Journal, 1995. **14**(21): p. 5350-5357.
95. Zhang, D.L., M.C. Ghosh, and T.A. Rouault, *The physiological functions of iron regulatory proteins in iron homeostasis - an update*. Front Pharmacol, 2014. **5**: p. 124.

96. Huynh, N., et al., *Glycogen branching enzyme controls cellular iron homeostasis via Iron Regulatory Protein 1 and mitoNEET*. Nature Communications, 2019. **10**(1).
97. Neves, J., et al., *Iron Homeostasis in the Lungs-A Balance between Health and Disease*. Pharmaceuticals (Basel), 2019. **12**(1).
98. Muckenthaler, M., et al., *Iron-regulatory protein-1 (IRP-1) is highly conserved in two invertebrate species*. European Journal of Biochemistry, 1998. **254**(2): p. 230-237.
99. Lind, M.I., et al., *Of two cytosolic aconitases expressed in Drosophila, only one functions as an iron-regulatory protein*. J Biol Chem, 2006. **281**(27): p. 18707-14.
100. Warren, J.T., et al., *Discrete pulses of molting hormone, 20-hydroxyecdysone, during late larval development of Drosophila melanogaster: correlations with changes in gene activity*. Dev Dyn, 2006. **235**(2): p. 315-26.
101. Ou, Q., et al., *The Insect Prothoracic Gland as a Model for Steroid Hormone Biosynthesis and Regulation*. Cell Rep, 2016. **16**(1): p. 247-262.
102. Hammond, G.L., *Plasma steroid-binding proteins: primary gatekeepers of steroid hormone action*. J Endocrinol, 2016. **230**(1): p. R13-25.
103. Freudzon, L., *Perioperative steroid therapy: where's the evidence?* Curr Opin Anaesthesiol, 2018. **31**(1): p. 39-42.
104. Dai, J.D. and L.I. Gilbert, *Metamorphosis of the corpus allatum and degeneration of the prothoracic glands during the larval-pupal-adult transformation of Drosophila melanogaster: a cytophysiological analysis of the ring gland*. Dev Biol, 1991. **144**(2): p. 309-26.
105. Kannangara, J.R., C.K. Mirth, and C.G. Warr, *Regulation of ecdysone production in Drosophila by neuropeptides and peptide hormones*. Open Biol, 2021. **11**(2): p. 200373.
106. Jones, D. and G. Jones, *Farnesoid secretions of dipteran ring glands: what we do know and what we can know*. Insect Biochem Mol Biol, 2007. **37**(8): p. 771-98.
107. Van der Horst, D.J., W.J.A. Van Marrewijk, and J.H.B. Diederer, *Adipokinetic hormones of insect: Release, signal transduction, and responses*, in *International Review of Cytology*. 2001, Academic Press. p. 179-240.

108. Christesen, D., et al., *Transcriptome Analysis of Drosophila melanogaster Third Instar Larval Ring Glands Points to Novel Functions and Uncovers a Cytochrome p450 Required for Development*. G3 (Bethesda), 2017. **7**(2): p. 467-479.
109. Yamanaka, N., G. Marques, and M.B. O'Connor, *Vesicle-Mediated Steroid Hormone Secretion in Drosophila melanogaster*. Cell, 2015. **163**(4): p. 907-19.
110. Okamoto, N., et al., *A Membrane Transporter Is Required for Steroid Hormone Uptake in Drosophila*. Dev Cell, 2018. **47**(3): p. 294-305 e7.
111. Shimada-Niwa, Y. and R. Niwa, *Neural control of steroid hormone biosynthesis during development in the fruit fly Drosophila melanogaster*. Genes & genetic systems, 2014. **89**: p. 27-34.
112. Yoshiyama, T., et al., *Neverland is an evolutionally conserved Rieske-domain protein that is essential for ecdysone synthesis and insect growth*. Development, 2006. **133**(13): p. 2565-74.
113. Yoshiyama-Yanagawa, T., et al., *The conserved Rieske oxygenase DAF-36/Neverland is a novel cholesterol-metabolizing enzyme*. J Biol Chem, 2011. **286**(29): p. 25756-62.
114. Niwa, R., et al., *Non-molting glossy/shroud encodes a short-chain dehydrogenase/reductase that functions in the 'Black Box' of the ecdysteroid biosynthesis pathway*. Development, 2010. **137**(12): p. 1991-9.
115. Niwa, R. and Y.S. Niwa, *Enzymes for ecdysteroid biosynthesis: their biological functions in insects and beyond*. Biosci Biotechnol Biochem, 2014. **78**(8): p. 1283-92.
116. Garen, A., L. Kauvar, and J.-A. Lepesant, *Roles of ecdysone in Drosophila development*. Proceedings of the National Academy of Sciences, 1977. **74**(11): p. 5099-5103.
117. Yamanaka, N., K.F. Rewitz, and M.B. O'Connor, *Ecdysone control of developmental transitions: lessons from Drosophila research*. Annu Rev Entomol, 2013. **58**: p. 497-516.

118. Munoz, M., J.A. Garcia-Erce, and A.F. Remacha, *Disorders of iron metabolism. Part I: molecular basis of iron homoeostasis*. J Clin Pathol, 2011. **64**(4): p. 281-6.
119. Perutz, M.F., et al., *Structure of haemoglobin: a three-dimensional Fourier synthesis at 5.5-Å resolution, obtained by X-ray analysis*. Nature, 1960. **185**(4711): p. 416-22.
120. Marengo-Rowe, A.J., *Structure-function relations of human hemoglobins*. Proceedings (Baylor University. Medical Center), 2006. **19**(3): p. 239-245.
121. De Domenico, I., D. McVey Ward, and J. Kaplan, *Regulation of iron acquisition and storage: consequences for iron-linked disorders*. Nat Rev Mol Cell Biol, 2008. **9**(1): p. 72-81.
122. Beutler, E., et al., *Mutation Analysis in Hereditary Hemochromatosis*. Blood Cells, Molecules, and Diseases, 1996. **22**(2): p. 187-194.
123. Guengerich, F.P., *Destruction of heme and hemoproteins mediated by liver microsomal reduced nicotinamide adenine dinucleotide phosphate-cytochrome P-450 reductase*. Biochemistry, 1978. **17**(17): p. 3633-3639.
124. Correia, M.A., P.R. Sinclair, and F. De Matteis, *Cytochrome P450 regulation: the interplay between its heme and apoprotein moieties in synthesis, assembly, repair, and disposal*. Drug Metab Rev, 2011. **43**(1): p. 1-26.
125. Olakkaran, S., et al., *Lead modulated Heme synthesis inducing oxidative stress mediated Genotoxicity in Drosophila melanogaster*. Science of The Total Environment, 2018. **634**: p. 628-639.
126. Heinemann, I.U., M. Jahn, and D. Jahn, *The biochemistry of heme biosynthesis*. Archives of Biochemistry and Biophysics, 2008. **474**(2): p. 238-251.
127. Layer, G., et al., *Structure and function of enzymes in heme biosynthesis*. Protein Sci, 2010. **19**(6): p. 1137-61.
128. Sachar, M., K.E. Anderson, and X. Ma, *Protoporphyrin IX: the Good, the Bad, and the Ugly*. J Pharmacol Exp Ther, 2016. **356**(2): p. 267-75.

129. Caughey, W.S. and J.A. Ibers, *Crystal and molecular structure of the free base porphyrin, protoporphyrin IX dimethyl ester*. Journal of the American Chemical Society, 1977. **99**(20): p. 6639-6645.
130. Llorens, J.V., et al., *Mitochondrial iron supply is required for the developmental pulse of ecdysone biosynthesis that initiates metamorphosis in Drosophila melanogaster*. J Biol Inorg Chem, 2015. **20**(8): p. 1229-38.
131. Ajioka, R.S., J.D. Phillips, and J.P. Kushner, *Biosynthesis of heme in mammals*. Biochim Biophys Acta, 2006. **1763**(7): p. 723-36.
132. Danielsen, E.T., et al., *A Drosophila Genome-Wide Screen Identifies Regulators of Steroid Hormone Production and Developmental Timing*. Dev Cell, 2016. **37**(6): p. 558-70.
133. Stolzel, U., M.O. Doss, and D. Schuppan, *Clinical Guide and Update on Porphyrias*. Gastroenterology, 2019. **157**(2): p. 365-381 e4.
134. O'Malley, R., et al., *Porphyria: often discussed but too often missed*. Pract Neurol, 2018. **18**(5): p. 352-358.
135. Kadish, K., K.M. Smith, and R. Guilard, *The Porphyrin Handbook, Volume 3*. Vol. 3. 2000: Elsevier.
136. Ramanujam, V.S. and K.E. Anderson, *Porphyria Diagnostics-Part 1: A Brief Overview of the Porphyrias*. Curr Protoc Hum Genet, 2015. **86**: p. 17 20 1-17 20 26.
137. Balwani, M. and R.J. Desnick, *The porphyrias: advances in diagnosis and treatment*. Blood, 2012. **120**(23): p. 4496-4504.
138. Erwin, A.L. and M. Balwani, *Porphyrias in the Age of Targeted Therapies*. Diagnostics (Basel), 2021. **11**(10).
139. Baldin, J.P., D. Barth, and M. Fronius, *Epithelial Na(+) Channel (ENaC) Formed by One or Two Subunits Forms Functional Channels That Respond to Shear Force*. Front Physiol, 2020. **11**: p. 141.
140. Mano, I. and M. Driscoll, *DEG/ENaC channels: a touchy superfamily that watches its salt*. Bioessays, 1999. **21**(7): p. 568-578.

141. Firsov, D., et al., *The heterotetrameric architecture of the epithelial sodium channel (ENaC)*. *Embo j*, 1998. **17**(2): p. 344-52.
142. Immke, D.C. and E.W. McCleskey, *Protons open acid-sensing ion channels by catalyzing relief of Ca²⁺ blockade*. *Neuron*, 2003. **37**(1): p. 75-84.
143. Fitzsimons, J.T., *The physiological basis of thirst*. *Kidney Int*, 1976. **10**(1): p. 3-11.
144. Choi, H.Y., H.C. Park, and S.K. Ha, *High Water Intake and Progression of Chronic Kidney Diseases*. *Electrolyte Blood Press*, 2015. **13**(2): p. 46-51.
145. Bianchi, L. and M. Driscoll, *Protons at the Gate: DEG/ENaC Ion Channels Help Us Feel and Remember*. *Neuron*, 2002. **34**(3): p. 337-340.
146. Garty, H. and L.G. Palmer, *Epithelial sodium channels: function, structure, and regulation*. *Physiological Reviews*, 1997. **77**(2): p. 359-396.
147. Zelle, K.M., et al., *The genetic architecture of degenerin/epithelial sodium channels in Drosophila*. *G3 (Bethesda)*, 2013. **3**(3): p. 441-50.
148. Drummond, H.A., N.L. Jernigan, and S.C. Grifoni, *Sensing tension: epithelial sodium channel/acid-sensing ion channel proteins in cardiovascular homeostasis*. *Hypertension*, 2008. **51**(5): p. 1265-71.
149. Kellenberger, S. and L. Schild, *Epithelial Sodium Channel/Degenerin Family of Ion Channels: A Variety of Functions for a Shared Structure*. *Physiological Reviews*, 2002. **82**(3): p. 735-767.
150. Swift, P.A. and G.A. MacGregor, *The Epithelial Sodium Channel in Hypertension*. *American Journal of Pharmacogenomics*, 2004. **4**(3): p. 161-168.
151. Hanukoglu, I. and A. Hanukoglu, *Epithelial sodium channel (ENaC) family: Phylogeny, structure-function, tissue distribution, and associated inherited diseases*. *Gene*, 2016. **579**(2): p. 95-132.
152. Cheng, Y.R., B.Y. Jiang, and C.C. Chen, *Acid-sensing ion channels: dual function proteins for chemo-sensing and mechano-sensing*. *J Biomed Sci*, 2018. **25**(1): p. 46.

153. Lingueglia, E., *ENaC, Degenerins, ASICs, and Related Channels*, in *Encyclopedia of Biophysics*, G.C.K. Roberts, Editor. 2013, Springer Berlin Heidelberg: Berlin, Heidelberg. p. 664-674.
154. Canessa, C.M., et al., *Amiloride-sensitive epithelial Na⁺ channel is made of three homologous subunits*. *Nature*, 1994. **367**(6462): p. 463-467.
155. Bhalla, V. and K.R. Hallows, *Mechanisms of ENaC regulation and clinical implications*. *J Am Soc Nephrol*, 2008. **19**(10): p. 1845-54.
156. Rotin, D., *Role of the UPS in Liddle syndrome*. *BMC Biochem*, 2008. **9 Suppl 1**: p. S5.
157. Bork, P. and M. Sudol, *The WW domain: a signalling site in dystrophin?* *Trends in Biochemical Sciences*, 1994. **19**(12): p. 531-533.
158. Kamynina, E., et al., *A novel mouse Nedd4 protein suppresses the activity of the epithelial Na⁺ channel*. *Faseb j*, 2001. **15**(1): p. 204-214.
159. Fotia, A.B., et al., *Regulation of neuronal voltage-gated sodium channels by the ubiquitin-protein ligases Nedd4 and Nedd4-2*. *J Biol Chem*, 2004. **279**(28): p. 28930-5.
160. Liu, L., W.A. Johnson, and M.J. Welsh, *Drosophila DEG/ENaC pickpocket genes are expressed in the tracheal system, where they may be involved in liquid clearance*. *Proc Natl Acad Sci U S A*, 2003. **100**(4): p. 2128-33.
161. Turi, J.L., et al., *Iron accumulation in bronchial epithelial cells is dependent on concurrent sodium transport*. *Biometals*, 2008. **21**(5): p. 571-80.
162. Hu, Y., et al., *An integrative approach to ortholog prediction for disease-focused and other functional studies*. *BMC Bioinformatics*, 2011. **12**: p. 357.
163. Eastwood, A.L. and M.B. Goodman, *Insight into DEG/ENaC channel gating from genetics and structure*. *Physiology (Bethesda)*, 2012. **27**(5): p. 282-90.
164. Ilyaskin, A.V., et al., *Activation of the Human Epithelial Sodium Channel (ENaC) by Bile Acids Involves the Degenerin Site*. *J Biol Chem*, 2016. **291**(38): p. 19835-47.

165. Frise, M.C., et al., *Clinical iron deficiency disturbs normal human responses to hypoxia*. J Clin Invest, 2016. **126**(6): p. 2139-50.
166. Giaccia, A.J., M.C. Simon, and R. Johnson, *The biology of hypoxia: the role of oxygen sensing in development, normal function, and disease*. Genes & development, 2004. **18**(18): p. 2183-2194.
167. Lendahl, U., et al., *Generating specificity and diversity in the transcriptional response to hypoxia*. Nat Rev Genet, 2009. **10**(12): p. 821-32.
168. Smith, T.G., P.A. Robbins, and P.J. Ratcliffe, *The human side of hypoxia-inducible factor*. Br J Haematol, 2008. **141**(3): p. 325-34.
169. Bigham, A.W. and F.S. Lee, *Human high-altitude adaptation: forward genetics meets the HIF pathway*. Genes Dev, 2014. **28**(20): p. 2189-204.
170. Carmeliet, P., et al., *Role of HIF-1alpha in hypoxia-mediated apoptosis, cell proliferation and tumour angiogenesis*. Nature, 1998. **394**(6692): p. 485-90.
171. Zelzer, E., P. Wappner, and B.Z. Shilo, *The PAS domain confers target gene specificity of Drosophila bHLH/PAS proteins*. Genes & development, 1997. **11**(16): p. 2079-2089.
172. Nambu, J.R., et al., *The Drosophila melanogaster similar bHLH-PAS gene encodes a protein related to human hypoxia-inducible factor 1a and Drosophila single-minded*. Gene, 1996. **172**(2): p. 249-254.
173. Ohshiro, T. and K. Saigo, *Transcriptional regulation of breathless FGF receptor gene by binding of TRACHEALESS/dARNT heterodimers to three central midline elements in Drosophila developing trachea*. Development, 1997. **124**(20): p. 3975-3986.
174. Sonnenfeld, M., et al., *The Drosophila tango gene encodes a bHLH-PAS protein that is orthologous to mammalian Arnt and controls CNS midline and tracheal development*. Development, 1997. **124**(22): p. 4571-4582.
175. Bacon, N.C.M., et al., *Regulation of the Drosophila bHLH-PAS Protein Sima by Hypoxia: Functional Evidence for Homology with Mammalian HIF-1a*. Biochemical and Biophysical Research Communications, 1998. **249**(3): p. 811-816.

176. Wilk, R., I. Weizman, and B.Z. Shilo, *trachealess encodes a bHLH-PAS protein that is an inducer of tracheal cell fates in Drosophila*. *Genes Dev*, 1996. **10**(1): p. 93-102.
177. Arquier, N., et al., *Analysis of the hypoxia-sensing pathway in Drosophila melanogaster*. *Biochem J*, 2006. **393**(Pt 2): p. 471-80.
178. Jiang, L. and S.T. Crews, *The Drosophila dysfusion basic helix-loop-helix (bHLH)-PAS gene controls tracheal fusion and levels of the trachealess bHLH-PAS protein*. *Mol Cell Biol*, 2003. **23**(16): p. 5625-37.
179. Heinrich, E.C., et al., *The effect of developmental stage on the sensitivity of cell and body size to hypoxia in Drosophila melanogaster*. *The Journal of experimental biology*, 2011. **214**(Pt 9): p. 1419-1427.
180. Callier, V. and H.F. Nijhout, *Control of body size by oxygen supply reveals size-dependent and size-independent mechanisms of molting and metamorphosis*. *Proc Natl Acad Sci U S A*, 2011. **108**(35): p. 14664-9.
181. Li, L., et al., *Binding and uptake of H-ferritin are mediated by human transferrin receptor-1*. *Proc Natl Acad Sci U S A*, 2010. **107**(8): p. 3505-10.
182. Todorich, B., et al., *Tim-2 is the receptor for H-ferritin on oligodendrocytes*. *J Neurochem*, 2008. **107**(6): p. 1495-505.
183. Li, J.Y., et al., *Scara5 is a ferritin receptor mediating non-transferrin iron delivery*. *Dev Cell*, 2009. **16**(1): p. 35-46.
184. Greenspan, R.J., *Fly pushing: the theory and practice of Drosophila genetics*. 2004: CSHL Press.
185. Mansilla, A., et al., *Ligand-independent requirements of steroid receptors EcR and USP for cell survival*. *Cell Death Differ*, 2016. **23**(3): p. 405-16.
186. Casas-Tinto, S., M. Arnes, and A. Ferrus, *Drosophila enhancer-Gal4 lines show ectopic expression during development*. *R Soc Open Sci*, 2017. **4**(3): p. 170039.
187. Fernandez-Moreno, M.A., et al., *Drosophila melanogaster as a model system to study mitochondrial biology*. *Methods Mol Biol*, 2007. **372**: p. 33-49.

188. Ou, Q., A. Magico, and K. King-Jones, *Nuclear receptor DHR4 controls the timing of steroid hormone pulses during Drosophila development*. PLoS Biol, 2011. **9**(9): p. e1001160.
189. Gerace, E. and D. Moazed, *Affinity Pull-Down of Proteins Using Anti-FLAG M2 Agarose Beads*. Methods Enzymol, 2015. **559**: p. 99-110.
190. Gao, M., et al., *An in vivo crosslinking approach to isolate protein complexes from Drosophila embryos*. J Vis Exp, 2014(86).
191. Mahmood, T. and P.C. Yang, *Western blot: technique, theory, and trouble shooting*. N Am J Med Sci, 2012. **4**(9): p. 429-34.
192. Richards, A.L., M. Eckhardt, and N.J. Krogan, *Mass spectrometry-based protein-protein interaction networks for the study of human diseases*. Mol Syst Biol, 2021. **17**(1): p. e8792.
193. Liu, X., et al., *Combined proximity labeling and affinity purification-mass spectrometry workflow for mapping and visualizing protein interaction networks*. Nat Protoc, 2020. **15**(10): p. 3182-3211.
194. Huynh, N.T., *Characterizing new players involved in iron homeostasis during Drosophila larval development: Shifting the classic paradigm of iron metabolism*, in *Department of Biological Sciences*. 2020, University of Alberta.
195. Tomoyasu, Y. and R.E. Denell, *Larval RNAi in Tribolium (Coleoptera) for analyzing adult development*. Dev Genes Evol, 2004. **214**(11): p. 575-8.
196. Orr, B.O., et al., *Composition and Control of a Deg/ENaC Channel during Presynaptic Homeostatic Plasticity*. Cell Rep, 2017. **20**(8): p. 1855-1866.
197. Snyder, P.M., *The epithelial Na⁺ channel: cell surface insertion and retrieval in Na⁺ homeostasis and hypertension*. Endocr Rev, 2002. **23**(2): p. 258-75.
198. Truman, J.W. and L.M. Riddiford, *The origins of insect metamorphosis*. Nature, 1999. **401**(6752): p. 447-452.
199. Dubrovsky, E.B., *Hormonal cross talk in insect development*. Trends in Endocrinology & Metabolism, 2005. **16**(1): p. 6-11.

200. Locke, M. and H. Leung, *The induction and distribution of an insect ferritin — A new function for the endoplasmic reticulum*. *Tissue and Cell*, 1984. **16**(5): p. 739-766.
201. Winzerling, J.J., et al., *Rapid and efficient isolation of transferrin and ferritin from *Manduca sexta**. *Insect Biochem Mol Biol*, 1995. **25**(2): p. 217-24.
202. Capurro Mde, L., et al., *Musca domestica hemolymph ferritin*. *Arch Insect Biochem Physiol*, 1996. **32**(2): p. 197-207.
203. Crichton, R.R. and M. Charlotiaux-Wauters, *Iron transport and storage*. *European Journal of Biochemistry*, 1987. **164**(3): p. 485-506.
204. Scott, M.S., et al., *Refining protein subcellular localization*. *PLoS Comput Biol*, 2005. **1**(6): p. e66.
205. Jernigan, N.L. and H.A. Drummond, *Vascular ENaC proteins are required for renal myogenic constriction*. *American Journal of Physiology-Renal Physiology*, 2005. **289**(4): p. F891-F901.
206. Rizzo, M.A., M.W. Davidson, and D.W. Piston, *Fluorescent protein tracking and detection: applications using fluorescent proteins in living cells*. *Cold Spring Harb Protoc*, 2009. **2009**(12): p. pdb top64.
207. Ratz, M., et al., *CRISPR/Cas9-mediated endogenous protein tagging for RESOLFT super-resolution microscopy of living human cells*. *Sci Rep*, 2015. **5**: p. 9592.
208. Swale, D.R., et al., *Role of inward rectifier potassium channels in salivary gland function and sugar feeding of the fruit fly, *Drosophila melanogaster**. *Pestic Biochem Physiol*, 2017. **141**: p. 41-49.
209. Arrese, E.L. and J.L. Soulages, *Insect fat body: energy, metabolism, and regulation*. *Annu Rev Entomol*, 2010. **55**: p. 207-25.
210. Faisal, M.N., et al., *Transcriptional regionalization of the fruit fly's airway epithelium*. *PLoS One*, 2014. **9**(7): p. e102534.

211. Liu, L., et al., *Contribution of Drosophila DEG/ENaC Genes to Salt Taste*. *Neuron*, 2003. **39**(1): p. 133-146.
212. Farkas, R., et al., *Vacuole dynamics in the salivary glands of Drosophila melanogaster during prepupal development*. *Dev Growth Differ*, 2015. **57**(1): p. 74-96.
213. Andrew, D.J., K.D. Henderson, and P. Seshaiyah, *Salivary gland development in Drosophila melanogaster*. *Mechanisms of Development*, 2000. **92**(1): p. 5-17.
214. von Mering, C., et al., *STRING: known and predicted protein-protein associations, integrated and transferred across organisms*. *Nucleic Acids Res*, 2005. **33**(Database issue): p. D433-7.
215. Menzies, F.M., et al., *Puromycin-sensitive aminopeptidase protects against aggregation-prone proteins via autophagy*. *Hum Mol Genet*, 2010. **19**(23): p. 4573-86.
216. Dorer, D.R., et al., *A Family of Genes Clustered at the Triplo-lethal Locus of Drosophila melanogaster Has an Unusual Evolutionary History and Significant Synteny With Anopheles gambiae*. *Genetics*, 2003. **165**(2): p. 613-621.
217. Shah, N., et al., *Evolution of a large, conserved, and syntenic gene family in insects*. *G3 (Bethesda)*, 2012. **2**(2): p. 313-9.
218. Scholl, A., et al., *Tracheal expression of Osiris gene family in Drosophila*. *Gene Expr Patterns*, 2018. **28**: p. 87-94.
219. Ando, T., et al., *Nanopore Formation in the Cuticle of an Insect Olfactory Sensillum*. *Curr Biol*, 2019. **29**(9): p. 1512-1520 e6.
220. Burmester, T., et al., *The evolution of hexamerins and the phylogeny of insects*. *J Mol Evol*, 1998. **47**(1): p. 93-108.
221. Roberts, D.B., S.A. Blackwell, and S.A. Loughlin, *Quantitative analysis of the amount of larval serum protein-1 (LSP-1) synthesized by flies with different doses of the LSP-1 coding sequences*. *Biochem Genet*, 1984. **22**(9-10): p. 783-95.

222. Wolfe, J., M.E. Akam, and D.B. Roberts, *Biochemical and Immunological Studies on Larval Serum Protein 1, the Major Haemolymph Protein of Drosophila melanogaster Third-Instar Larvae*. European Journal of Biochemistry, 1977. **79**(1): p. 47-53.
223. Roberts, D., *Chapter 6 Drosophila Antigens: Their Spatial and Temporal Distribution, Their Function and Control*. 1975. **9**: p. 167-189.
224. Massey, H.C., et al., *The Drosophila Lsp - 1 β Gene*. European Journal of Biochemistry, 1997. **245**(1): p. 199-207.
225. Rulifson, E., et al., *A Systematic Screen for Tube Morphogenesis and Branching Genes in the Drosophila Tracheal System*. PLoS Genetics, 2011. **7**(7): p. e1002087.
226. Ziello, J.E., I.S. Jovin, and Y. Huang, *Hypoxia-Inducible Factor (HIF)-1 regulatory pathway and its potential for therapeutic intervention in malignancy and ischemia*. The Yale journal of biology and medicine, 2007. **80**(2): p. 51-60.
227. Jarecki, J., E. Johnson, and M.A. Krasnow, *Oxygen Regulation of Airway Branching in Drosophila Is Mediated by Branchless FGF*. Cell, 1999. **99**(2): p. 211-220.
228. Wagner, P.D., *The biology of oxygen*. Eur Respir J, 2008. **31**(4): p. 887-90.
229. Ong, S.T., et al., *Iron-withholding strategy in innate immunity*. Immunobiology, 2006. **211**(4): p. 295-314.
230. Branon, T.C., et al., *Efficient proximity labeling in living cells and organisms with TurboID*. Nat Biotechnol, 2018. **36**(9): p. 880-887.
231. Cho, K.F., et al., *Proximity labeling in mammalian cells with TurboID and split-TurboID*. Nat Protoc, 2020. **15**(12): p. 3971-3999.
232. Astle, J., T. Kozlova, and C.S. Thummel, *Essential roles for the Dhr78 orphan nuclear receptor during molting of the Drosophila tracheal system*. Insect Biochemistry and Molecular Biology, 2003. **33**(12): p. 1201-1209.

233. Klok, C.J., et al., *Critical oxygen partial pressures and maximal tracheal conductances for Drosophila melanogaster reared for multiple generations in hypoxia or hyperoxia*. J Insect Physiol, 2010. **56**(5): p. 461-9.

234. Beitel, G.J. and M.A. Krasnow, *Genetic control of epithelial tube size in the Drosophila tracheal system*. Development, 2000. **127**(15): p. 3271-3282.